THE LATE CRETACEOUS-EARLY TERTIARY POLAR FORESTS OF NORTHWEST ELLESMERE ISLAND, NUNAVUT, CANADA: PALAEOBOTANY, PALAEOECOLOGY AND PALAEOCLIMATOLOGY

Adam Zoltan Csank

Submitted in Partial Fulfillment of the Requirements

for the Degree of Bachelor of Science, Honours

Department of Earth Sciences

Dalhousie University, Halifax, Nova Scotia

April 2002

Dalhousie University

Department of Earth Sciences
Halifax, Nova Scotia
Canada B3H 3J5
(902) 494-2358
FAX (902) 494-6889

DATE *April, 15 2002*

AUTHOR *Adam Zoltan Csank*

TITLE *The Late Cretaceous Polar Forests of Northwest Ellesmere Island, Nunavut, Canada: Palaeobotany, Palaeoecology and Palaeoclimatology*

Degree *B.Sc.*　　Convocation _____　　Year *2003*

Permission is herewith granted to Dalhousie University to circulate and to have copied for non-commercial purposes, at its discretion, the above title upon the request of individuals or institutions.

Abstract

During the Mesozoic to Early Cenozoic greenhouse climate phase forests grew well within the polar circle. These unique polar forest ecosystems flourished in a warm, high-latitude environment where trees were subjected to months of unbroken winter darkness followed by continuous daylight in the summer and elevated atmospheric carbon dioxide levels (c. 800 ppm).

This thesis describes five anatomically preserved wood specimens from a new, Late Cretaceous-Earliest Tertiary, high-latitude (palaeolatitude of 74-78°N) fossil plant assemblage from Emma Fiord and Phillips Inlet, NW Ellesmere Island. The fossil wood occurs in the Campanian/Maastrichtian to Danian Hansen Point Volcanics of the Eureka Sound Group, Sverdrup Basin, a stratigraphic unit interpreted as originating in a volcanically disturbed, alluvial plain/peat mire setting close to the margins of the palaeo-Arctic Ocean. Quantitative analysis of anatomical features in petrographic thin sections enabled the wood specimens to be assigned to two conifer families, the Taxodiaceae and Pinaceae. One taxodiaceous species (*Taxodioxylon albertense* (Penhallow) Shimakura, 1937) and three pinaceous species (*Piceoxylon ellesmerensis* (Falcon-Lang, MacRae and Csank, unpub. subm.), *Pinuxylon woolardii* (Tidwell, Parker and Folkman, 1986), and *Pinuxylon* sp. 1 were identified.

Biometric analysis of the permineralized trunks suggests that the forest canopy was in the order of 15-20 m. Well-preserved growth rings indicate that these trees grew under a temperate climate with a high year-to-year variability characterized by frequent disturbances. Common traumatic rings indicate that one such disturbance process was the occurrence of sharp frosts towards the end of the growing season, while abundant false rings suggest that another may have been occasional flooding or ash falls. Finally, intra-annual phenological studies of growth rings suggest that trees possessed a mixture of habits, some being evergreen and other being deciduous.

Although pinaceous conifers are the most common group represented by the permineralized woods, additional studies of charred woods, compressed foliage, and palynomorphs from the same site by other authors demonstrate that taxodiaceous conifers were actually the dominant vegetation with pinaceous conifers occurring in only subordinate numbers, together with gingkos, angiosperms and ferns. Physiognomically, the nearest extant equivalent to these polar forests would be the cool-temperate *Sequoia-Pseudotsuga* forests of British Columbia. The data presented in this thesis therefore shed considerable new light on the community-scale ecology of North Hemisphere, Late Cretaceous-Early Tertiary polar forests, and may provide a useful long-term context for the response of modern boreal forest ecosystems to future global climate change.

Acknowledgements

This thesis would not have been possible without the help of the people mentioned bellow. Their guidance, support and encouragement kept me going throughout the project. Thanks everyone.

- My supervisor Dr. H. J. Falcon-Lang for the encouragement, guidance and instruction he provided throughout the thesis. His deadlines kept me on track and his contributions in the form of corrections and suggestions made this thesis what it is.
- G. Brown for making the thin sections on which much of this project is based.
- Dr. R.A. MacRae for certain key figures, the use of his field notes and for collecting the samples in the first place
- Dr. G.K. Muecke who, along with RAM, collected the samples and who stored them here at Dalhousie.
- Dr. R.A. Jamieson and A.M. Grist for use of their photographic equipment.
- Dr. M. Zentilli for encouragement and advice.
- M. & L. Kitzmiller for corrections.
- Lastly to the 2001-2002 Honours class for moral support.
- AZC would also like to thank the Killam Trust for partial funding of this thesis.

Table of contents

Table of tables

Table of figures

1. Introduction

1.1 Present-day global change

The recognition that forests covered the polar circle throughout most of the Mesozoic and Cenozoic represents one of the greatest palaeontological discoveries of the past twenty years. This research is particularly important in assessing the long-term impact of present day global warming (Beerling, 1998).

Since the 1900's the Earth's mean surface temperature has risen by $0.6^{\circ}C$ (Ruddiman, 2001). This global warming is caused by the greenhouse effect, in which long wave solar radiation reflected from Earth's surface is trapped by greenhouse gases (H_2O, CH_4 and CO_2) and re-radiated back to the surface. Since the industrial revolution there has been a 30% increase in atmospheric CO_2 (from 280 ppm-371 ppm) (Ruddiman, 2001). At present, estimates of anthropogenic CO_2 emissions into the atmosphere are 6 Gt C per year. Of that 6 Gt C, 2.3 Gt C remains in the atmosphere, 1.7 Gt C is thought to be absorbed by the oceans, whilst 2.0 Gt C is sequestered by the terrestrial biosphere (Beerling, 1999). Predictions by the Intergovernmental Panel on Climate Change indicate that atmospheric CO_2 concentration of 450-800ppm by the year 2100 (Houghton *et al.*, 1996). This is important because of the close relationship between temperature and CO_2 levels (Fig. 1.1).

Concerns about the possible impact of elevated CO_2 levels and resultant global warming has increased interest in the likely response of vegetation. At the Kyoto Summit in 1998, the uptake of carbon by forests was proposed as a method of reducing net CO_2 emissions to the atmosphere (UNFCCC, 1998). However, Betts (2000) suggests that this would not prove effective, as the albedo effect of boreal forests would offset any temperature reduction by carbon sequestration. Albedo is a measure of the degree to which a surface of a particular colour absorbs light. Light-coloured surfaces, the Antarctic Ice sheet for example, reflect a high proportion of solar radiation and so have a high albedo. Dark-coloured surfaces, evergreen forests for example, absorb relatively more solar radiation and as such have a low albedo. If boreal forests were to grow further north they would act as a sink for CO_2 however, during seasons of snow cover the impact

1

of decreased albedo would be large enough to outweigh the benefit gained by CO_2 removal (Betts, 2000).
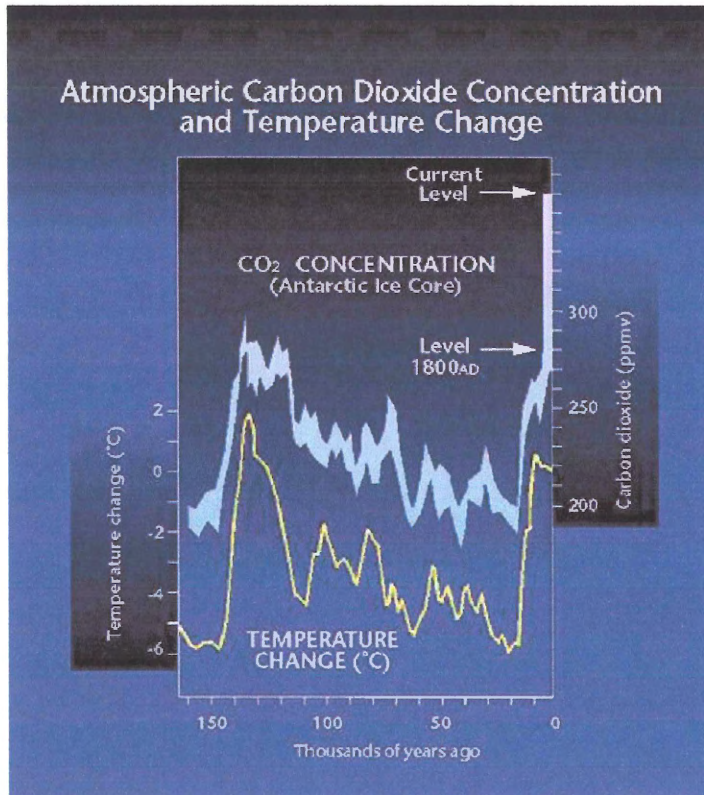
Figure 1.1: A plot of carbon dioxide levels and temperature showing how they relate to each other. (After Barnola *et al.*, 1987).

1.2 The Late Cretaceous-Early Tertiary Greenhouse world: an overview

During the Cretaceous and Early Tertiary, atmospheric CO_2 concentrations were even higher than those predicted by the IPCC for 2100, probably on the order of 1000-2000 ppm (Retallack, 2001). Consequently, temperatures on Earth were considerably warmer than today (Fig. 1.2), resulting in a pole-to-equator temperature contrast of between 17 and 28° C the Late Cretaceous compared to the present contrast of 41° C (Barron, 1983). The mean annual temperature (MAT) at the poles was between 2 and 10° C in the Cretaceous (Parrish and Spicer, 1988a; Barron, 1983) compared to a MAT of -5 to -20° C at the poles today (Alaska Climate Research Center, 2002).

2

In the Early Cretaceous, global climate was changing from the relatively arid climate of the Jurassic to a much more humid environment (Spicer and Chapman, 1990). Fossils of warm-adapted species of both animal and plant have been found at both poles (Axelrod, 1984; Tarduno *et al*, 1998). For much of the Cretaceous there is no record of ice in polar regions, although there was a cooling phase in the Early Cretaceous evidenced by ice-rafted deposits (Frakes and Francis, 1988). Tree-rings and sediments from this period show a strong seasonality at the poles evidenced by traumatic parenchyma (scar tissue formed by freezing temperatures during the growing season) and false rings (temporary interruptions in growth) in trees, and by the widespread occurrence of varves in the sediment (Francis and Frakes, 1993). Oxygen isotope data taken from foraminifera and nanoplankton indicate sea-surface temperatures of 28° C and bottom water temperatures of 11° C at the beginning of the Cretaceous. These cooled by 2-3° C from the Berriasian to the Barremian before rising to a peak in the late Albian/early Cenomanian. Temperatures dropped with a final cooling episode in the Maastrichtian (Fig. 1.2) (Francis and Frakes, 1993). In the early Paleocene temperatures had started to warm again before stabilizing until the early Oligocene when climate cooled quite suddenly; this time also witnessed the demise of the polar forest biome (Spicer and Chapman, 1990.). The low pole-to-equator temperature contrast hints at a sluggish ocean circulation with poorly mixed waters (Francis and Frakes, 1993). The lack of polar ice caps would have meant there was no source of cold oxygen-rich bottom water as there is today. Instead bottom water would have consisted of cool, high-latitude water or saline low-latitude water, sourced from epieric seas (Francis and Frakes, 1993).

On land, leaf and vegetation analyses from high latitude forests in Alaska have indicated mean annual temperatures of 12-13° C in the Coniacian (the warmest part of the Cretaceous) and 2-8° C during the Campanian and Maastrichtian (Francis and Frakes, 1993), the mean annual temperature high latitude regions today is -19.6 °C (Jahren and Sternberg, 2002). The latest Maastrichtian appears to have been especially cool, with low, even freezing, temperatures at high latitudes similar perhaps to the early Cretaceous (Francis and Frakes, 1993). Studies by Spicer and Parrish (1990b) suggest that although permanent ice did not develop at sea level during the Maastrichtian it likely was present above 1000m at 85° N. Conditions such as those described above indicate that the

Cretaceous-Tertiary poles were more habitable environments than the poles today and would have been able to sustain more complex and diverse ecosystems than those in existence today.

Time x10^6 yrs	Average Global Temperature		
	Period	Cooler Present Warmer	
0	Quaternary		
1.67	Pliocene		
5.1	Miocene		
24	Oligocene		
36	Eocene		
55	Paleocene		
65	Cretaceous		
140	Jurassic		
210	Triassic		
250	Permian		
290	Carboniferous		
360	Devonian		
410	Silurian		
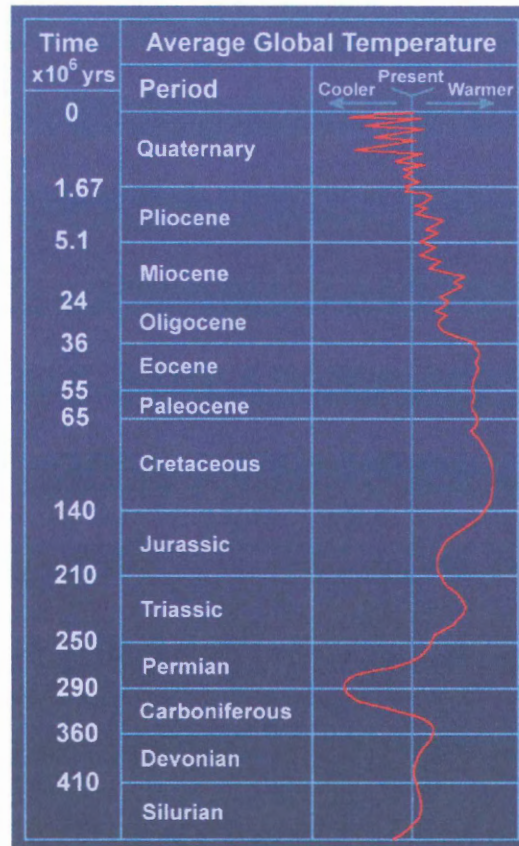
Figure 1.2: This curve shows average global temperature over geologic time. Note the greenhouse temperatures during the Cretaceous and Early Tertiary. The slight cooling in the Maastrichtian should be noted as well as the cooling period in the Early Oligocene. (after Spicer and Chapman, 1990).

1.3 Polar forests: an extinct biome

One of the more interesting facets of the greenhouse world were the temperate rainforests inhabited by dinosaurs that existed at both poles. Rich fossil floras have been described from Alaska (Spicer and Parrish, 1990a), Australia (Douglas and Williams, 1982), Antarctica (Falcon-Lang and Cantrill, 2000), Arctic Canada (Christie and McMillan, 1991) and Siberia (Herman and Spicer, 1996); all located well above the polar

circles during the Cretaceous (Fig. 1.3). These forests existed at palaeolatitudes of 66-85°. The most northerly modern forest is at Ary-Mas 72° N in Northern Russia, and in some parts of the world the tree-line is as far south as 59° N (Spicer and Chapman, 1990). It is interesting to note that these high-latitude floras would have had to survive through the dark winter months with no sunlight whatsoever. Beerling (1998) mentions that increased CO_2 causes certain physiological changes in plants, such as more efficient water uptake and larger leaf area that may help them adapt to cooler temperatures and less light. Experiments have shown that under a polar light regime higher CO_2 levels help to significantly reduce the rate of dark respiration in plants enabling them to survive the long months of winter darkness (Beerling and Osborne, 2002). The unique conditions in existence at the poles made the Late Paleozoic-Early Tertiary polar forests unique biomes without any close modern analogues.

Interestingly both modern boreal forests and high-latitude Cretaceous forests are dominated by gymnosperms (Poole and Cantrill, 2001). High-latitude Cretaceous floras of the Southern Hemisphere were be dominated by bennettites (an extinct plant group, resembles modern cycads) and other gymnosperms in the pre-angiosperm under-storey. Araucarian (monkey puzzle) and podocarp conifers formed the majority of the over-storey of Southern Hemisphere forests (Falcon-Lang *et al.*, 2001). The Northern Hemisphere pre-angiosperm flora consisted of cycadophytes and ferns, with taxodioid and pinoid conifers forming the majority of the overstorey (Axelrod, 1984; Spicer and Parrish, 1986). Angiosperm diversification in the Cretaceous brought colour and smell to the polar forests with species such as Illiciaceae (star anise), Winteraceae (winter's bark), Moniniaceae (lemon) and *Nothofagus* (southern beech) appearing in the austral forests (Poole and Cantrill, 2001). The Northern hemisphere flora was rich in herbs as well as species such as *Dryas* (mountain avens), *Betula* (birch), *Cassiope* and *Grewia* (Axelrod, 1984; Spicer and Chapman, 1990).

In the Early Tertiary, continued evolution of polar vegetation resulted in the appearance of several new species of conifer including *Pseudotsuga* (douglas fir) and *Larix* (larch) (Basinger, 1991; Obst *et al.* 1991; LePage and Basinger, 1991b). By the Eocene angiosperms had become much more dominant members of the polar forest biome and deciduous trees had begun to take over from the evergreens (Herman and

5

Spicer, 1995; Kumagai *et al.*, 1995). Polar forests continued to thrive as an ecosystem well into the Tertiary, before migrating south in the Early-Oligocene as climate began to cool resulting in the demise of this unique biome.
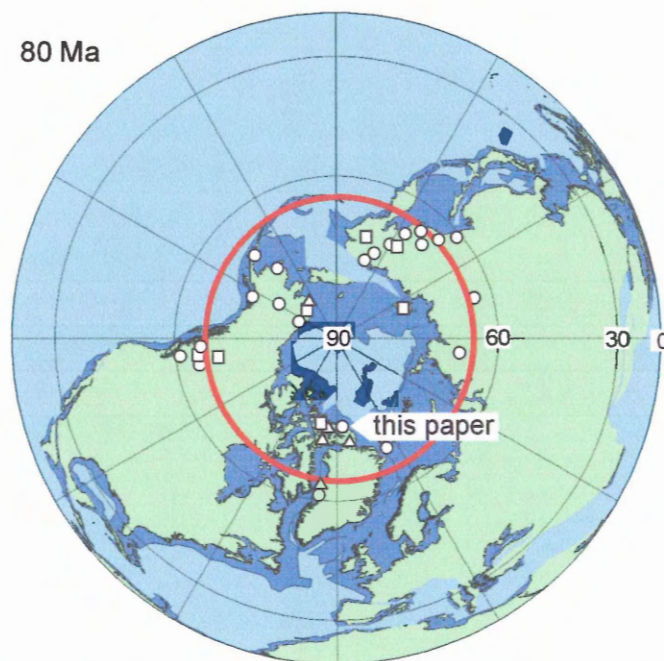
△ Early Tertiary ○ Late Cretaceous □ Early-Middle Cretaceous ▬ Average modern tree line 64° N

Figure 1.3: A pole centred map showing the locations of all known fossil forest sites. (adapted from Cambridge Palaeomap Project, 2002, pers. comm.).

1.4 Aims and Objectives

This thesis aims to improve our knowledge of the unique ecosystems and climate of the poorly understood Late-Cretaceous and Early Tertiary polar biome. A secondary aim of this project is to develop an understanding of polar conditions in a Greenhouse world and show how this knowledge can be useful in understanding our future in this time of global climate change. After all, as one researcher noted, "the past is the key to the future"(Beerling, 1998). Two objectives fulfill these aims:

(1) Taxonomy of fossil woods from Emma Fiord and Phillips Inlet, Northwest Ellesmere Island is studied to determine forest composition at a previously unstudied site (Chapter 3)

6

(2) Tree-rings in the fossil woods are analyzed to determine growth patterns, which will shed light on the tree ecology, growing conditions and growing climate (Chapter 4).

2. Geological background

2.1 Geological setting

The fossil forest sites studied in this report are located in North Western Ellesmere Island, the most northerly of the Canadian Arctic Islands. Site one, hereafter referred to as the Emma Fiord site, is located on an unnamed peninsula which lies between Emma Fiord and Audhild Bay. Site two, referred to as the Phillips Inlet site, is located just to the South of Phillips Inlet on the north coast of Ellesmere Island (Fig 2.1, 2.2). Both sites lie stratigraphicaly within the Hansen Point Volcanic unit of the Eureka Sound Group which forms part of the Sverdrup Basin (Fig. 2.3).

The Canadian Arctic Islands form part of the North American continental margin and as such possess a complex geologic history. Thorsteinsson and Trettin (1972) published the first geological maps of the area and since that time a handful of other researchers have offered their interpretations. Most recent research on Ellesmere Island has centered on the petroleum potential (Chen *et al.*, 2000) and tectonic evolution (Miall, 1986; Embry and Osadetz, 1988; Harrison *et al.*, 1999; Arne *et al.*, 1998; Arne *et al.*, 2002) of the Sverdrup Basin. The following summary draws elements from these diverse sources as well as from information collected by MacRae and Muecke (unpublished report) on a field excursion in 1987. These data are used to assemble a plausible geologic history for the Hansen Point Volcanics (in which the fossil forests occurs) and the Eureka Sound Group as well as providing a generalized look at the Sverdrup basin. This will provide the background for the geologic environment of the fossil forests.
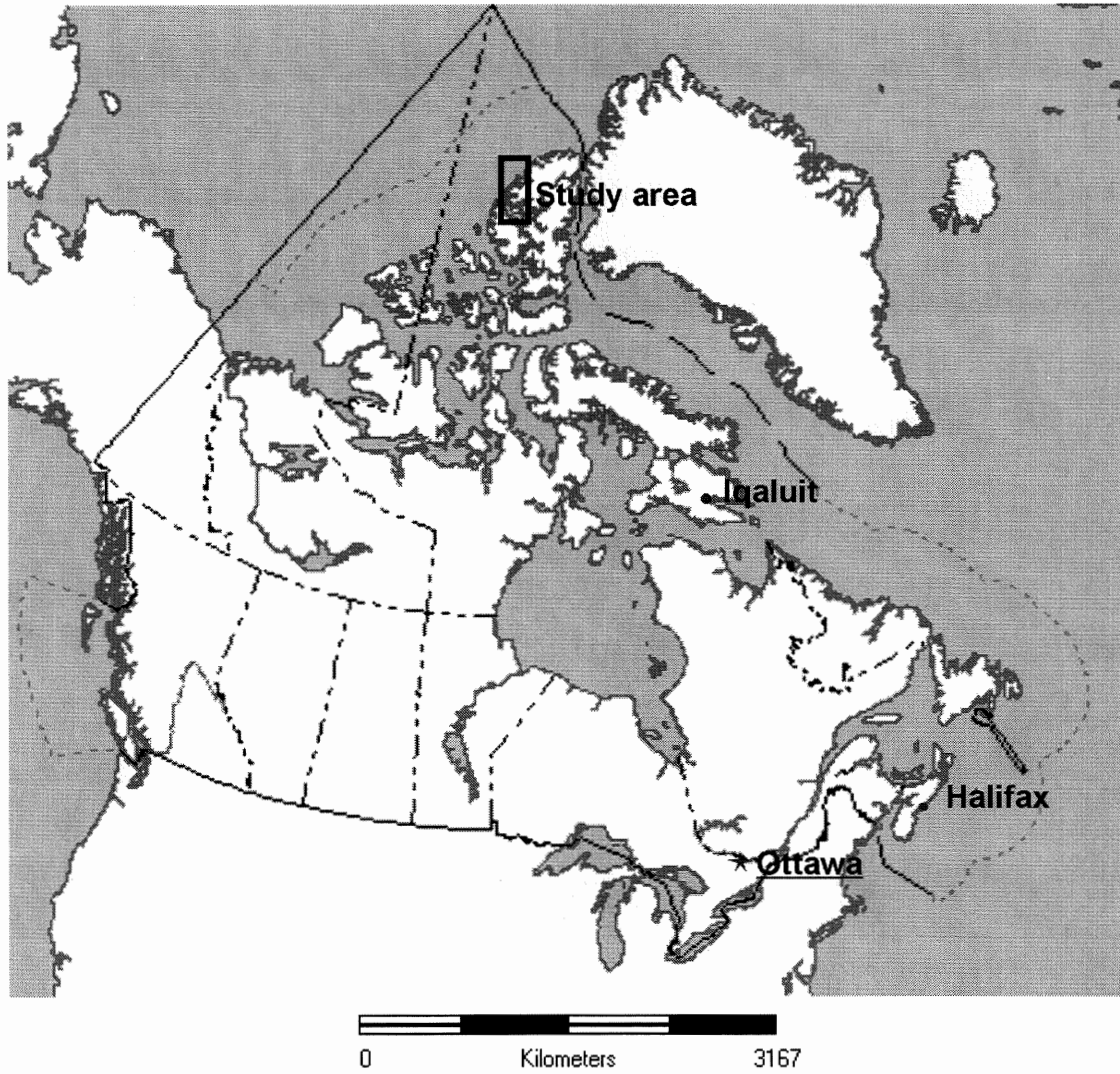
Figure 2.1: Map of Canada showing the location of the study area. Adapted from the National Atlas of Canada, 2001.
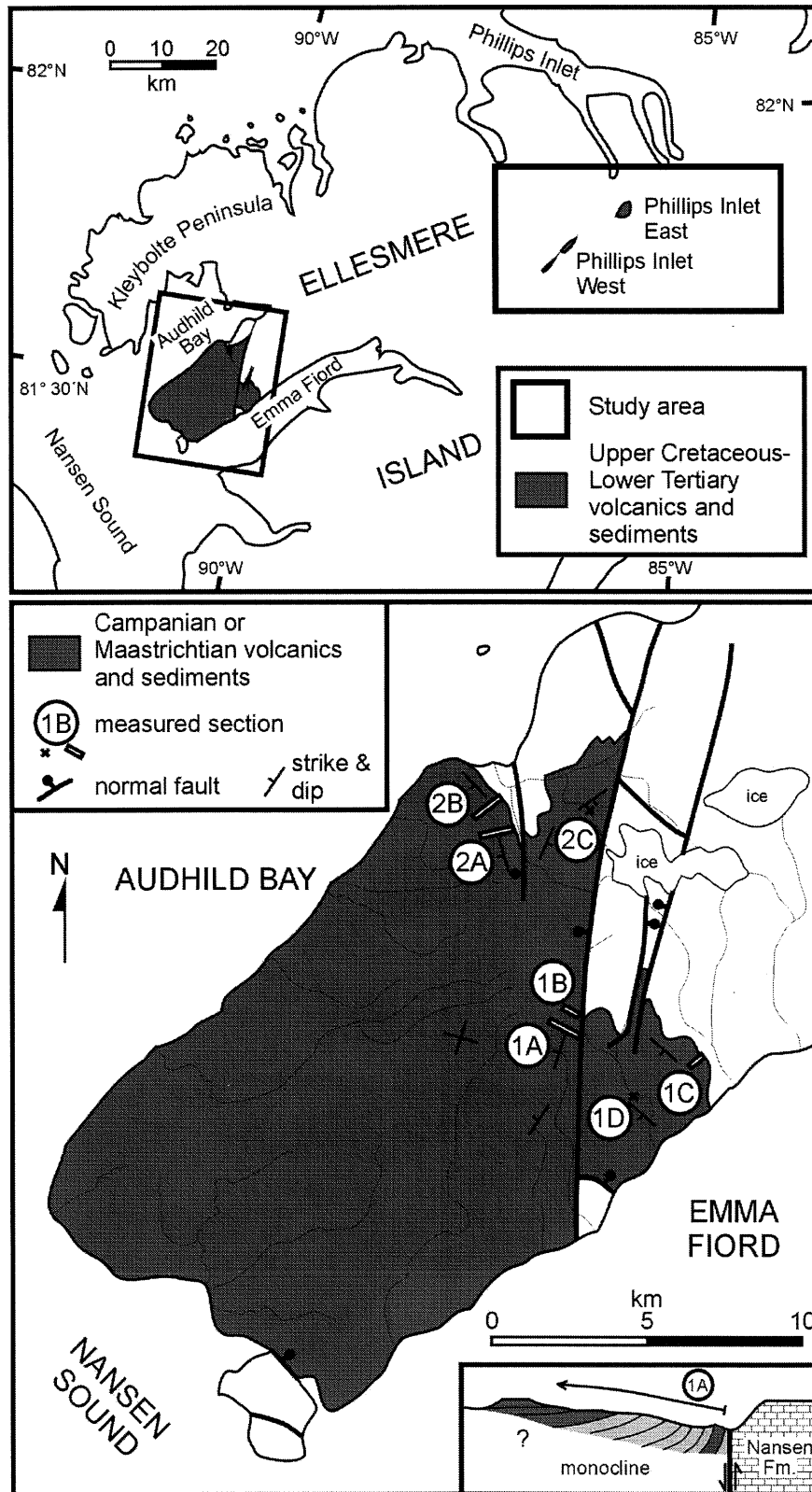
Figure 2.2: Detailed map of the study area showing faults sedimentary units and locations of the stratigraphic columns. (Graphic courtesy of R.A. MacRae)

Figure 2.3: A generalized stratigraphic column of the Eureka Sound Group and associated units showing the position of the Hanson Point Volcanics (HPV) and the position of the two fossil forest sites. (After Falcon-Lang *et al.* unpubl. subm.).

2.1.1 The Sverdrup Basin

Continental rifting of the Franklinian Mobile belt during the Early Carboniferous resulted in the formation of the Sverdrup Basin, a northeast trending basin occupying the northwestern portion of the Canadian Arctic Archipelago (Fig. 2.4) (Cameron and Muecke, 1996). Approximately 13 km thickness of sediment recording 220 million years of deposition fill the basin (Arne *et al.*, 2002). The earliest deposits consist of localized lacustrine marlstones, shales and siltstones but later progressed to marine type deposits during the Upper Carboniferous and Permian (Cameron and Muecke, 1996). A hiatus occurred near the Permian-Triassic boundary just prior to the deposition of a thick Mesozoic-Cenozoic sequence (Arne *et al.*, 2002). The 4000 m thick succession of the

11

Kanguk Formation and Eureka Sound Group records a major change in the formation of the basin during which time Sverdrup Basin was fragmented into several small, syntectonic basins over the course of 40-45 million years during the Tertiary (Ricketts and Stephenson, 1994). This fragmentation of the Sverdrup Basin corresponds with the early onset of Eurekan tectonism in the Late Cretacous/Paleocene and the formation of the Canada Basin (Arne *et al.*, 1998).
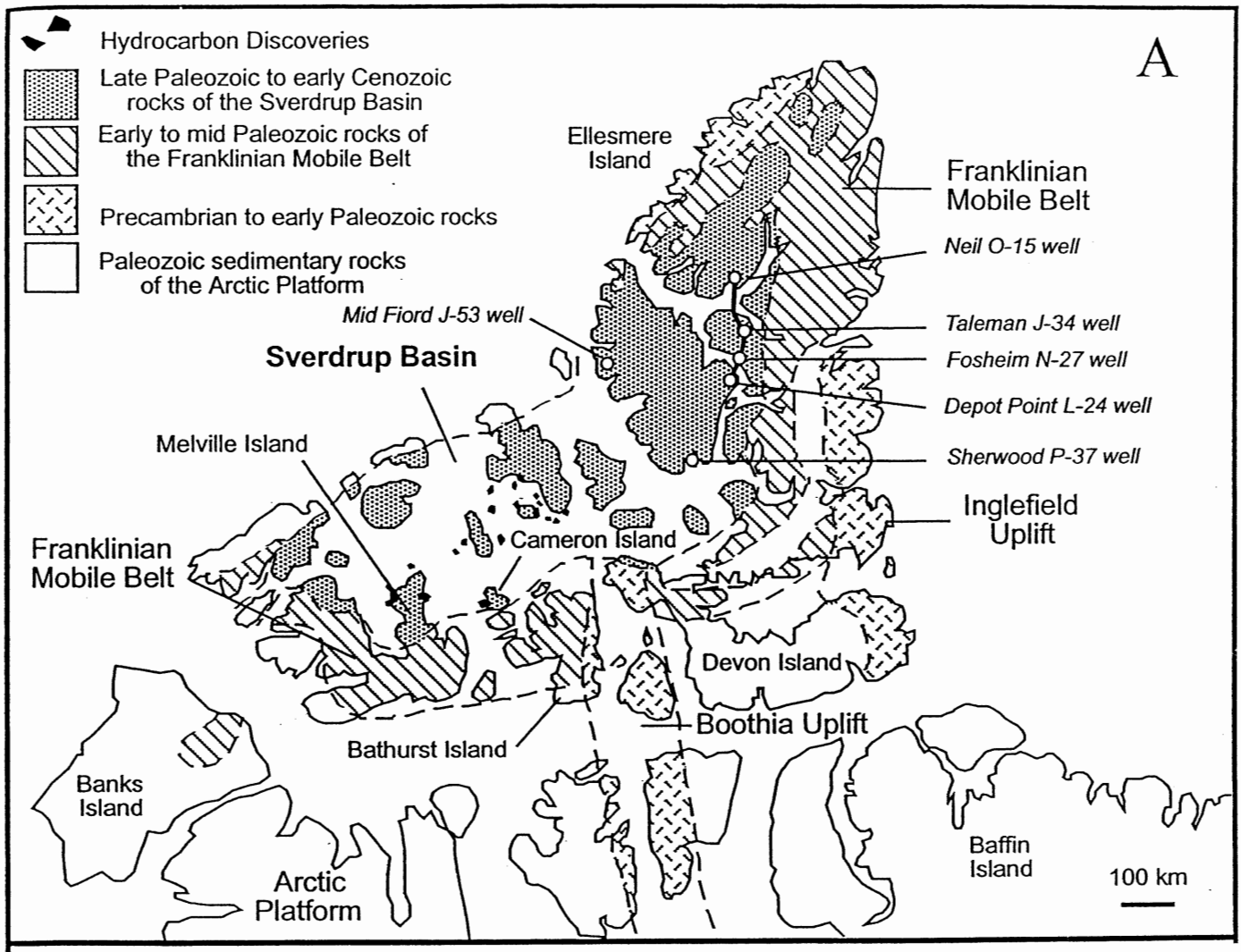
Figure 2.4: A map of the Sverdrup Basin showing all major tectonostratigraphic elements (After Arne, *et al.*, 2002).

2.1.2 The Eureka Sound Group

The Eureka Sound Group was first formally defined by Miall (1986) and consists of coal-bearing sediments Late Cretaceous to Early Tertiary in age intercalated locally with bimodal, alkali volcanic units. Numerous outcrops of the Eureka Sound Group have been studied throughout the Sverdrup Basin, many of them containing fossil plants (Fortier *et al.*, 1963; Miall, 1986). Some units in the Eureka Sound Group have been interpreted as marine units based on fossils found within the sediments, while other facies include prodelta and delta sequences which led to the interpretation by Ricketts and Stephenson, (1994) of the depositional setting as being a series of transgressive/regressive deltaic events. Work conducted by MacRae (1987, unpubl. field notes) indicates an absence of any unequivocal marine units in the study area indicating an entirely terrestrial depositional setting.

2.1.3 Sedimentology of the Emma Fiord and Phillips Inlet region

The Hansen Point Volcanics (HPV) are a poorly defined volcanic/sedimentary unit (Embry and Osadetz, 1988). Two major facies associations occur in the HPV, a bimodal volcanic suite and a poorly exposed clastic sedimentary unit containing lignite beds.

In the Emma Fiord section, sedimentary units comprise 40% of the succession and contain 5 main facies (Falcon-Lang *et al.*, unpubl. subm.) (Fig. 2.5). Two of the facies contain arkosic channel sandstones and conglomerates suggesting a fluvial setting of deposition (Falcon-Lang *et al.*, unpubl. subm.). Facies 7 consists of lignite beds containing some pyroclastics, which grade into bituminous shale. At some horizons numerous closely spaced tree trunks are found (Falcon-Lang *et al.*, unpubl. subm.). This facies was most likely deposited in a peat mire setting. Facies 9 consists of fine to course grained planar-bedded sandstone intercalated with lignite and containing abundant foliage impressions (Falcon-Lang *et al.*, unpubl. subm.). These are most likely crevasse splay deposits, the megaflora was most likely trapped in these sandstones during flood

events (Ricketts and Stephenson, 1994). Thick lignite beds associated with the sandstone suggest this was a peat mire/alluvial floodplain environment. The most likely source of sediment for these sandstone units is the intercalated volcanic units present in the group. Coeval units of the Lower Expedition Formation on Axel Heiberg Island have been interpreted as a wave-dominated, fluvio-deltaic environment containing peat mires, barrier islands, strandplains and distributary channels (Ricketts, 1991).

In the Phillips inlet section sediment is similar to the Emma Fiord section consisting of sediment with intercalated volcanics and lignite beds (MacRae, 1987, unpubl. field notes). Units in this section consist of conglomerates, channelized sandstones and bituminous shale/lignite beds. Some conglomeratic facies consists of matrix supported conglomerate with angular basaltic grains fining upwards and ending in dark grey shale beds with abundant flattened wood fragments, probably a debris flow (MacRae, 1987, unpubl. field notes). These units exist throughout the section. Other sedimentary facies consist of highly cemented medium sandstone, siltstone and mudstone beds containing siderite. These units fine upwards and contain cross beds, probably flood deposits (MacRae, 1987, unpubl. field notes). Other conglomeratic units consist of well sorted clast supported conglomerate grading into coarse to medium sandstone suggesting a well fluvial setting. Sporadic lignites suggest that the Phillips Inlet section was much better drained than the peat mire/floodplain dominated Emma Fiord. The presence of debris flows suggests that this section was near a slope perhaps deposited as fans coming down the scarps of the rift. Plant fossils were either transported from further up slope or were caught in the debris flow as it reached the floor of the rift valley.
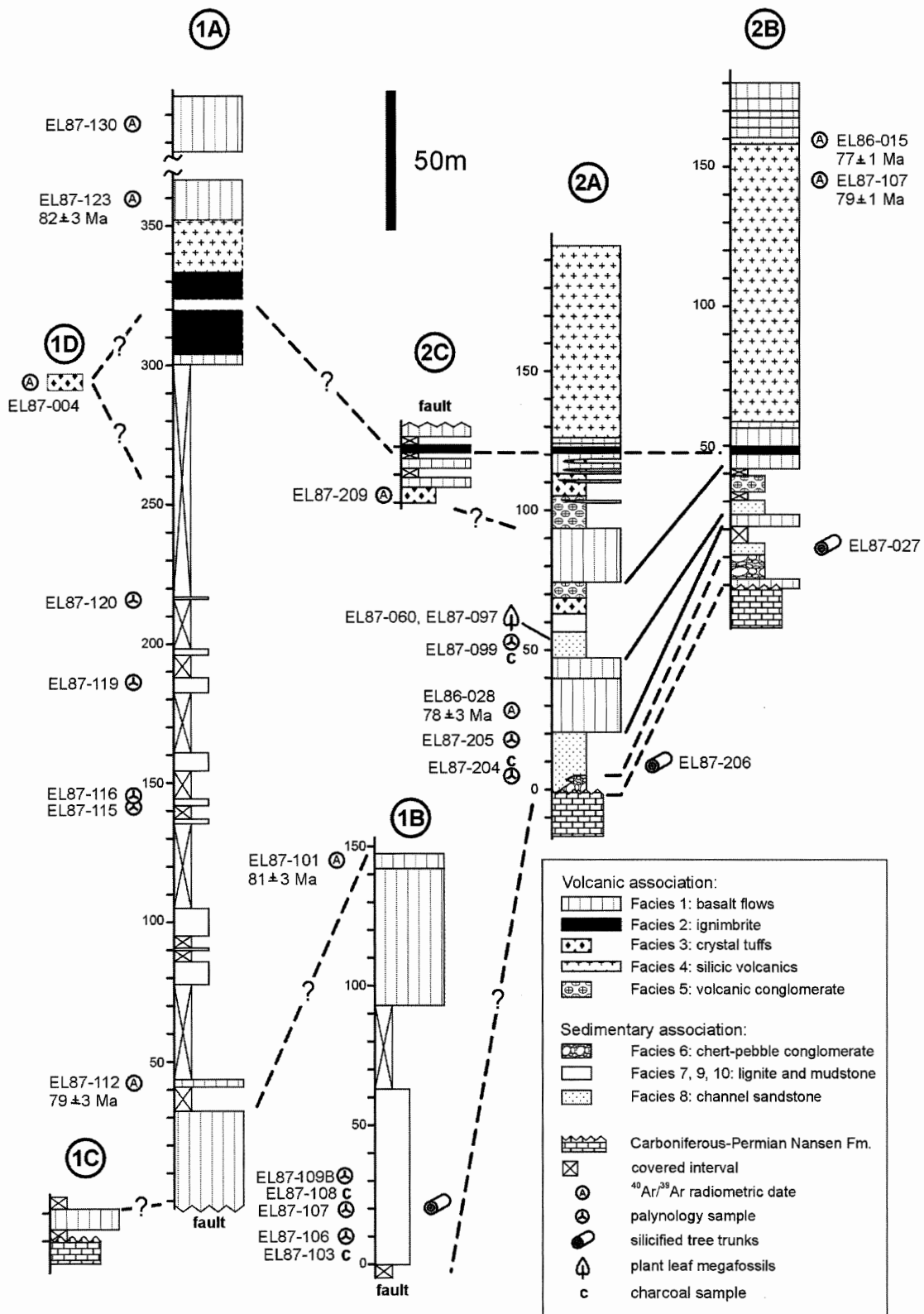
Figure 2.5: Stratigraphic column of the Emma Fiord section of the Eureka Sound Group. Shows locations of all samples. Column is correlated using the pervasive ignimbrite unit. (Graphic courtesy of R.A. MacRae).

15

2.1.4 Age constraints and palaeolatitude

The volcanic units consist of bimodal suites of alkali basalts, acidic volcanics and pyroclastics (MacRae *et al.*, 1990). The volcanic suites have yielded ^{40}Ar/^{39}Ar ages of 80 ± 2 Ma for Emma Fiord and 65 ± 3 Ma for Phillips Inlet (Muecke *et al.*, 1990). Discovery of the palynomorph *Wodehousia* at Emma Fiord, a taxon definitive of the Maastrichtian (MacRae *et al.*, 1990), by MacRae (1989 unpubl. BSc thesis) is interesting because the ^{40}Ar/^{39}Ar age of 80 ± 2 Ma would place the sediments in the Early Campanian. Further work is needed to resolve these conflicting ages, but in general, this places our the Emma Fiord samples in the Latest Campanian-Earliest Maastrichtian. There is no similar problem for the Phillips Inlet sample, however, the error on the ^{40}Ar/^{39}Ar date of 65 ± 3 Ma could place these samples in either the Latest Maastrichtian or Earliest Danian (MacRae *et al.*, 1990). Presently the fossil forests of Ellesmere Island lie between 77° and 82° N latitude but this was not always the case. The magnetic palaeopole was displaced by $6.6° \pm 1.6°$ towards northeastern Siberia in the Early Eocene. Palaeomagnetic data collected in the Eocene fossil forest localities of Axel Heiberg Island and Ellesmere Island indicate a palaeolatitude of 74-80° N latitude (Irving and Wynne, 1991). Wynne *et al.* (1988) provides palaeomagnetic data indicating that in the Late Cretaceous the fossil forests probably grew at between 74-79° N palaeolatitude.

2.2 Previous work on fossil forests of Ellesmere and Axel Heiberg Island

Fossil forests on Ellesmere Island have been known since 1883 when they were found by Brainard, a member of the ill-fated Greely expedition, and mentioned in Greely's report in 1886 (Fortier *et al.*, 1963). The next expedition to make mention of fossil forests was the GSC sponsored Operation Franklin, carried out in 1955 and spanning some 200,000 square miles of the Canadian Arctic Archipelago (Fortier *et al.*, 1963). The report contained numerous mentions of fossil plant material extending from the Triassic to the Early Tertiary. Other than a report describing some of the fossil wood by Bannon and Fry (1957) none of these data were published in anything other than a GSC Memoir (Fortier *et al.*, 1963). In the 1980's some work was done examining the

potential of the Eureka Sound Group as a petroleum reservoir. These studies resulted in several advances in the sedimentological knowledge of the area, such as the recognition of the Eureka Sound Group as a valid designation (Miall, 1986; Ricketts and Stephenson, 1994). Petroleum research in the Sverdrup Basin recently has concentrated on the offshore units since they hold the currently recognised reservoirs in the Canadian Arctic (Chen *et al.*, 2000). Fossil forests in the Canadian Arctic were back in the spotlight in 1991 when a group of scientists interested in global change and Greenhouse worlds traveled to Axel Heiberg Island to study an Eocene fossil forest site located in the Geodetic Hills. This study was a comprehensive analysis of all aspects of this fossil forest site from the geology to the biology, and was the first time a comprehensive study had been conducted on the fossil forests of the Canadian Arctic (Christie and McMillan, 1991). Studies of this fossil forest site are ongoing with new geochemical research on oxygen isotopes obtained from the wood revealing the complex polar weather patterns of the Eocene (Jahren and Sternberg, 2002). Also studies by Francis (1988) examined some of the fossil woods from Ellesmere Island. Palynological studies of Emma Fiord were carried out by MacRae (1989 unpubl. BSc. thesis) as well as a stratigraphic description of the units around Emma Fiord. Some minor research has been conducted on vertebrate fossils from the Eureka Sound Group (Dawson, 2001; Tarduno *et al.*, 1998). There remains enormous potential for more research to be carried out in stratigraphy, tectonics and especially palaeontology to fully understand the unique polar forest ecosystem of Ellesmere Island and the Canadian Arctic. Hopefully interest and concern over current global change may encourage more projects such as this one.

3. Wood taxonomy

3.1 Study Material

This chapter will deal with the identification of five fossilized wood specimens collected from two locations on Northwestern Ellesmere Island in the Canadian Arctic (81° 30' N, 90° 00' W). Samples EL87-027 and EL87-206 were collected from the peninsula between Emma Fiord and Auldhild Bay (Fig. 2.2) and lie stratigraphically in the Late Cretaceous Hansen Point Volcanics of the Eureka Sound Group. Volcanics bracketing the sediments have been $^{40}Ar/^{39}Ar$ dated at 80 ± 2 Ma or Early Campanian in age (Muecke *et al.*, 1990). Samples EL87-257, EL87-268 and Phillips-86 come from Phillips inlet located on the north coast of Ellesmere Island and lie stratigraphically in the Eureka Sound Group. Volcanics from this location have been dated at 65 ± 3 Ma or Late Maastrichtian-Early Danian (Muecke *et al.*, 1990).

3.2 Introduction to wood anatomy

To give the reader an understanding of the fossil wood descriptions which follow in Section 3.4, a brief guide to certain key features is first needed. There are two basic wood types: conifer wood and angiosperm wood.

3.2.1 Conifer wood

The greater part of conifer wood (softwood) consists of tracheids, vertically arranged lignified cells. These conduct water and nutrients from the roots of the tree to the top as well as well as acting as mechanical supporting tissue (Jane, 1970). Tracheids of the early wood (wood formed in the spring in temperate climates) are often of relatively large diameter with thin cell walls. As they grow radially they retain their tangential size and so form fairly regular files of cells (Jane, 1970). Towards the end of the growth increment tracheids are smaller with thick walls and often have a flattened

appearance; this is known as latewood (wood formed in the fall in temperate climates). Inside the tracheids are features known as bordered pits, small circular doughnut-shaped pits with apertures used to transport water and nutrients around the circumference of the tree. Bordered pits can be uniseriate, one row of pits, biseriate, two rows, or triseriate, three rows (Fig. 3.1). When they are multiseriate (more than one row) they can be oppositely (pits side by side) or adjacently (alternating pits) arranged (Fig. 3.2). Bordered pits usually only occur in the radial section of the trunk although some genera like the *Picea* (spruces) have bordered pits occurring in the tangential tracheid walls (Greguss, 1955).

Running radially through the trunk are features known as rays, which transport sugars from the centre of the tree out towards the edge of the trunk. The rays can be seen running horizontally in thin section cutting across the tracheids. Where the rays and the tracheids intersect we find what are known as cross-field pits, used to transfer water and sugars from the tracheids to the rays. Cross-field pits form different apertures specific to certain families of tree giving us a clue to the identity of a particular tree. Figure 3.3 shows some of the different types of cross-field pits. Viewed in a tangential orientation, rays can be uniseriate (one row of cells), biseriate (two rows of cells), or fusiform (containing a horizontal resin duct) (Fig 3.4). Normal resin ducts are only present in members of the Pinaceae Family. Resin ducts are large cylindrical tubes lined by a layer of cells known as epithelial cells and exist to transport and store resin (sap); this is why Pinaceous conifers are also known as resinous conifers. There are two types of resin duct; horizontal resin ducts run radially through the tree and axial resin ducts run vertically; both types are not always found in the same tree. Conifers that are not part of the Pinaceae Family may form what are known as traumatic resin ducts that form when the tree is stressed. Compression wood checks, or spiral thickenings form mostly in wood growing under the influence of gravity, such as in branches or trees growing on an angle (Creber, 1975). Compression wood checks also occur in two wood genera regardless of gravity effects. These genera are *Tsuga* (yew) and *Pseudotsuga* (Douglas fir) (Jane, 1970). Figure 3.5 details some of the anatomical features present in softwood.
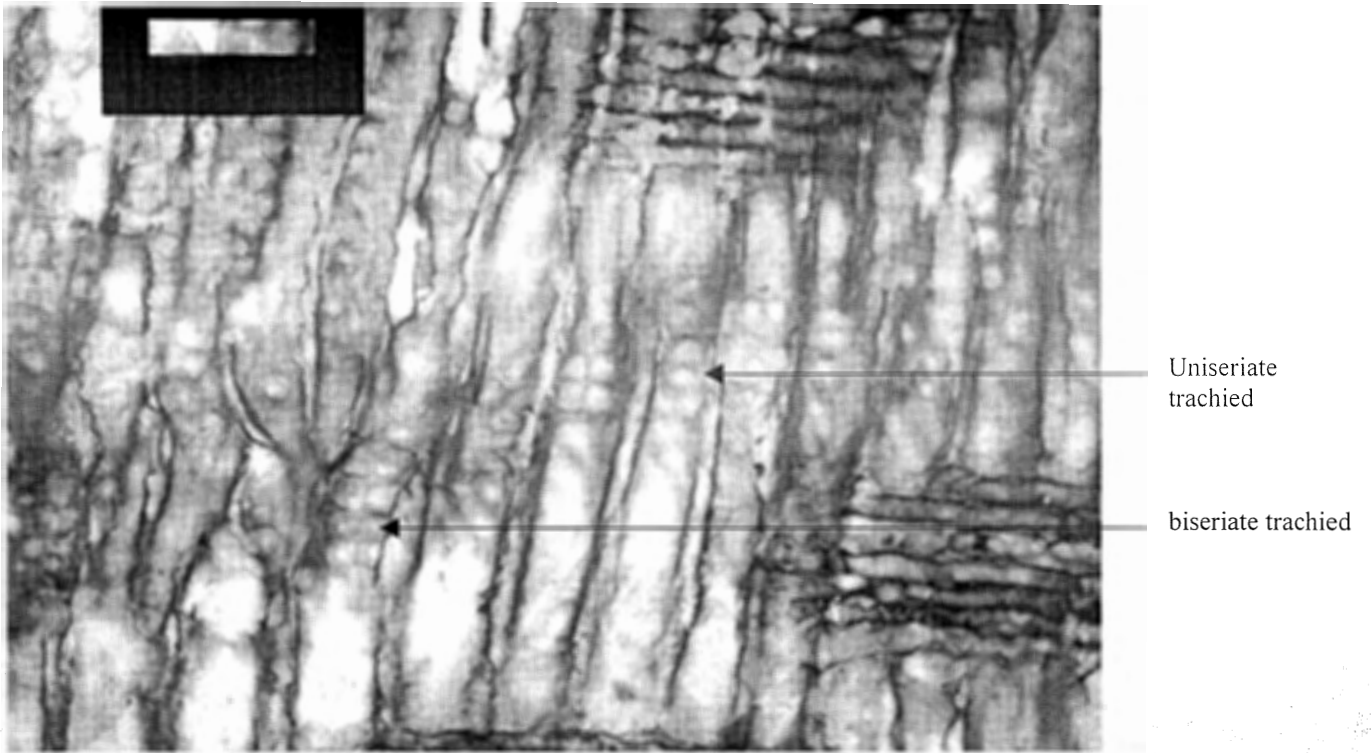
Figure 3.1: Two of the three types of bordered pitting are shown in this figure from sample Phillips-86. Scale bar (edge to edge) represents 100 μm.
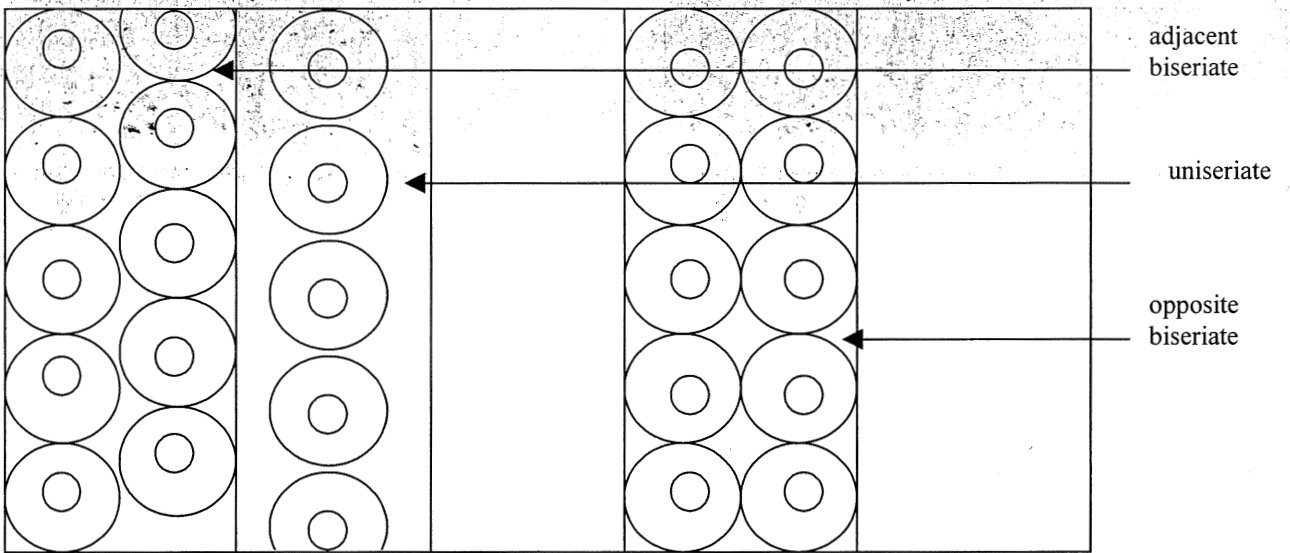
Figure 3.2: Shows the different ways in which multiseriate pits can be arranged.

20

taxodioid

cupressoid

piceoid
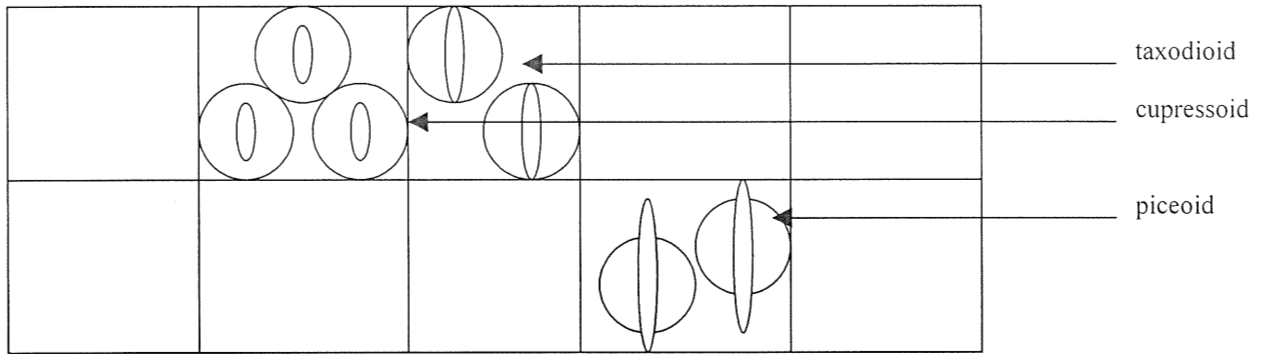
Figure 3.3: Cartoon showing the different types of cross-field pits present in the samples.

Figure 3.4: shows the various types of rays present in a sample. (EL87-257) Scale bar represents 100 μm.

3.2.2 Angiosperm wood

Angiosperm wood (hardwood) is considerably more complex than softwood. There is relatively little variation in general structure between various conifer woods, however, the same cannot be said for angiosperm wood (Jane, 1970). Hardwood consists of four or five different major elements known as the vessel element, parenchyma cell, libriform fibre, tracheid and the fibre-tracheid (Jane, 1970). Hardwood tracheids like those in softwoods conduct water and act as supporting tissue, although in hardwoods their primary purpose is mechanical support. Tracheids contain small, sparse bordered pits and unlike softwood tracheids hardwood tracheids do not arrange themselves in regular files.

One of the most distinctive features of hardwood is the presence of vessel elements whose sole purpose is water conduction. Vessel elements appear as rather large cylindrical cells. Tangentially there are different types of ray forms present in hardwoods some have exclusively uniseriate rays while other have large fusiform multiseriate aggregate rays which act like lateral vessel members (Jane, 1970). Libriform fibres are elongated tracheid like cells which serve as the main supporting tissue in hardwoods with the assistance of the fibre-tracheids. In hardwood the axial elements show considerable variation and thus in describing hardwoods, attention is paid to the vessel elements (distribution and shape), the tracheids (bordered pits), the fibres and the parenchyma. Figure 3.6 illustrates some of the features found in hardwoods.

3.3 Methods

To identify wood specimens, wood anatomy must be viewed in three directions (Fig. 3.7). Standard petrographic thin sections (30 µm thick) were prepared for each fossil wood specimen. Transverse thin-sections (TS), cut horizontally across the trunk; radial thin sections (RLS) cut vertically through the centre of the trunk and tangential thin sections (TLS) cut vertically along the edge of the trunk were prepared (Fig. 3.8). Each of these planes provides specific information about the wood type. All my wood specimens
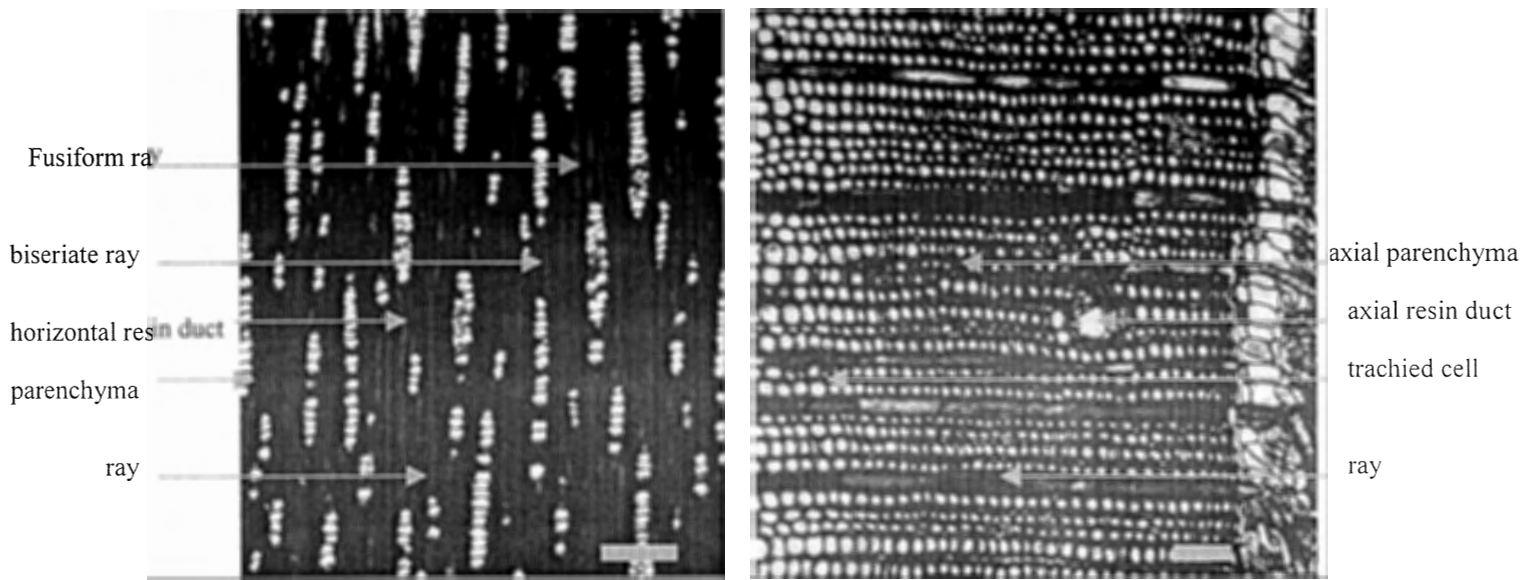
Figure 3.5: Some of the anatomical features present in softwood. Sample EL87-027, tangential thin section on the right, transverse thin section on the left. Scale bars each represent 100 μm.
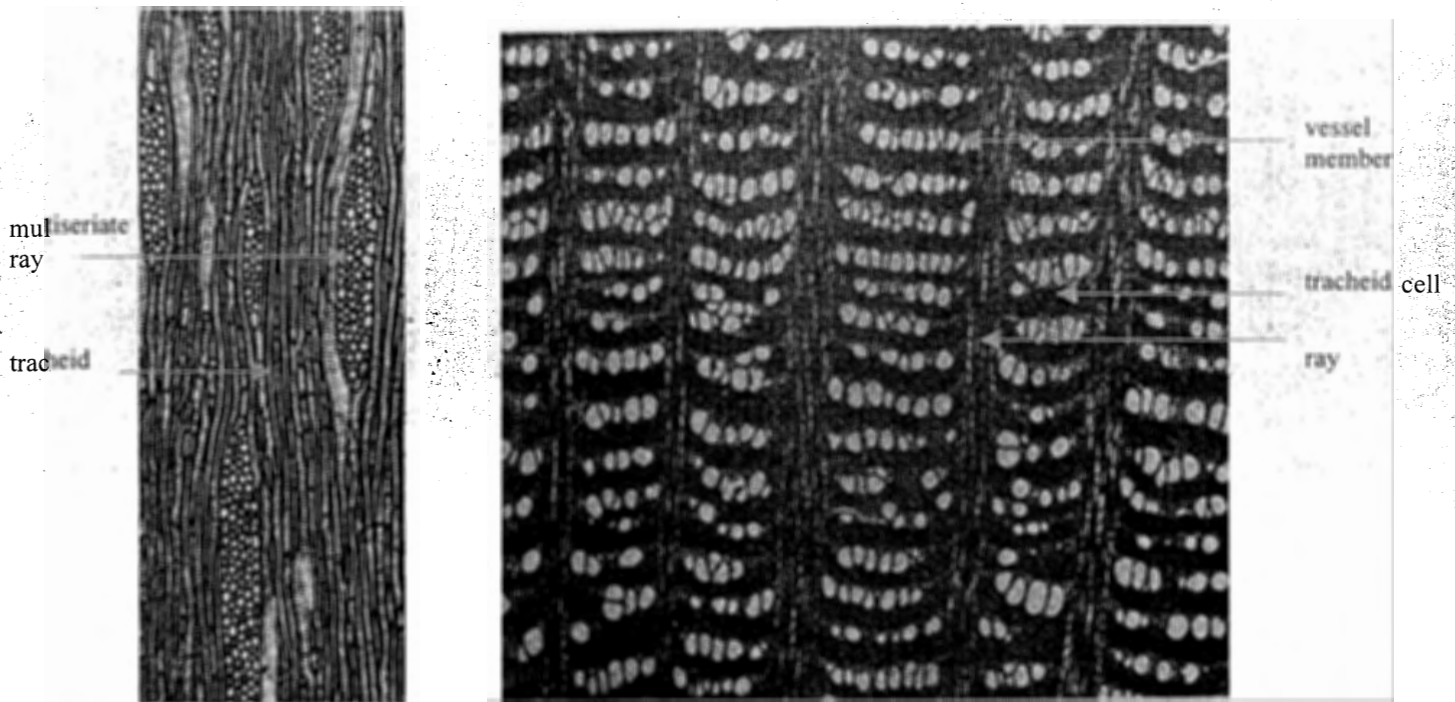
Figure 3.6: Details some of the features present in angiosperm wood. On left TLS (170X) of *Ilex aquifolium* (holly) showing the large multiseriate rays present in some angiosperm wood. On right TS (16X) of *Orites excelsa* (southern silky oak) showing vessels and their arrangement in between large rays (after Jane, 1970).

23

were coniferous, therefore, only those features present in conifer wood needed to be analyzed.

In TS the growth rings are visible as well as features such as false rings, axial parenchyma, axial resin ducts, ray and tracheid cells. Ray lengths were measured for ten rays then averaged and ray cell lengths were measured in each of the ten rays to give an average ray cell length for the sample. Where present the diameter of the axial resin ducts was measured as well as the density of the resin ducts and the diameter and number of epithelial cells.

In RLS one can see the tracheid cells running longitudinally in the thin-section. One hundred tracheids were analyzed as to whether they possesed uniseriate or multiseriate; opposite or adjacent bordered pitting. Contiguity (the number of adjoining bordered pits) was measured as the number of connecting pits. Also in RLS widths of bordered pits were measured and one hundred cross-fields were measured to determine the types of cross-field pitting was present as well as the number of cross-field pits present in each cross-field.

In TLS we are able to see the rays as stacks of cells. One hundred rays were measured to determine what percentage was uniseriate, multiseriate or fusiform. Ray height, measured in number of cells high, and the width and height of the individual ray cells was also measured. The number of rays over a 2 mm distance in TLS was measured to provide a number for how many rays per linear mm there were in each sample. If present, horizontal resin ducts were measured as well as the epithelial cell diameter.

For this project I have adopted the mostly quantitative method of analysis used by Falcon-Lang and Cantrill (2000). The reason for this is the more precise nature of the analysis needed. There is little variation in wood anatomy at the family level and small differences that only evidence themselves in a quantitative study are needed to differentiate between genera. Also anatomy varies in a single tree from the base of the trunk to the top and a quantitative analysis is needed to determine what variations are genuine generic differences (Falcon-Lang and Cantrill, 2000).

Some problems encountered in the analysis were that some samples had been folded as they were buried resulting in both tangential and radial planes being present on

24
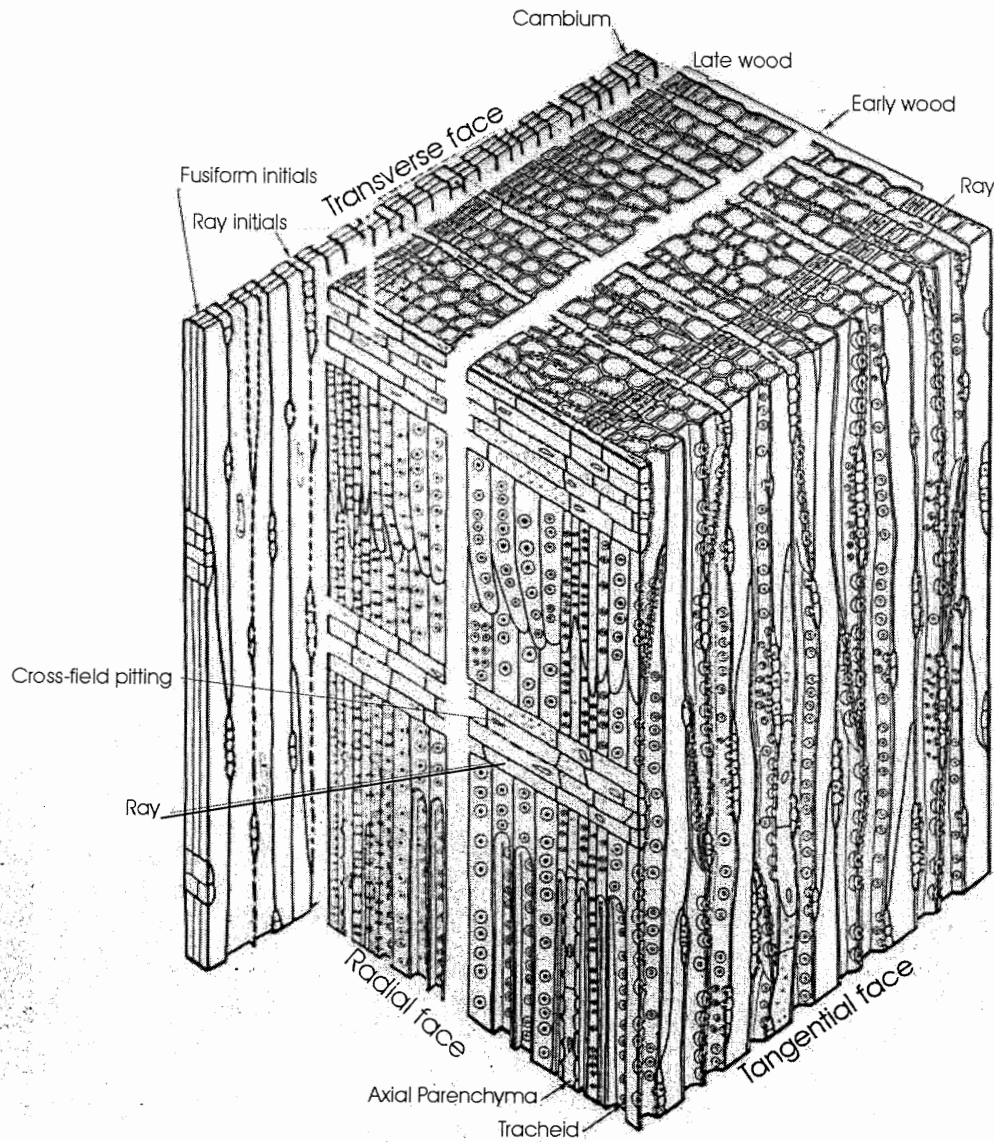
Secondary Xylem

Figure 3.7. Block diagram of the cambium and secondary xylem of *Thuja occidentalis*. Example of conifer wood. This figure shows the different faces along which thin sections are cut for analysis. This figure also shows some of the features to look for on each face. (Adapted from Meylan, 1972).
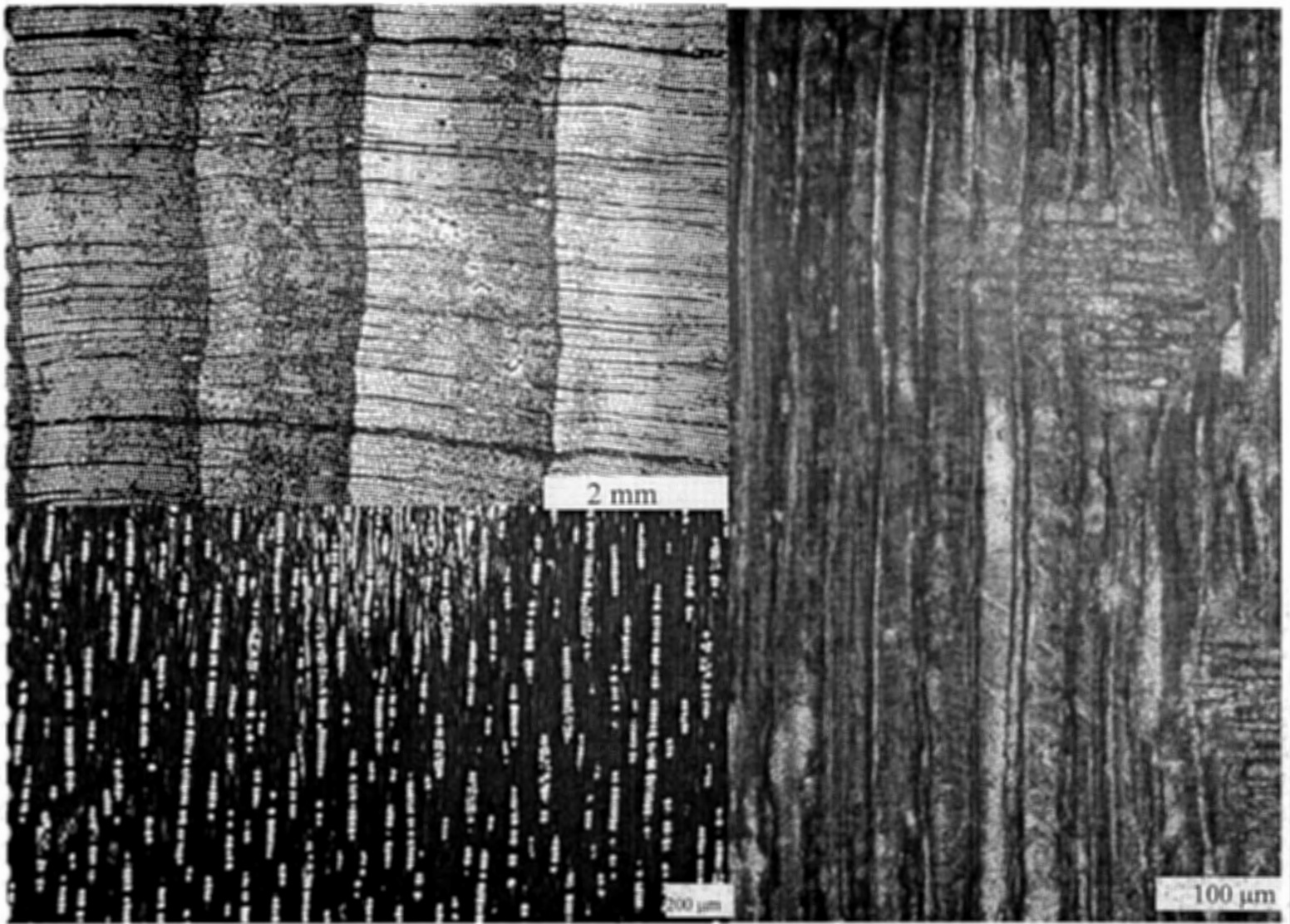
Figure 3.8: Shows the three different planes in thin-section. Transverse (top left) EL87-027 shows growth rings, axial resin ducts, rays and axial parenchyma. Tangential (bottom left) EL87-027 shows stacked rays and horizontal resin ducts. Radial (right) EL87-257 shows wood checks bordered pits and cross-fields.

the same slide. Also one sample was not very well preserved which made it difficult to observe certain features, such as the small cross-field pits.

3.4 Description of fossil wood anatomy

3.4.1 EL87-027

In RLS, tracheids show uniseriate (48 % measured in early-wood (EW); 58.25 % measured in the late-wood (LW)), biseriate (22 % EW; 0 % LW) and triseriate (3 % EW; 0 % LW) bordered pits. Pits are circular with circular apertures, diameters of 18.62 μm, and almost always touching (97 %) or rarely more than one pit apart (3 %). Multiseriate pits are almost always arranged oppositely (96%) and almost never alternately (4 %). In TLS tracheid walls show rare uniseriate pits that when present are never touching. Rays are 1.94 mm long and are composed of 63.84 μm long parenchymatous cells with thin, pitted horizontal cell walls, cells are 15.96 μm wide and 21.28 μm high. Cross-field pitting is cupressoid, piceoid or taxodioid, and consists of 1-4 alternately arranged circular pits per field. In TLS, rays are uniseriate (77.67 %) or biseriate (14.56 %), 2-35 cells high and spaced 14 rays/ linear mm. Fusiform rays (7.77 %) contain horizontal resin ducts (23.94 μm high and 23.94 μm wide) are present ringed by 8-14 4.25 μm thick epithelial cells. Horizontal resin ducts are randomly distributed with about 1 duct per mm^2. Pyrite crystals are present in some tracheids as well as spiral thickening of the tracheids. In TS rare axial resin ducts (42.56 μm long and 47.88 μm wide) are present ringed by 8-12 7.98 μm thick epithelial cells. Axial resin ducts seem to be distributed in the centre of growth rings and are distributed with about 0.3 ducts per mm^2, on average. Axial parenchyma is common, with pitted transverse walls. Bordered pits are present inside the transverse rays as well as contained within some axial parenchyma. False rings are present in some growth rings. In TS the specimen contains bark which consists of concave growing layers of cells. Bark cells are 18.62-26.6 μm in diameter for the early

bark and 5.32 μm in diameter for the late bark. In hand sample the bark is 1.5 cm thick and shows a jagged triangular pattern consistent with its formation on a growing tree. The trunk shows distinct growth rings in hand sample and has a radius of 7.25 cm (Table 3.1; Plate I).

3.4.2 EL87-206

In RLS tracheids are uniseriate (42.24 %) and biseriate (34.48 %) as well as rare triseriate (4.31 %) bordered pits. Pits are circular with circular apertures and always touching, or never more than one pit space apart. Where multiseriate pits are present they are almost exclusively arranged oppositely (95.83 %) and rarely are they alternately arranged (4.17 %). Rays are 1.25 mm long and are composed of parenchymatous cells, 63.84 μm long, 12.24 μm high and 10.64 μm wide with thin horizontal cell walls. Cross-field pitting is taxodioid consisting of 1-3 pits in each field arranged oppositely (difficult to discern because of poor preservation). In TLS tracheid walls are blank. Rays are almost exclusively uniseriate (87.38 %), or rarely biseriate (12.62 %), and 2-40 cells high spaced 14 rays/linear mm horizontally. In TS traumatic parenchyma, frost rings and false rings are present at regular intervals usually positioned in the ring shortly after the first appearance of the early wood. Rare axial parenchyma is present as well as spiral thickening on some trachieds. It was difficult to analyze some of the features of this sample because of poor preservation. In hand sample growth rings are visible and the trunk has a radius of 12 cm (Table 3.1; Plate II).

3.4.3 EL87-257

In RLS tracheids showed uniseriate (31.34 %), biseriate (52.24 %) or triseriate (2.24 %) bordered pitting. Pits are circular and almost always touching (98 %) (rarely spaced more than 1 pit apart (2 %). Multiseriate pits are oppositely arranged (98 %) or rarely alternately arranged (2 %). Cross-field pitting is piceoid and taxodioid consisting of 1-4 alternately arranged, where more than two, circular pits per field. Bordered pits are spherical and 15.96 μm in diameter. Rays are 2.39 mm long and have thick walled

parenchymatous cells 79.8 μm long, 10.64 μm high, 15.96 μm wide. In TLS trachied walls are blank. TLS, rays are predominantly uniseriate (75.20 %) with rare biseriate rays (16.80 %) and 4-37 cells high spaced with 16.1 rays/mm. Fusiform rays (8 %) contain horizontal resin ducts, 37.24 μm high and 34.58 μm wide, with a ring of 6-12, 7.98 μm in diameter epithelial cells. This specimen showed spiral thickening of some of the tracheids. In TS (111.7 μm wide, 95.76 μm high) axial resin ducts ringed by 12-15 (21.28 μm long, 26.6 μm wide) epithelial cells are observed in this sample. Axial resin ducts are distributed at the zone of transition between early wood and late wood and in that area are distributed at a density of 1-2 per mm^2. The permineralizing material is calcite. This sample exhibited alternating RLS/TLS sections (i.e was buckled) which made some features harder to identify. Compression wood checks are present in the sample. In hand sample the specimen shows distinct growth rings and has a radius of 11 cm. No bark is present on this sample (Table 3.1; Plate III).

3.4.4 EL87-268

In RLS tracheids exhibit uniseriate (30.82 % LW; 44.53 % EW) or biseriate (52.05 % LW; 3.65 % EW) bordered pitting. Pits are circular with circular apertures with a diameter of 18.62 μm and are almost always touching (98 %) or rarely more than one pit space apart (2 %). Multiseriate pits are oppositely arranged (100 %). Rays are 2.01 mm long and have thick walled parenchymatous cells 85.12 μm long, 13.3 μm wide and 15.96 μm high. Cross-field pitting is piceoid and taxodioid consisting of 1-4 alternately arranged, where more than two, or oppositely arranged, where less than two, circular pits. In TLS, trachied walls are blank and rays are predominantly uniseriate with rare biseriate rays (13.64 %). Rays are 3-23 cells high spaced 16.9 rays/linear mm. Fusiform rays (18.18 %) contained horizontal resin ducts, 42.56 μm by 39.9 μm in diameter, with a ring of 6-8, 6.92 μm thick epithelial cells. Horizontal resin ducts tend to appear in groups of 2-3 side by side. In TS 85.12 μm by 79.8 μm diameter axial resin ducts are present ringed by 10-14 18.62 μm thick, 21.28 μm wide epithelial cells. Axial resin ducts are randomly distributed with 3-4 ducts per mm^2. The permineralizing material is calcite. This sample

also showed alternating RLS/TLS. Compression wood checks are present. The hand samples, although fragmented shows distinct growth rings and includes a branch sample with a diameter of 6 cm. The trunk section has a radius of 10 cm (Table 3.1; Plate IV).

3.4.5 86-Phillips

In RLS, tracheids exhibit uniseriate (30 %), biseriate (51.33 %) or triseriate (2 %) bordered pitting. Pits are circular with a diameter of 17.56 µm and are always touching, or never more than one pit space apart. Where there are multiseriate pits they are oppositely arranged (99 %) or very rarely alternately arranged. TLS tracheid walls are blank. Rays are 1.59 mm long and are composed of parenchymous cells 53.2 µm long, 21.28 µm wide, 15.96 µm high with thick horizontal cell walls. Cross-field pitting is piceoid and taxodioid with 1-4, oppositely arranged circular pits per field. In TLS, rays are normally uniseriate (55.70 %) and sometimes biseriate (27.52 %) and are 3-29 cells high spaced 20rays/mm horizontally. Fusiform rays (16.78 %) contained horizontal resin ducts 37.24 µm high and 42.57 µm wide surrounded by 7-12 10.64 µm thick epithelial cells. Compression wood checks were present in TLS. In TS axial parenchyma is present, as are 101.1 µm by 106.4 µm diameter axial resin ducts. The ducts are ringed by 8-10 epithelial cells with diameters of 21.28 µm. Some traumatic parenchyma is present between growth rings. In hand sample rings are visible, however, there was no piece large enough to obtain a trunk radius from (Table 3.1; Plate V).

3.5 Identification of form taxa

3.5.1 *Piceoxylon ellesmerensis* Falcon-Lang, MacRae and Csank,   (unpubl. subm.)

Holotype: EL87-027

Specimens: no other samples

Plate: I

Etymology: after Ellesmere Island, the sample's locality

Taxon		Piceoxylon		Taxodioxylon	Pinuxylon sp. 1			Pinuxylon sp. 2
Slide		EL87-027(EW)	EL87-027(LW)	EL87-206	EL87-257	EL87-268(EW)	EL87-268(LW)	86-Phillips
Uniseriate	number (%)	47 (44.76)	60 (58.25)	49 (42.24)	42 (31.34)	45 (30.82)	61 (44.53)	45 (30.00)
Biseriate	number (%)	43 (40.95)	0 (0)	40 (34.48)	70 (52.24)	76 (52.05)	5 (3.65)	77 (51.33)
Triseriate	number (%)	15 (14.28)	0 (0)	5 (4.31)	3 (2.24)	0 (0)	0 (0)	3 (2.00)
Blank	number (%)	27 (27)	43 (41.75)	22 (18.97)	19 (14.18)	25 (17.12)	71 (51.82)	25 (16.67)
Alternate	number (%)	4 (4)	N/A	2 (4.17)	2 (2)	0 (0)	0 (0)	1 (1)
Opposite	number (%)	96 (96)	N/A	46 (95.83)	98 (98)	100 (100)	5 (100)	99 (99)
Contiguous Chains of: (Mode)		1-11 pits (8)	1-8 pits (7)	1-10 pits (8)	1-9 pits (5)	2-8 pits (4)	2-8 pits (4)	2-8 pits (5)
Cross-field pit type		Piceoid, Cupressioid and Taxodioid		Taxodioid	Piceoid and Taxodioid	Piceoid and Taxodioid		Piceoid and Taxodioid
# cross-field pits (mode)		1-4 (3)	1-4 (3)	1-3 (2)	1-4 (2)	1-4 (2)	1-4 (2)	1-4 (2)
Ray Length		1.94 mm	1.94 mm	1.25 mm	2.39 mm	2.01 mm	2.01 mm	1.59 mm
Ray Height (Mode)		2-35 cells (15)		2-40 cells (16)	4-37 cells (10)	3-23cells (8)		3-29 cells (7)
Ray Cell Height		21.28 µm		12.24 µm	10.64 µm	15.96 µm		15.96 µm
Ray Cell Width		15.96 µm		10.64 µm	15.96 µm	13.3 µm		21.28 µm
Ray Cell Length		63.84 µm		63.84 µm	79.8 µm	85.12 µm		53.2 µm
Uniseriate	number (%)	80 (77.67)		90 (87.38)	94 (75.20)	75 (75)		83 (55.70)
Biseriate	number (%)	15 (14.56)		13 (12.62)	21 (16.80)	15 (15)		41 (27.52)
Fusiform	number (%)	8 (7.77)		0 (0)	10 (8.00)	10 (10)		25 (16.78)
Number of Rays/ linear mm		14		14	16.1	16.9		20
Resin Ducts present		Axial and Horizontal		NONE	Axial and Horizontal	Axial and Horizontal		Axial and Horizontal
	Height	A: 42.56 µm H: 23.94µm		N/A	A:95.76 µm, H: 37.24 µm	A: 79.8 µm H: 42.56 µm		A:106.4 µm H: 37.24 µm
	Width	A: 47.88 µm H: 23.94µm		N/A	A: 111.7 µm H: 34.58 µm	A: 85.12 µm H: 39.9 µm		A: 101.1 µm H: 42.57 µm
# epithelial cells		A: 8-12 H: 8-14		N/A	A: 12-15 , H: 6-12	A: 10-14 H: 6-8		A: 8-10 H: 7-12
epithelial cell thickness		A: 7.98 µm H: 4.25µm		N/A	A: 26.6 µm , H: 7.98 µm	A: 18.62 µm H: 6.92 µm		A: 21.28 µm H: 10.64 µm
Tangential tracheid pitting		Uniseriate non-contiguous		NONE	NONE	NONE		NONE

(Left margin vertical labels: radial tracheid pitting; Rays; Resin ducts)

Table 3.1: Table of data for quantatative wood descreiption, summary of Section 3.2. EW=early wood, LW=late wood. Actual recorded number is outside of parentheses the number in parentheses is the percentage expresion of the actual number {e.g 80 (77.67)}. For Ray height, number of cross-field pits and contiguous chains the number in parentheses is the mode while the other numbers are the range of values measured. A=axial resin duct and H=horizontal resin duct.

Diagnosis: Contains small axial (47.88 μm) and horizontal (23.94 μm) resin ducts, spiral thickening in all tracheids and piceoid, cuppressoid, taxodioid cross-field pits. Contains bordered pits inside the transverse ray walls and in the axial parenchyma. Bordered pits were also present in the tangential tracheid walls.

Comparison: Gothan (1905) erected the genus *Piceoxylon* to describe wood with the above features and the name has been assigned to this sample based on the wood classification scheme established by Kraüsel (1949). Key characteristics of *Piceoxylon* based on Kraüsel's (1949) scheme are resin ducts with thick walled epithelial cells, bordered pits in both radial and tangential tracheid walls. *Piceoxylon* wood can be broadly placed into two categories, those with spiral thickenings and those without spiral thickenings (Roy and Hills, 1972); my sample falls into the first group. Other members of *Piceoxylon* lack horizontal resin ducts such as *Piceoxylon dongguanensis* (Chongyang *et al.*, 1996) while containing axial resin ducts. *Piceoxylon piceae* (Rossler, 1937) and *Piceoxylon beaufortense* (Roy and Hills, 1972) contain spiral thickenings only in the late wood as well as having shorter rays (2-12 cells high), no xylem parenchyma and dominantly uniseriate bordered pitting. *Piceoxylon christopheri* (Bannon and Fry, 1957) has much larger axial resin ducts (90x180 μm) and small ray heights (1-16 cells high). *Piceoxylon thomsoni* (Bannon and Fry, 1957) bears a striking similarity to our sample with its common biseriate pitting and 1-4 cross-field pits. *Piceoxylon thomsoni,* however, differs by having larger resin ducts (up to 150 μm) and shorter rays (1-16 cells high). As my specimen differs from all previously described *Piceoxylon* samples, except *Piceoxylon ellsmerensis*, I call this species by that name.

Biological affinity: The presence of axial and horizontal resin ducts with thick walled epithelial cells, piceoid and taxodioid cross-field pits and spiral thickenings show this wood to have characters of the pinaceous conifers *Picea*, *Larix* and *Pseudotsuga* (Greguss, 1955). *Piceoxylon ellesmerensis* is most similar to the modern *Picea* and *Pseudotsuga* genera as it contains spiral thickenings in all trachieds and abundant axial parenchyma features common to both genera. *Pseudotsuga* is not known in the fossil record prior to the Eocene (Obst *et al.*, 1991) *Piceoxylon ellesmerensis* lies

stratigraphicaly in the Cretaceous. The most similar Cretaceous specimen is *Piceoxylon thomsoni* (Bannon and Fry, 1957) from the Late Cretaceous (Albian) of Amund Ringnes Island also in the Canadian Arctic (Table 3.2).

3.5.2 *Taxodioxylon albertense* (Penhallow) Shimakura, 1937

Specimen: EL87-206

Plate: II

Diagnosis: Does not contain resin ducts. Cross-field pits are taxodioid. Rays are long (up to 40 cells high) and ray cells are small (12.24 μm). Bordered pitting is dominantly uniseriate. Gross trunk morphology (Sect. 4.1) shows a fluted trunk appearance indicative of buttressing common in taxodiaceous and podocarpaceous conifers (Greguss, 1955).

Comparison: The fluted growth rings, large tracheids, abundant resinous axial parenchyma, high rays and the taxodioid cross-field pits in number indicate that this sample is a typical taxodiaceous wood. Thus this fossil has been assigned to the genus *Taxodioxylon* (Kraüsel, 1949). When compared to other taxodiaceous woods our sample is identical to *Taxodioxylon albertense* (Penhallow, 1908; Shimakura, 1937; Meijer, 2000) with its high rays (1-70 cells high), small ray cells, dominantly uniseriate bordered pitting, cross-field pits which do not exceed 3 in number and a lack of traumatic resin ducts. *T. albertense* lacks the nodular trachied walls and alternate bordered pitting of *Taxodioxylon gypsaceum* (Ramanujam and Stewart, 1969) as well as having a smaller number of cross-field pits. *Taxodioxylon drumhellerense* and *Taxodioxylon antiquum* (Ramanujam and Stewart, 1969) also have a higher number of cross-field pits (2-4 and 2-5 respectively). *T. drumhellerense* has pits in the parenchymatous walls which are missing in our sample and *T. antiquum* has rays which exceed 80 cells in height (Table 3.3).

	EL87-027	*Piceoxylon dongguanensis*	*Piceoxylon beufortense*	*Piceoxylon christopheri*	*Piceoxylon thomsoni*
bordered pitting	uniseriate (44.76%) biseriate (40.95%)	biseriate	uniseriate occasionaly biseriate	uniseriate seldom biseriate	uniseriate often biseriate
cross-field pit type	piceoid, taxodioid and cupressoid	piceoid, abietinious	piceoid and taxodioid	abietinious	piceoid
Number of cross-field pits	1-4 pits	2-5 pits	4-5 pits	2-4 pits	1-4 pits
spiral thickenings	present in both early and late wood	absent	present in late wood	absent	absent
ray height	2-35 cells high	2-20 cells high	2-12 cells high	1-16 cells high	1-16 cells high
resin ducts	A: 47.88 µm H: 23.94 µm	Axial only		A: 90-180 µm H: 30-70 µm	A: 30-150 µm H: 20X50-100X180 µm
epithelial cells	A: 8-12 H: 8-14 thick walled		A: 6-8 H: thick walled epithelial cells	A: thick walled H: thick walled	A: thick walled H:thick walled
parenchyma	abundant		absent	abundant	abundant
reference	Csank, 2002	Chongyang et al., 1996	Roy and Hills, 1972	Bannon and Fry, 1957	Bannon and Fry, 1957
location	Emma Fiord, NW Ellesmere Island	China	Banks Island, Canadian Arctic	Amund Ringnes Island, Canada	Amund Ringnes Island, Canada
age	Campanian/Maastrichtian	Cretaceous	Tertiary	Late Cretaceous (Albian)	Lower Cretaceous

Table 3.2: Comparison chart for some fossil species of *Piceoxylon*. Percent abundance in parentheses. A=Axial resin duct H=horizontal resin duct. ray height expresed as a function of the number of cells high. Blank fields mean there was no available data. Note the differences between EL87-027 and all other Piceoxylon's.

	EL87-206	*Taxodioxylon albertense*	*Taxodioxylon gypsaceum*	*Taxodioxylon drumhellerense*	*Taxodioxylon multiseriatum*
bordered pitting	uniseriate (42.24%) biseriate (34.48%)	uniseriate occasionaly biseriate	mostly biseriate some uniseriate and triseriate	uniseriate occasionaly biseriate	biseriate or triseriate occasionaly uniseriate
cross-field pit type	taxodioid	taxodioid, cupressoid	taxodioid, cupressoid	taxodioid, glyptostroboid	taxodioid
number of cross-field pits	1-3 pits	1-3 pits	2-8 pits	1-2 pits	2-5 pits
ray height	2-40 cells high	6-40 cells high	2-35 cells high	biseriate 2-25 cells high	2-90 cells high mostly multiseriate
parenchyma	diffusely distributed	diffusely distributed	abundant	abundant	abundant
reference	Csank, 2002	Penhallow, 1908; Shimakura, 1937; Meijer, 2000	Kraüsel, 1949	Ramanujam and Stewart, 1968	Ramanujam and Stewart, 1968
location	Emma Fiord, NW Ellesmere Island	Southern Alberta, Northeast Belgium	Alberta, Belgium, Saskatchewan	Alberta	Alberta
age	Campanian/Maastrichtian	Late Cretaceous (Santonian)	Late Cretaceous, Tertiary	Late Cretaceous	Late Cretaceous

Table 3.3: Comparison chart for some fossil species of *Taxodioxylon*. Percent abundance in parentheses. Number of cross-field pits and ray height expressed as a range of values. Note the similarity between EL87-206 and *Taxodioxylon albertense*.

Biological affinity: This sample bears closest affinity to the modern genera of *Sequoia*, because of the high rays (upwards of 100 cells high), and *Sequoiadendron*, which has dominantly uniseriate bordered pitting even in wide tracheids (Meijer, 2000).

3.5.3 *Pinuxylon woolardii* Tidwell, Parker and Folkman, 1986
Specimens: EL87-257, EL87-268
Plates: III, IV

Diagnosis: This specimen contains piceoid and taxodioid cross-field pits. Bordered pitting is dominantly biseriate with some triseriate pitting. Large resin ducts both axial (79.8-111.7 μm) and horizontal (34.58-42.56 μm). Rays are quite long up to 2.39 mm in length.

Comparison: The sample can be identified as *Pinuxylon woolardii* (Tidwell *et al.*, 1986) Because of its large axial resin ducts (110-125 μm), 1-3 cross-field pits and grouped resin ducts (2-3). *Pinuxylon woolardii* differs from other *Pinuxylon* woods because of its higher rays and multiple cross-field pits (Tidwell *et al.*, 1986). *Pinuxylon woolardii* is most similar to *Pinuxylon parryoides* (Kraüsel, 1949). It differs in having smooth ray tracheid walls and slightly shorter rays (Tidwell *et al.*, 1986) (Table, 3.4). *Pinuxylon tarnocziense* (Greguss, 1967) has 2 sometimes 3 pits per cross-field and generally shorter rays. *Pinuxylon* cf. *P. vateri* (Platen) Rossler, (1937) differs on the basis of fewer horizontal resin ducts, lower rays, and only one or two large pits per cross-field.

Biological Affinity: According to Tidwell *et al.* (1986) five living species show features similar to *P. woolardii*. *Pinus aristata,* which differs in its low rays (7-9 cells) and few horizontal resin ducts. *Pinus monophylla* is the most similar having high rays and numerous large resin ducts arranged in two's or three's, however, *P. monophylla* has thinner walled ray parenchyma and only ever two cross-field pits which lack borders. *Pinus cembroides* has high rays (20-25 cells high), but differs in having circular ray cells.

35

Pinus edulis differs by the low rays (8-10 cells) and larger resin ducts. *Pinus balfouriana* is similar to *Pinuxylon woolardii* except for having dentate ray tracheid walls

3.5.4 *Pinuxylon* sp. 1 (not previously identified)

Holotype: Phillips-86

Specimens: no other samples

Etymology: After "Gemini", for the high number of biseriate rays which make this specimen unique.

Plate: V

Diagnosis: Has short rays (1.59 mm long) with large ray cells (21.28 μm). Rays are more abundant in tangential section than other specimens and there are more biseriate rays (16.78%). Bordered pitting is dominantly biseriate (51.33%). Trachied walls are dentate in appearance.

Comparison: This sample differs from all other *Pinuxylon* samples because of its greater number of biseriate rays in tangential section and the high number of rays present in tangential section. *Pinuxylon woolardii* (Tidwell *et al.*, 1986) differs in its lower percentage of biseriate rays. *Pinuxylon parryoides* (Kraüsel, 1949) has dentate ray tracheids, high rays and a high percentage of biseriate bordered pits, however, it lacks biseriate rays and circular axial resin ducts. As my sample differs from all previously described *Pinuxylon* samples I erect a new species, *Pinuxylon geminii* (Table 3.4).

Biological affinity: This sample shows some affinity with both *Pinus edulis* and *Pinus balfouriana* both of the *Aristata (Parryanna)* group defined by Greguss (1955). *Pinus aristata* and *Pinus balfouriana* have the closest match to my sample *P. balfouriana* especially because of occasionally high rays (up to 45 cells high), its abundance of rays and its dentate tracheid walls, however, lacking lacks the biseriate rays of my sample (Greguss, 1955).

	EL87-257	EL87-268	*Pinuxylon woolardii*	*Pinuxylon parryoides*	*Pinuxylon tarnocziense*	*Pinuxylon* cf. *vateri*	*Pinuxylon haploxyloides*
bordered pitting	biseriate (52.24%) uniseriate (31.34%)	biseriate (52.05%) uniseriate (30.82%)	Uniseriate commonly biseriate	uniseriate occasionaly biseriate	biseriate occasionaly uniseriate	uniseriate occasionaly biseriate	uniseriate occasionaly biseriate
cross-field pit type	piceoid and taxodioid	piceoid and taxodioid	pinoid	pinoid, piceoid	piceoid, pinoid	pinoid	pinoid
Number of cross-field pits	1-4 pits	1-4 pits	2-5 pits	1-3 pits	2-3 pits	1-2 pits	1
ray height	4-37 cells high	3-23 cells high	8-21 cells high	1-20 cells high	2-18 cells high	1-16 cells high	1-12 cells
rays	uniseriate rarely biseriate	uniseriate rarely biseriate	uniseriate rarely biseriate				
resin ducts	A: 111.7 µm H: 37.24 µm	A: 85.12 µm H: 42.56 µm	A: 110-125 µm H: moderate in size		A: 100-115 µm H: moderate in size		A: 70-100 µm H:
epithelial cells	A: 12-15 thin walled H: 6-12 thin walled	A: 10-14 thin walled H: 6-8 thin walled	A: 5-7 thin walled H: 5-6 thin walled	A: thin walled H: thin walled	thin walled both A and H	Thin walled both A and H	A:thin walled H: thin walled
reference	Csank, 2002	Csank, 2002	Tidwell *et al.*, 1986	Kraûsel, 1949	Greguss, 1967	Rossler, 1937	Kraûsel, 1949
location	Phillips Inlet, NW Ellesmere Island	Phillips Inlet, NW Ellesmere Island	Oregon		Hungary		
age	Latest Cretaceous/Eariest Tertiary	Latest Cretaceous/Earliest Tertiary	Miocene		Miocene		

	Phillips-86	*Pinuxylon albicauloides*	*Pinuxylon haploxyloides*	*Pinuxylon woolardii*	*Pinuxylon parryoides*	*Pinuxylon tarnocziense*	*Pinuxylon* cf. *vateri*
bordered pitting	biseriate (51.33%) uniseriate (30%)	biseriate occasionaly uniseriate	uniseriate occasionaly biseriate	Uniseriate commonly biseriate	uniseriate occasionaly biseriate	biseriate occasionaly uniseriate	uniseriate occasionaly biseriate
cross-field pit type	piceoid and taxodioid	pinoid	pinoid	pinoid	pinoid, piceoid	piceoid, pinoid	pinoid
Number of cross-field pits	1-4 pits	1-2 pits	1	2-5 pits	1-3 pits	2-3 pits	1-2 pits
ray height	3-29 cells high	3-21 cells high	1-12 cells	8-21 cells high	1-20 cells high	2-18 cells high	1-16 cells high
rays	uniseriate occasionaly biseriate			uniseriate rarely biseriate			
resin ducts	A: 106.4 µm H: 42.57 µm		A: 70-100 µm H:	A: 110-125 µm H: moderate in size		A: 100-115 µm H: moderate in size	
epithelial cells	A: 8-10 thin walled H: 7-12 thin walled	Thin walled both A and H	A:thin walled H: thin walled	A: 5-7 thin walled H: 5-6 thin walled	A: thin walled H: thin walled	thin walled both A and H	Thin walled both A and H
reference	Csank, 2002	Greguss, 1967	Kraûsel, 1949	Tidwell *et al.*, 1986	Kraûsel, 1949	Greguss, 1967	Rossler, 1937
location	Phillips Inlet, NW Ellesmere Island	Hungary		Oregon		Hungary	
age	Latest Cretaceous/Earliest Tertiary	Miocene		Miocene		Miocene	

Table 3.4: Comparison chart for some fossil *Pinuxylon* species. A=Axial resin duct H=horizontal resin duct. Blank fields represent unavailable data.

Plate I
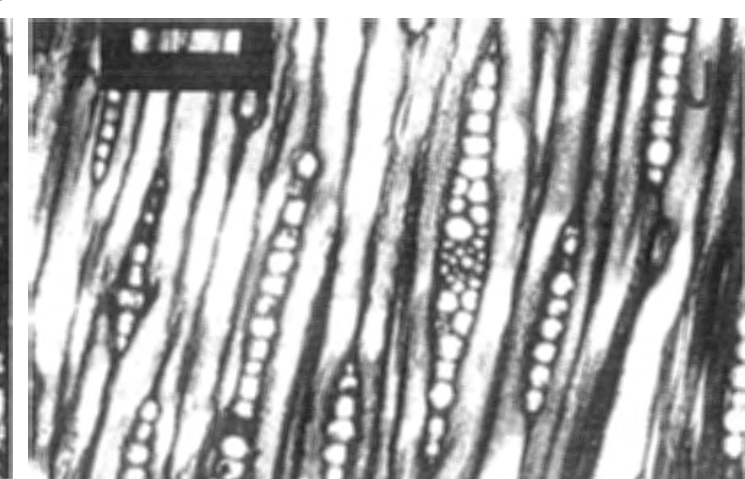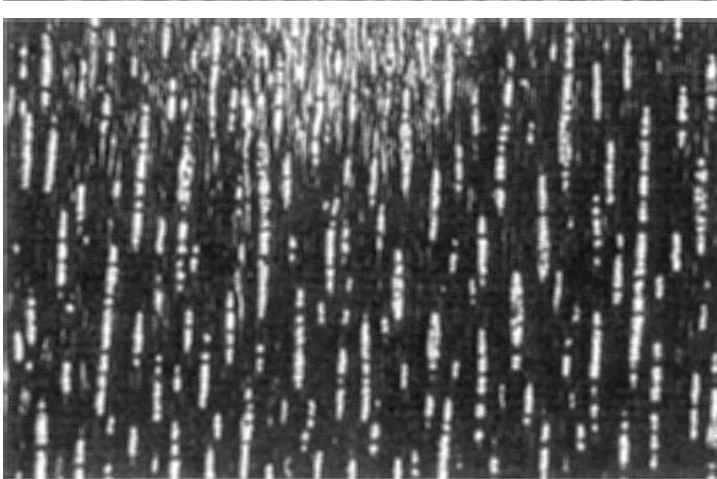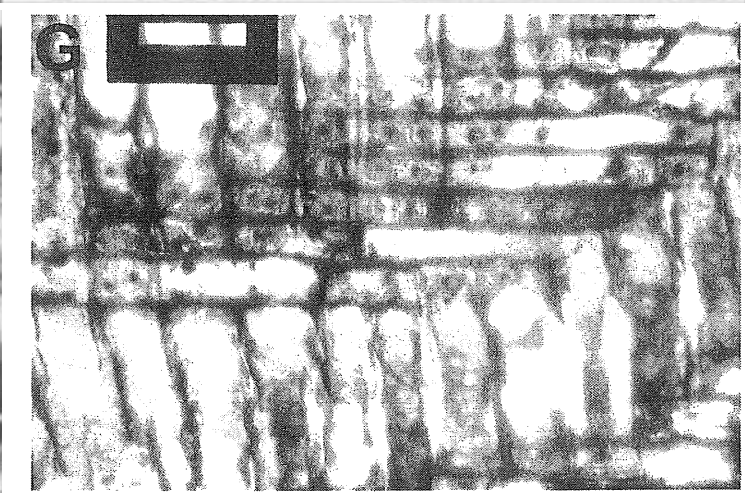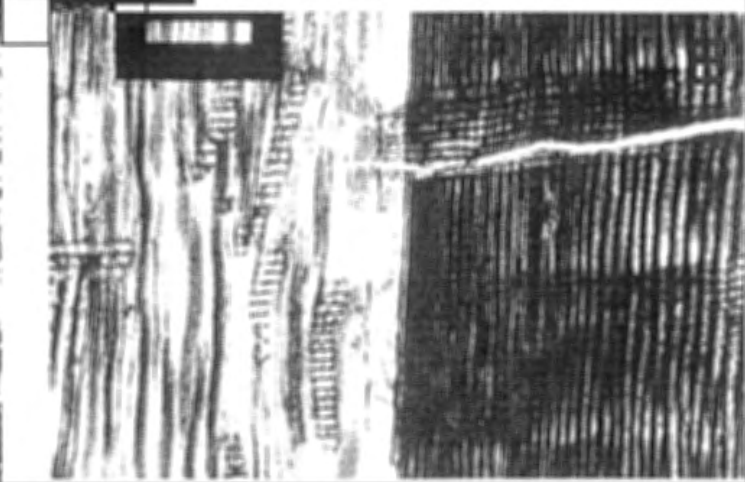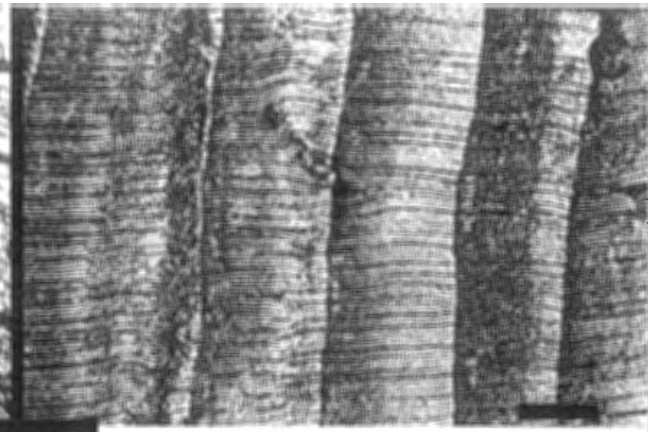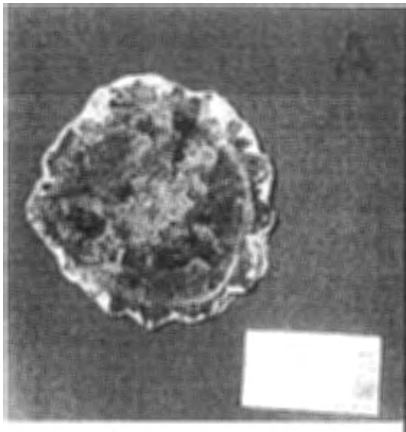
Plate I: Sample EL87-027, (*Piceoxylon ellesmerensis*). A: photograph of the trunk section showing the growth rings and the bark (scale bar = 9 cm). B: TS photomicrograph of a growth ring showing an axial resin duct (scale bar = 100 μm). C: TS wide view photomicrograph showing growth rings, a false ring is visible on the left of this picture (scale bar = 1 mm). D: TS photomicrograph of a growth ring showing the earlywood/latewood transition as well as some bordered pitting in the tangential rays (scale bar = 200 μm). E: RLS photograph showing tracheids running longitudinally, rays running horizontally and a growth ring boundary. Bordered pits are visible in this picture (scale bar = 250 μm). F: RLS showing spiral thickenings in the tracheids (scale bar = 200 μm). G: RLS showing cross-field pitting (scale bar = 75 μm). H: TLS showing the various ray sizes present in this sample (scale bar = 100 μm). J: TLS close-up view of a horizontal resin duct. The small duct ringed by epithelial cells is visible (scale bar = 125 μm).
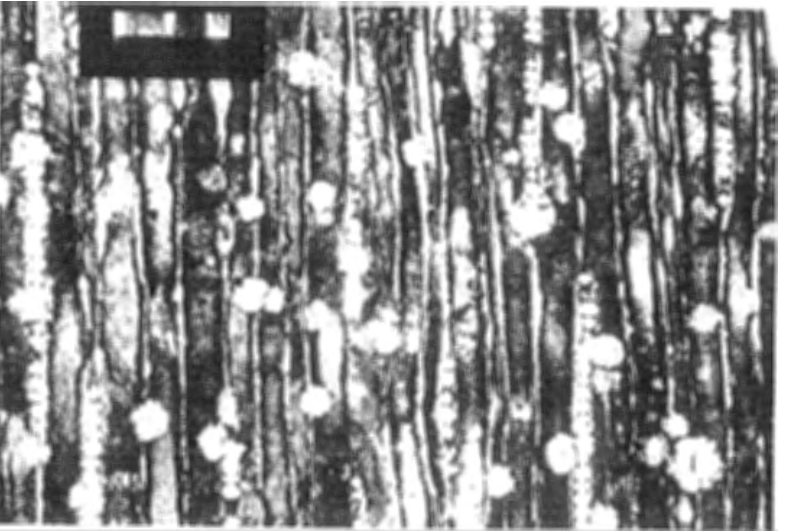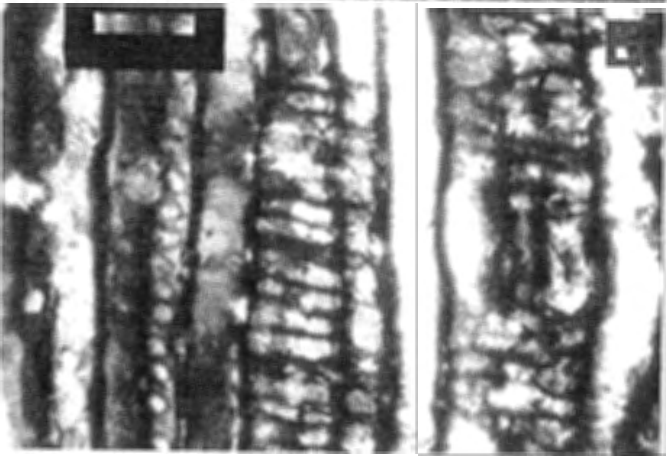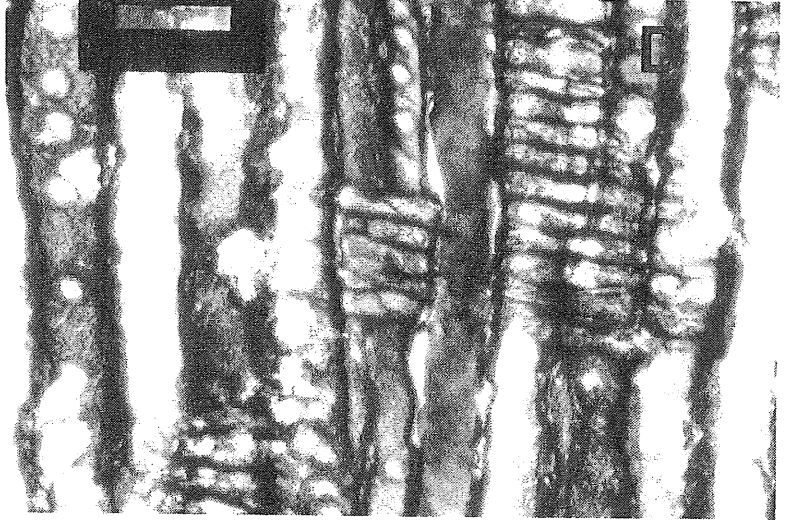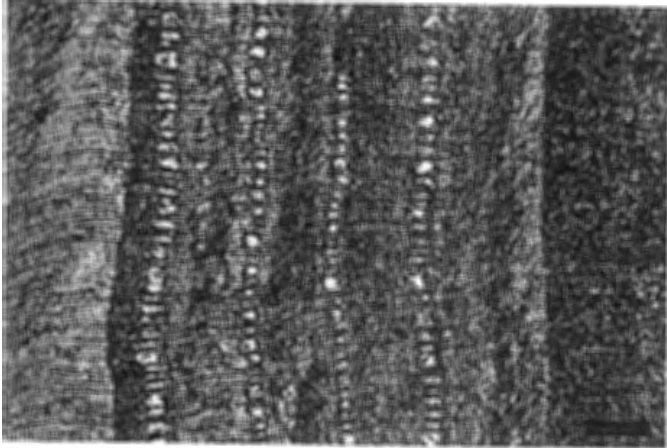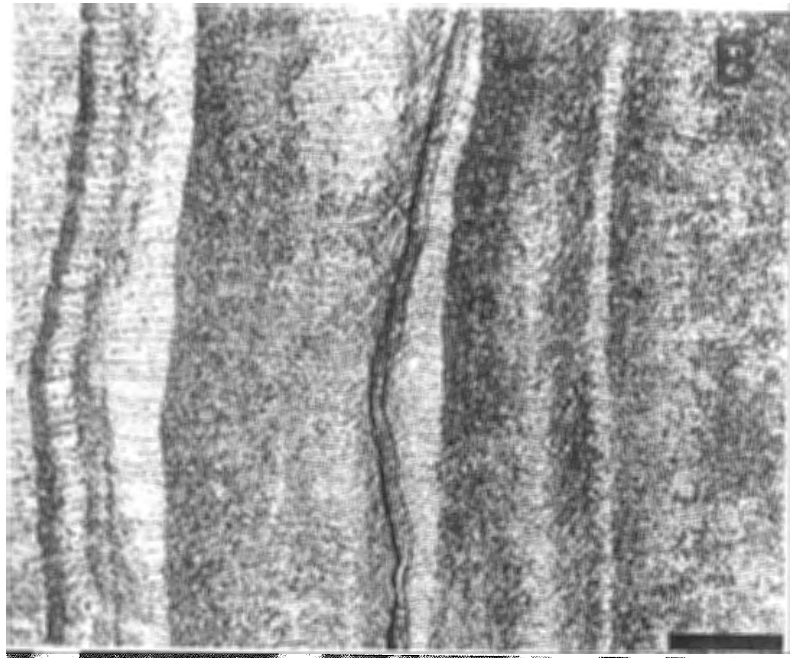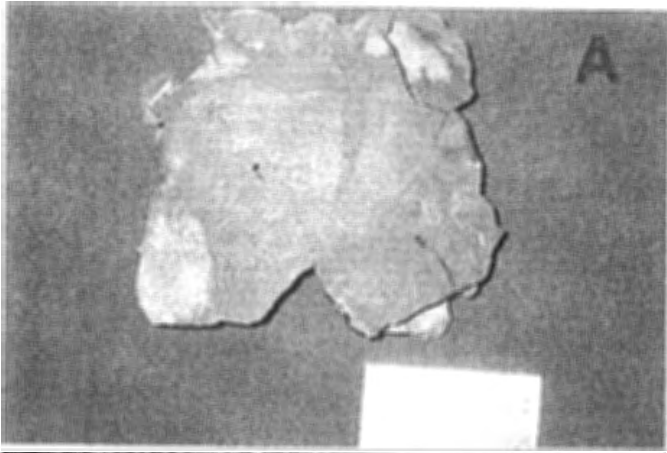
Plate II

Plate II: Sample EL87-206, (*Taxodioxylon albertense*) A: Photograph of the trunk section for EL87-206 showing the fluted growth ring pattern indicative of buttressing (scale bar = 9 cm). B: TS photograph of the growth rings, a false ring and a frost ring are present in this photograph (scale bar = 1 mm). C: TS photograph of frost rings this photo shows 4 frost rings occurring in the same growth ring (scale bar = 200 μm). D: RLS shows bordered pits, rays and some taxodioid cross-field pits (scale bar = 75 μm). E: RLS shows tracheids running longitudinally, with uniseriate bordered pits (scale bar = 100 μm). F: TLS shows rays (scale bar = 100 μm). G: TLS shows the high rays present in this sample (scale bar = 150 μm).
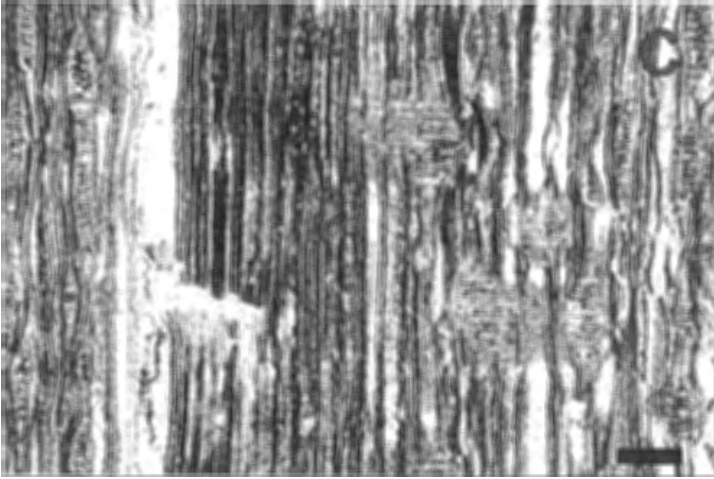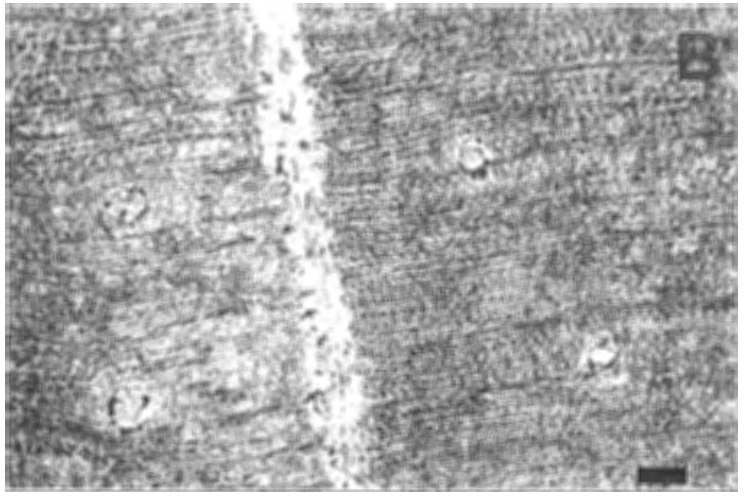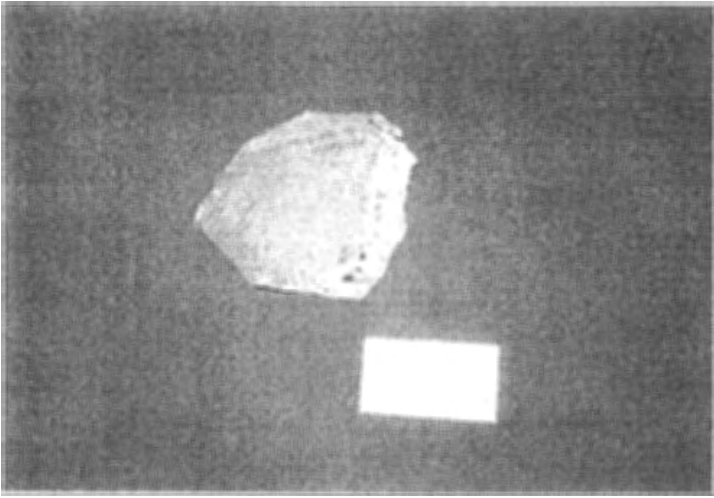
Plate III

Plate III: Sample EL87-257, (*Pinuxylon woolardii*) A: photograph of the trunk section showing the growth rings (scale bar = 9 cm). B: TS photograph of a growth ring showing the common axial resin ducts (scale bar = 100 μm). C: RLS photograph showing the alternate TLS RLS folding of this sample as well as rays, tracheids and bordered pits. An axial resin duct is visible as the column with no tracheids on the right of the picture (scale bar = 100 μm). D: RLS showing both uniseriate and biseriate bordered pitting (scale bar = 150 μm). E: RLS, showing bordered pitting and rays with some cross-field pits (scale bar = 100 μm). F: TLS, showing a fusiform ray with a horizontal resin duct and rays (scale bar =100 μm).
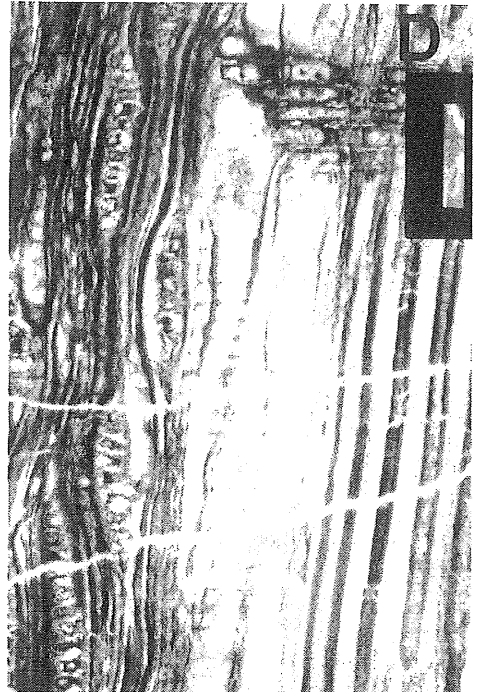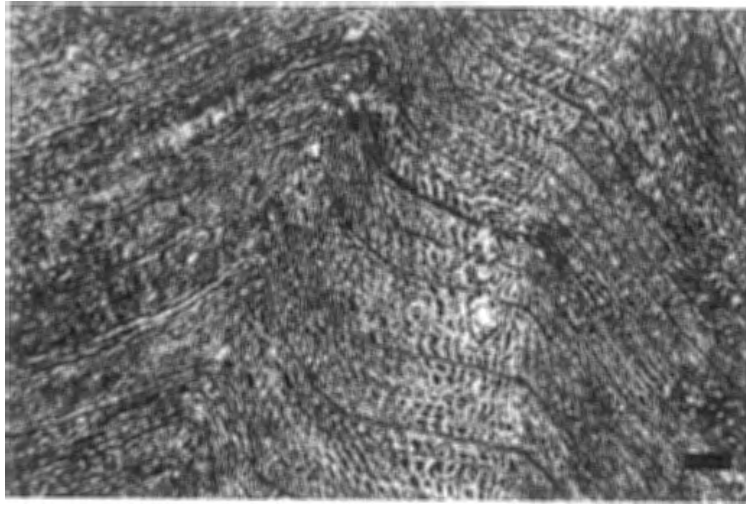
Plate IV

Plate IV: Sample EL87-268, (*Pinuxylon woolardii*) A: TS, photograph of a growth ring showing grouped axial resin ducts (scale bar = 100 μm). B: RLS, photograph of tracheids showing the bordered pits (scale bar = 100 μm). C: RLS, photograph of the cross-fields, showing some cross-field pits (scale bar = 75 μm). D: RLS shows biseriate bordered pits, some cross-field pits and the folded RLS/TLS (scale bar = 100 μm). E: TLS, shows grouped horizontal resin ducts and some rays (scale bar = 100 μm).
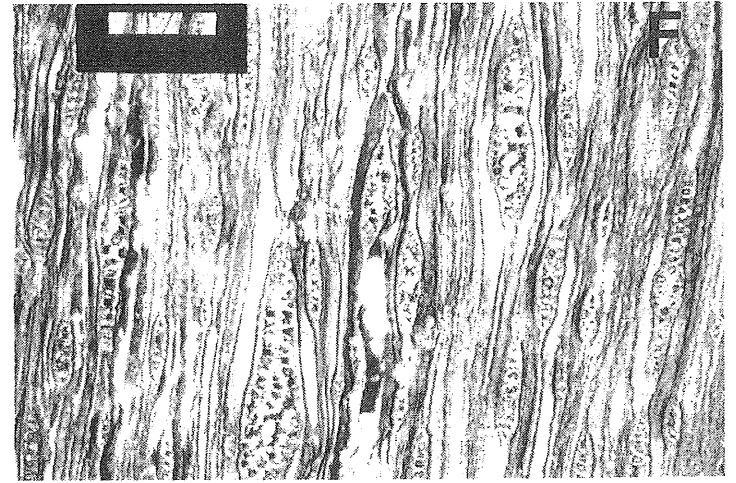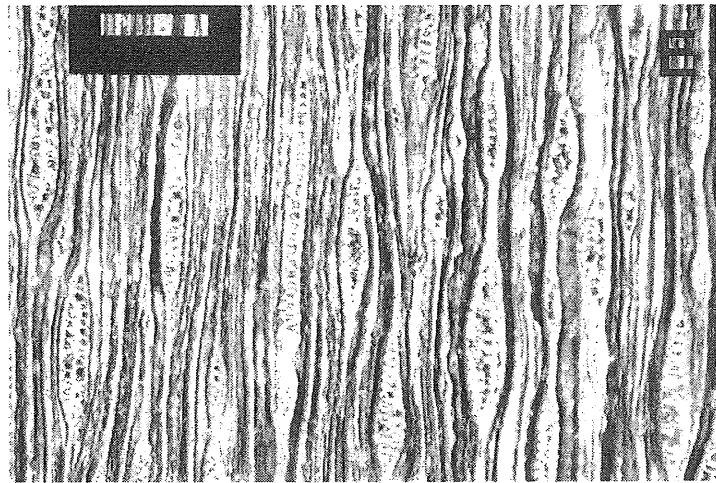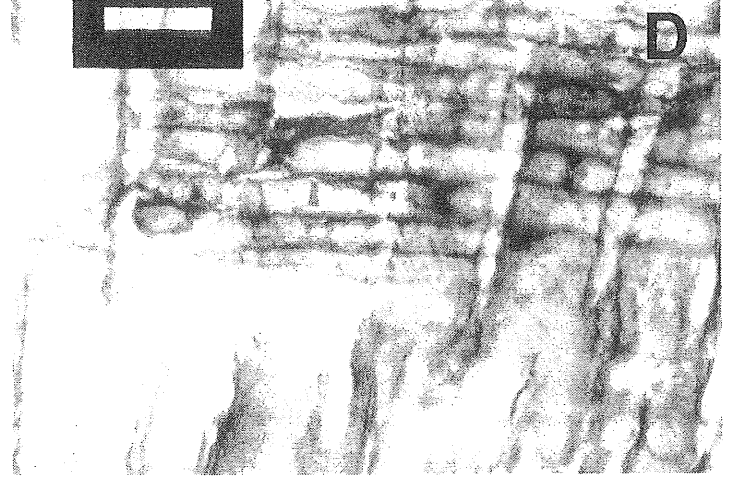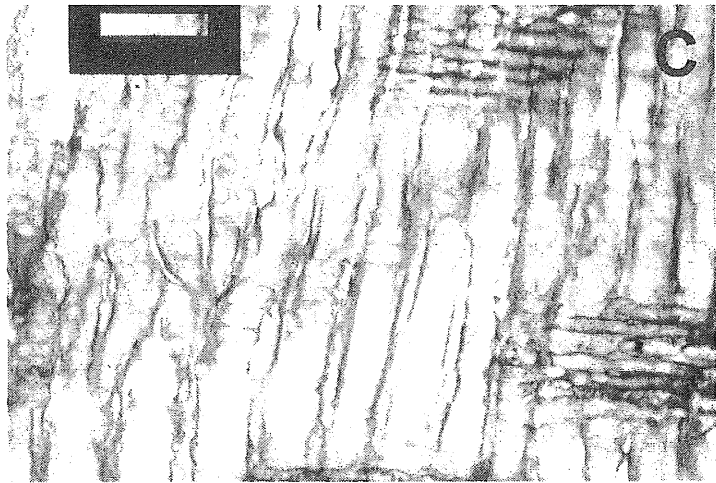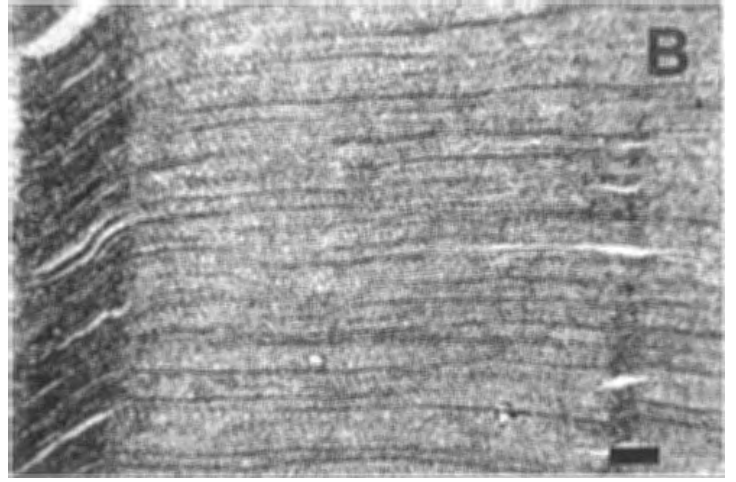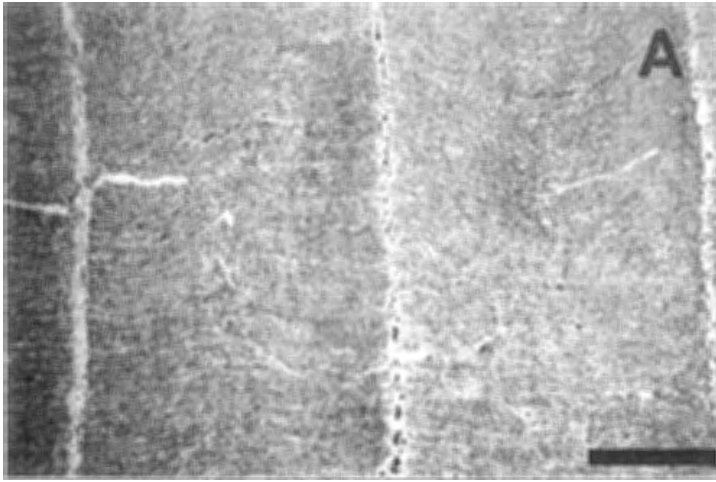
Plate V

Plate V: Sample Phillips-86 (*Pinuxylon* sp. 1) A: TS, photograph of the growth rings some axial resin ducts are visible in this picture (scale bar = 1 mm). B: TS, photograph of a growth ring two resin ducts are visible (scale bar = 200 μm). C: RLS, photo showing the dominant biseriate bordered pitting present in this sample (scale bar = 100 μm). D: RLS, showing the cross-field pits (scale bar = 75 μm). E: TLS, showing the biseriate rays present in this sample (scale bar = 100 μm). F: TLS, showing a fusiform ray with a horizontal resin duct (scale bar = 100 μm).

4. Tree growth data

4.1 Introduction

This chapter will examine the features produced by the growth of trees. Analysis of these growth features is important for climatologic analysis since tree growth factors are extremely dependent on climate. These growth factors include tree height, gross morphology and tree-rings of woody fossil trunks. Tree growth information is also extremely useful for the study of palaeoecology.

4.2 Trunk gross morphology analysis

4.2.1 Methodology

Trunk morphology can be informative as to the type of tree and the growing conditions of the plant. Features to look for are phenomena such as buttressing in the trunk and asymmetry of the growth rings.

Tree height is quite a significant factor because tree height can be correlated with spore dispersal, the ability to shade other plants and certain broad ecological effects such as water availability, nutrient content and forest density (Niklas, 1994; Lehman and Wheeler, 2001). Niklas (1994) found that tree height can be mathematically related to the tree diameter through the use of a simple biometric equation (Eq. 4.1, below). This calculation is based the observation that as a tree grows in height it also grows in width. This leads to the one problem with Niklas' equation, which is that for the tree height to be completely accurate you must measure the diameter at the base of the trunk. This is not always possible in paleobotany where your sample may come from any point along the trunk. This means that any calculation using this equation must be taken as the tree height above the measured tree trunk section, not the absolute tree height. Niklas (1994) provides equations for many different types of trees. The diameter to height relationship among angiosperm wood ("nonwoody") differed from that of conifer (or "woody") material. Because the Ellesmere material is conifer wood the equation we used is the equation for "woody" species:

$$\log_{10}H = 1.59 + 0.39(\log_{10}D) - 0.18(\log_{10}D)^2 \qquad (4.1)$$

Where H is the tree height in meters and D is the trunk diameter in meters. Application of this equation to my specimens gives the following results:

4.2.2 Data

Specimen: *EL87-027*

This is a silicified trunk preserved in sandstone. It contains a double core and circular rings forming an asymmetric pattern (Fig 4.1). It is the only sample with preserved bark. The bark is 1.5 cm in width at its maximum point and is longitudinally fissured, forming a ridged structure. The trunk itself is 16 cm in diameter, including the bark. Applying Niklas' biometric equation, tree height for this specimen is 14.66 m. However, since we cannot be certain that this trunk section is from the base of the tree, this is only a minimum estimate (Fig. 4.2).

Specimen: *EL87-206*

This is also a silicified trunk. This sample does not show the same degree of preservation as the previous sample. The trunk has a "fluted" growth ring pattern of ridges and troughs. Trunk diameter is 24 cm. Minimum tree height using Niklas' equation is 19.50 m (Fig. 4.3).

Specimen: *EL87-257*

This trunk is a calcified sample and shows a series of rings, which decrease in width as one moves outwards towards the edge. The outside rings are quite crushed, probably during burial. Trunk diameter is 22 cm. Minimum tree height is 18.02 m. This is a conservative estimate since the diameter would have been larger had the outside rings not been crushed (Fig. 4.4).
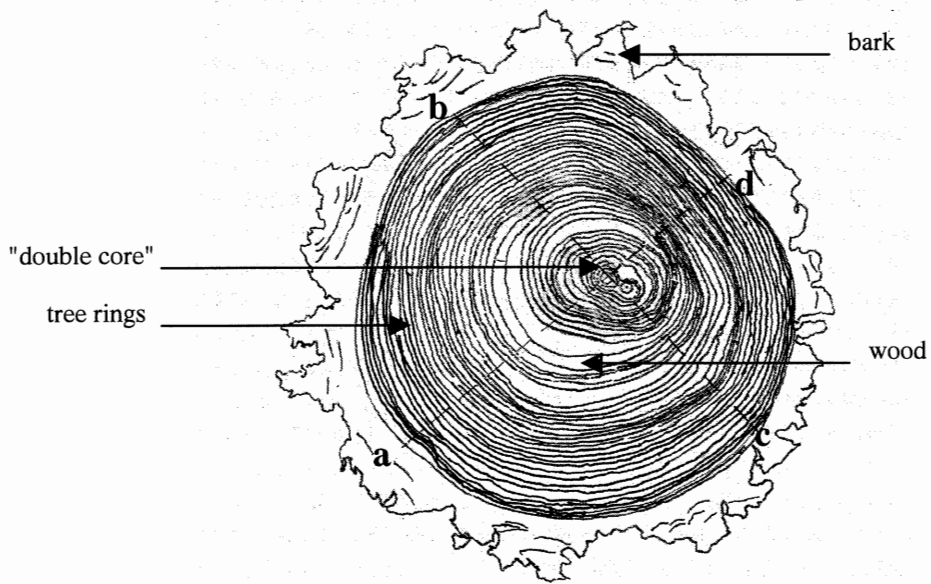
Figure 4.1: A sketch of the growth ring pattern from EL87-027. a,b,c,d are the axis along which the growth rings were measured to obtain mean sensitivity values (TS section).
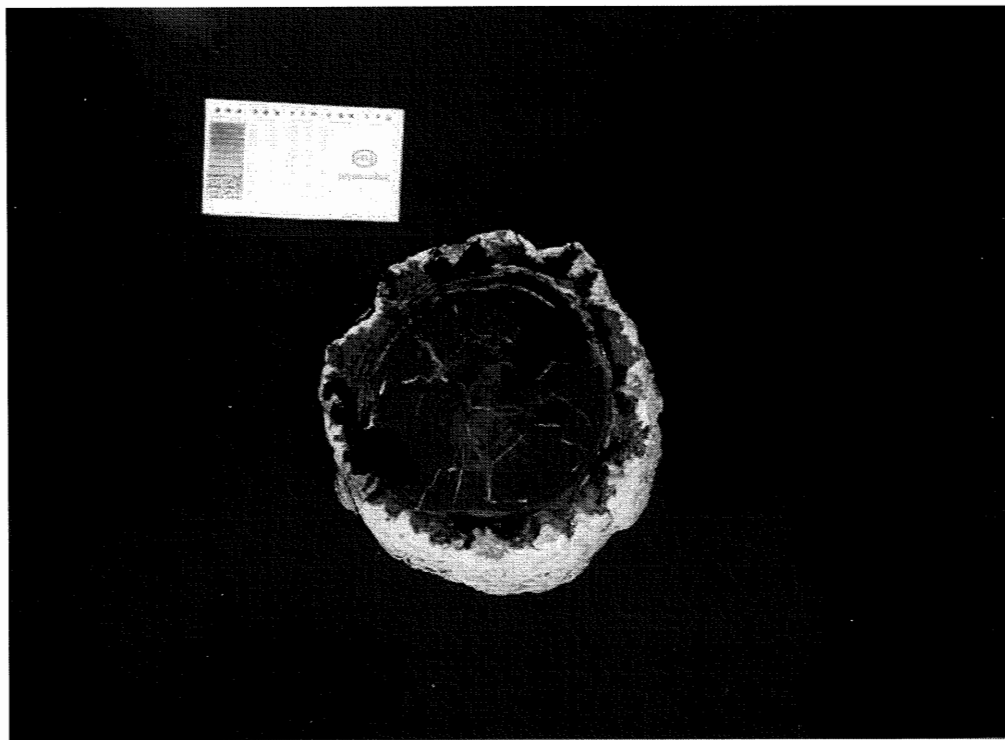
Figure 4.2: Photograph of trunk section EL87-027. Shows well preserved growth rings and bark. Scale bar is equal to 9 cm.

Figure 4.3: Photograph of sample EL87-206 trunk section. This photograph clearly shows the fluted patern of the growth rings and the trunk itself. Scale bar is equal to 9 cm.

rings too crushed to measure

Figure 4.4: Photograph of sample EL87-257 trunk section. You can make out the outer zone (arrow) in which the rings were too crushed to allow accurate measurments.

4.2.3 Interpretation

In modern forests tree height can be used as an indication of favorable growing conditions with taller trees existing in areas of favorable conditions and shorter trees found in areas where conditions are not so good. Short trees in modern forests are found in environments where water is a scarce commodity, such as arid climates or tundra. Tall trees are found in areas with a steady water supply, such as rainforests (Lehman and Wheeler, 2001). Water isn't the only factor that contributes to the height of trees (soil type and nutrients also play a vital role). For example trees growing in densely populated forests also are shorter than those growing where trees are spaced further apart (Lehman and Wheeler, 2001). Temperature affects tree height as well, colder conditions will cause the tree to form smaller growth rings and thus prevent it from growing as tall because more of the tree's energy is going into keeping fluids moving not growth. The Late Cretaceous-Early Tertiary forests of Ellesmere, forming as they were in a peat mire environment would have been growing in soil with low nutrient content (peat mires typically have low nutrient values; Wall and Hytönen, 1996). The same peat mire setting tells us that access to water would not have been a problem for these forests. Tree spacing based on *in situ* trunks found in a lignite bed appears to have been rather dense causing the trees to be shorter than they could be otherwise. Temperatures of the forest, as we will see elsewhere in this chapter, were definitely not tropical and while not tundra either they would certainly have been cool enough to reduce the growth potential of the trees. Fossil trees from Ellesmere Island show heights between 15 and 20 metres these are in the moderate height range for conifers. Modern forests in cool temperate climates show tree heights between 10 and 30 metres (Krüssmann, 1991), with taller trees growing in areas of constant temperatures and high rainfall (the coastal rainforests of the Pacific Northwest for example). Trees growing in Nova Scotia are usually between 15-20 metres high suggesting that climate in the Arctic forests may have been similar to the climate of Nova Scotia today.

4.3 Tree ring analysis

4.3.1 What are tree rings? How do they form

A single active layer known as the vascular cambium forms new tracheid cells in trees. As the tree grows the cambium is pushed outward forming a new layer of tracheid cells centripetally around the trunk. Seasonal changes in temperature, amount of water and amount of light can cause the cambium to shut down until conditions become favorable for growth again (Creber, 1975). It is this process which forms growth rings in trees.

Growth rings can tell us a considerable amount about the environment in which the tree found itself as well as providing information on the tree itself (Creber, 1977). To obtain this information growth rings were measured in hand sample and thin-section. In hand sample ring widths were measured in millimeters starting from the centre of the trunk and moving out towards the edge.

4.3.2 Inter-ring studies

4.3.2.1 Growth ring width and mean sensitivity: methods

When rings are measured in hand sample the ring width can provide information on how favorable the growing conditions were (Creber and Francis, 1999). On its own growth ring width can say something about the types of conditions existing during the growth of the tree. Large growth rings can be said to have grown under favorable conditions while small growth rings would indicate unfavorable conditions (Creber and Francis, 1999). Creber and Chaloner (1985) show that growth ring width can be used to indicate whether or not a fossil forest was situated in a temperate, semi-arid or arid setting. They show that in tropical settings growth rings are faint or absent and in drier climates growth rings are smaller than those found in wet climates (Table 4.1). There are two ways to measure the year-to-year variability in growth ring diameter. Annual

Locality	Age	Site on map	Palaeo-latitude	Ring details (mm)	Reference
Northern Alaska	L.C.	1	80°N	L: 4.0	Arnold, 1932
Amund Ringnes Island	L.C.	2	75°N	L: 6.5	Bannan and Fry, 1957
Ellesmere Island	L.T.	3	74°N	L: 3.0	Christie, 1964; Bradley, 1982 (pers. comm.)
Spitzbergen, King Charles Land	L.T.	4	61°N	L: 4.4	Gothan, 1907
Hare Island, West Greenland	L.T.	5	62°N	L: 5.4	Creber (unpublished)
Chilko Lake, British Columbia	L.C.	6	59°N	L: 5.6	Fry, 1958
Rosedale, Alberta, Canada	U.C.	7	51°N	L: 1.8	Ramunajam and Stewart, 1969
Dakota, U.S.A.	L.C.	8	48°N	L: 1.25	Read, 1932
East Sutherland	U.J.	9	43°N	L: 9.0	Creber, 1972
Sonora, Mexico	L.C.	10	35°N	L: 7.5	Cevallos-Ferriz, 1984; Cevallos-Ferriz and Gonzalez-Leon, 1983
Coahuila, Mexico	U.C.	11	30°N	L: 10	Cevallos-Ferriz, 1984; Cevallos-Ferriz and Weber (unpublished)
North Carolina, U.S.A.	U.C.	12	28°N	F	Boeshore and Gray, 1936
South Portugal	U.J.	13	31°N	A	Boureau, 1949
Dorset	U.J.	14	36°N	L: 3.7	Francis, 1983
Hopeh, China	U.J.	15	37°N	L: 5.0	Chang, 1929
Liaotung, Manchuria	L.C.	16	35°N	L: 2.5	Shimakura, 1937
Pyong-yang	M.J.	17	43°N	L: 13.0	Shimakura, 1936
Koryak, U.S.S.R.	U.J.	18	72°N	L: 3.0	Shilkina, 1963
South Sakhalin, Japan	U.C.	19	56°N	L: 3.7	Shimakura, 1937
Chiba, Japan	L.C.	20	36°N	A	Nishida, 1973
Koti-ken, Japan	U.J.	21	36°N	L: 3.0	Shimakura, 1936
Nong-son, Vietnam	L.J.	22	28°N	F	Boureau, 1950
Changwat Kalasin, Thailand	L.J.	22	28°N	F	Asama, 1982
Soegi, Indonesia	L.J.	23	21°N	A	Roggeveen, 1932
Afghanistan	J.	24	22°N	F	Sitholey, 1940
Uzbekistan, U.S.S.R.	U.C.	25	32°N	F	Khudayberdyev, 1962
Morocco	U.J.	26	24°N	F or A	Boureau, 1951
Tripolitania	M.C.	27	13°N	F or A	Negri, 1914
Niger	L.C.	28	2°N	F	Williams, 1930
Cairo	L.T.	29	5°N	F or A	Unger, 1859
Tchad	L.C.	30	7°S	F	Boureau, 1952
Tanzania	U.C.	31	28°S	F or A	Potonié, 1902
Madagascar	U.C.	32	31°S	A	Flicne, 1900
Bihar, India	M.J.	33	40°S	L: 1.2	Kräusel and Jain, 1963
East Pondo Land, South Africa	U.C.	34	48°S	F or A	Mädel, 1960; Schultze-Motel, 1966
Santa Cruz, Argentina	U.J.	35	53°S	L: 2.5	Calder, 1953
Alexander Island, Antarctica	L.C.	36	70°S	L: 9.0	Jefferson, 1982
New Zealand, South Island	M.J.	37	70°S	L: 1.1	Pole, 1982
New Zealand, South Island	U.C.	38	67°S	L: 1.0	Stopes, 1916

Species	Map site	Widest ring (mm)	Locality	Latitude (°N)
Larix dahurica	A	2.0	River Novaja	72
Larix dahurica	A	1.9	River Boganida	71
Larix dahurica	A	5.0	Between Amginsk and the River Aldan	60
Pinus sylvestris	B	2.1	Leningrad	60
Pinus sylvestris	B	9.0	Estonia	59
Pseudotsuga menziesii	C	5.0	British Columbia	55
Betula nana	D	0.14[a]	Kaiser Franz Joseph's Fjord, East Greenland	73
Betula nana	D	1.6[a]	Wurzburg, Germany	48
Vaccinium uliginosum	E	0.032[a]	Kaiser Franz Joseph's Fjord, East Greenland	73
Vaccinium uliginosum	E	0.7[a]	Erlanger, Germany	49
Alnus tenuifolia	F	2.7[a]	Glacier Bay, Alaska	59
Salix arctica	G	0.07[a]	Cornwallis Island	75
Salix arctica	H	0.2[a]	Axel Heiberg Island	79
Betula pubescens	I	0.5[a]	S.W. Greenland	61

Table 4.1: (*top*) Jurassic, Cretaceous and Lower Tertiary fossil woods plotted showing ring widths and palaeolatitude. J= Jurassic; L.C.= Lower Cretaceous; L.J.= Lower Jurassic; L.T.= Lower Tertiary; M.C.= Middle Cretaceous; M.J. = Middle Jurassic; U.C. = Upper Cretaceous; U.J.= Upper Jurassic. A= absent; F=faint; L= largest. (*bottom*) Table of average modern ring widths and latitude (After Creber and Chaloner, 1985).

Sensitivity is the variability in growth ring width from one year to the next and is measured using Equation 4.2 (modified from Douglass, 1928).

$$\text{Annual Sensitivity} = 2(X_t - X_{t+1})/(X_t + X_{t+1}) \qquad (4.2)$$

Where X is the ring width in mm, t is the ring number counting from the centre of the trunk and n is the number of rings in the sequence. Mean sensitivity, or tree sensitivity is a forestry term used to describe disturbances in forest growth. Uniform ring width would indicate favorable conditions (termed complacent) and is indicated by a mean sensitivity below 0.3. Trees with highly variable growth ring widths would indicate disturbed conditions (termed sensitive) and would have mean sensitivity values above 0.3 (Creber, 1977). Under favorable conditions trees will grow to their maximum genetic potential and therefore have uniform ring widths. In stressful years, environmental conditions will limit growth preventing the tree from reaching its genetic potential and producing variable ring widths (Creber, 1977). Mean sensitivity is calculated as the sum of all annual sensitivities divided by one less than the total number of growth rings (Eq. 4.3) (modified from Douglass, 1928).

$$\text{Mean sensitivity} = 1/n\text{-}1 \sum_{t=1}^{t=n-1} 2(X_t - X_{t+1})/(X_t + X_{t+1}) \qquad (4.3)$$

Where X is the ring width in mm, t is the ring number counting from the centre of the trunk and n is the number of rings in the sequence. Sensitive conditions would indicate that a tree's water supply had been highly variable from year to year this could take on a variety of forms such as unpredictable weather conditions (hurricanes, drought), flooding, or fire (Creber, 1977).

4.3.2.2 Results

EL87-027

Ring widths for EL87-027 were measured along 4 different axes to use the complete trunk specimen to its full advantage. Ring widths ranged in size from 0.2 mm to 5.5 mm with a mode of 1 mm and a mean of 1.2 mm (Appendix B; Fig. 4.5). Annual sensitivities calculated by Equation 4.2 (below) range from 0 to 1.3. Mean sensitivities calculated using Equation 4.3 are 0.38, 0.43, 0.35, 0.46 (Fig. 4.7).

EL87-206

Ring widths were measured along two axis one through a "ridge" and one through a "furrow". Ring widths ranged in size from 0.1 to 5.3 mm with a mode of 1.5 mm and a mean of 1.66 mm (Appendix B; Fig. 4.6). Annual sensitivities range from 0 to 1.5. Mean sensitivities calculated for this sample are 0.36 for both the ridge and the furrow (Fig. 4.8).

EL87-257

Ring widths were measured along one axis because it is a partial trunk. Widths ranged from 1 to 8 mm with a mode of 2.2 mm and a mean of 2.8 mm (Appendix B). Annual sensitivities range from 0 to 0.86. The mean sensitivity for this sample is calculated as 0.28 (Fig. 4.8).

4.3.3 Intra-rings studies

4.3.3.1 Cell-by-cell measurements: methods

Cell-by-cell measurments measure the diameter of each tracheid cell along one file cells throughout an entire growth ring starting in the earlywood. The cell-by-cell count plots the diameter of each cell against where the cell falls along the growth ring. The cell diameter steadily decreases with distance along the ring as shown in Figure 4.9. This method of measuring growth rings can be used to find growth rings when they are

EL87-027 rings
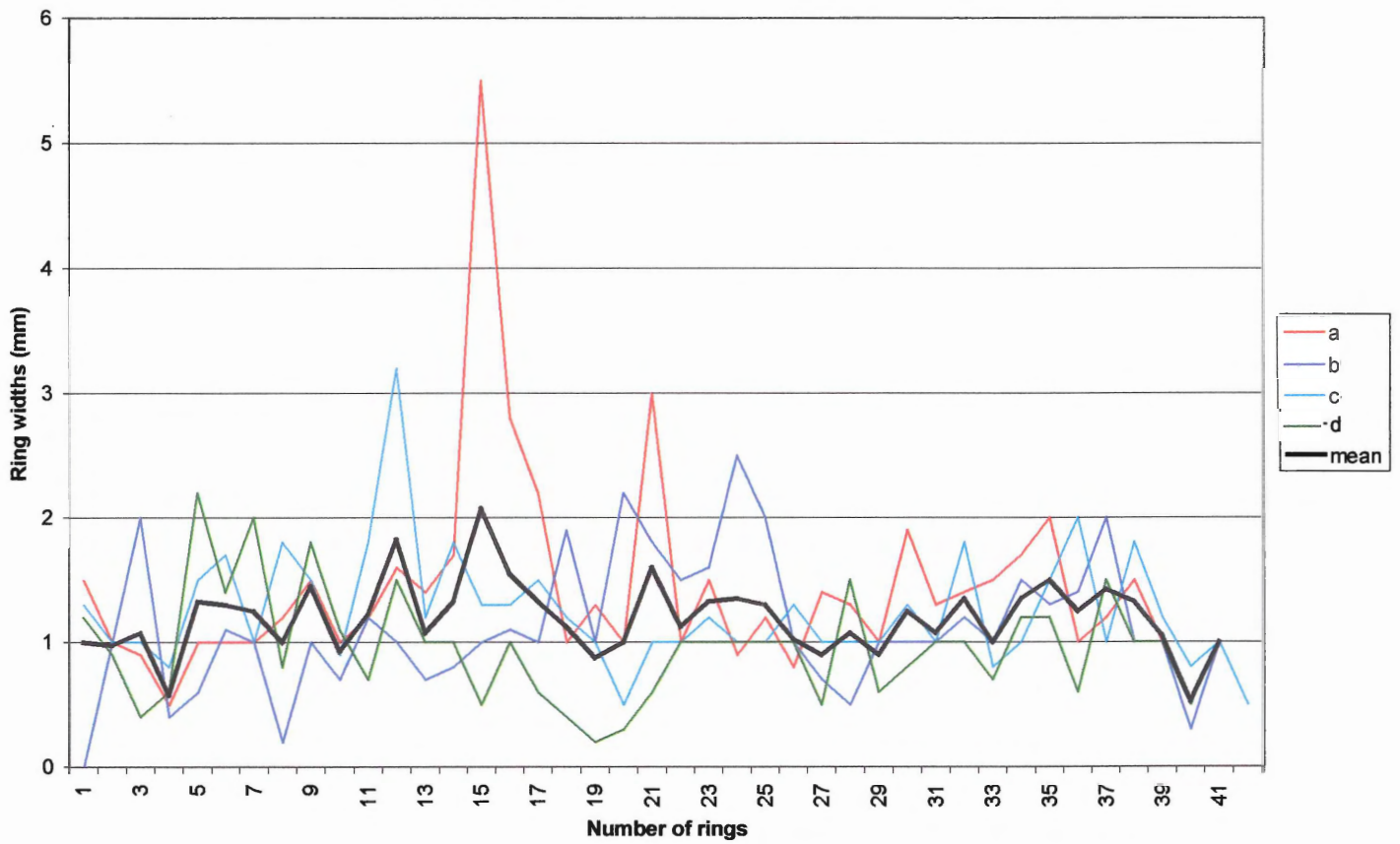
Figure 4.5: Graph of growth ring widths in millimetres along all files in sample EL87-027 measured as shown in Figure 4.1. Ring widths on the y axis and number of rings on the x axis.

EL87-206
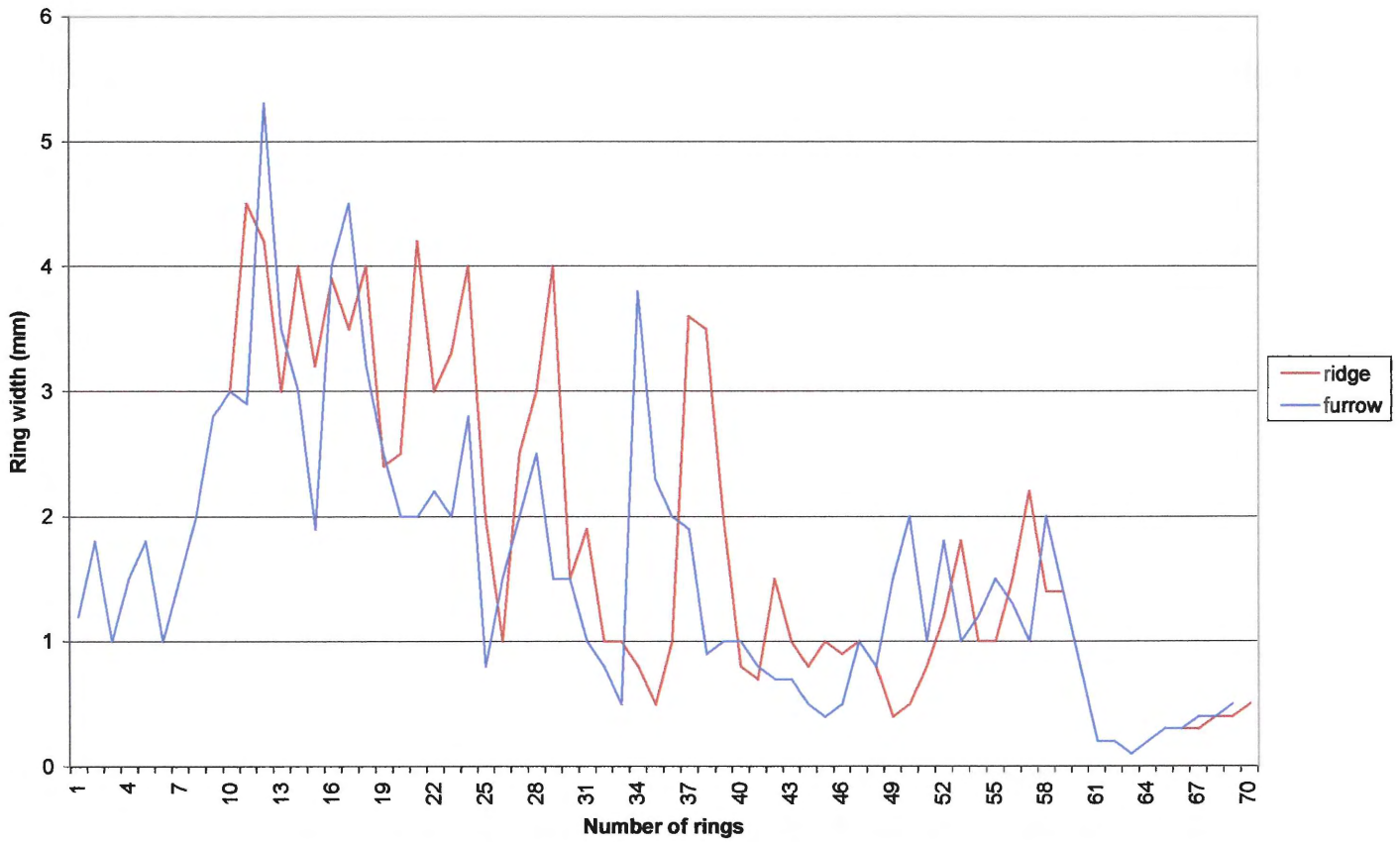
Figure 4.6: Graph of growth ring widths for sample EL87-206 measured in millimetres along a ridge of the fluted trunk and a furrow of the fluted trunk. Ring widths on the *y* axis and number of rings on the *x* axis.
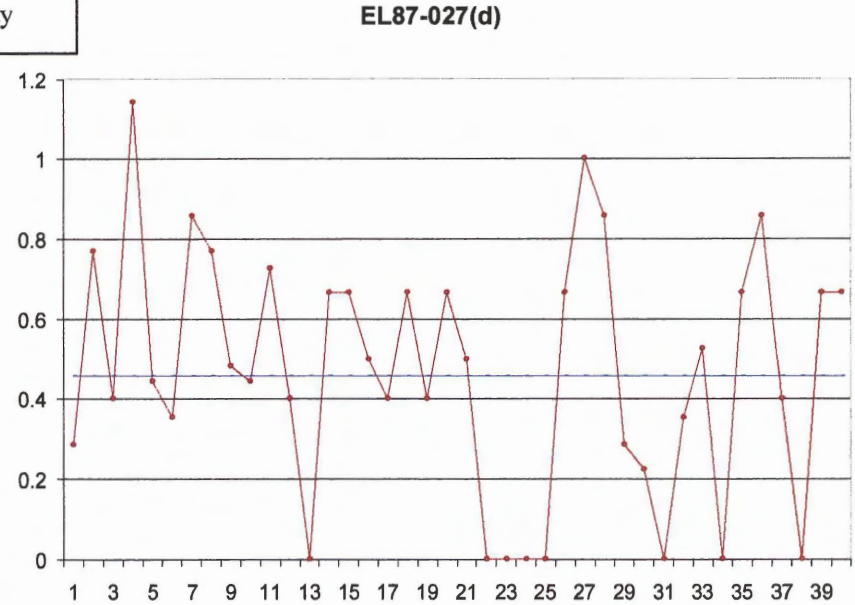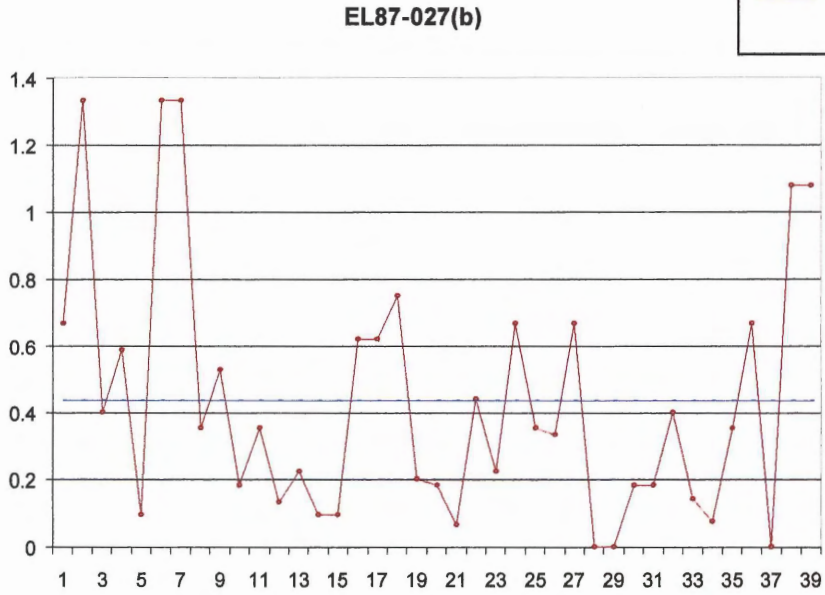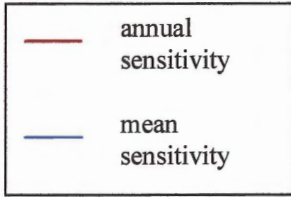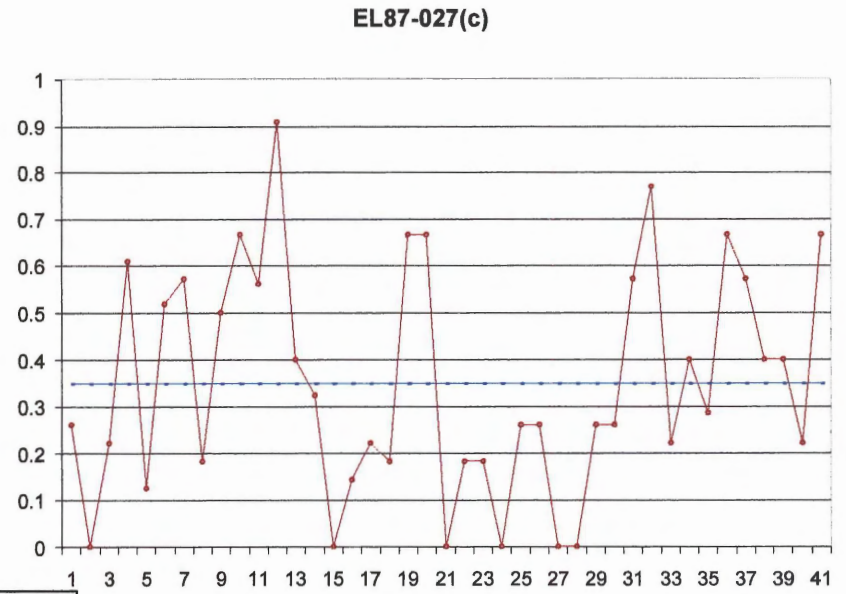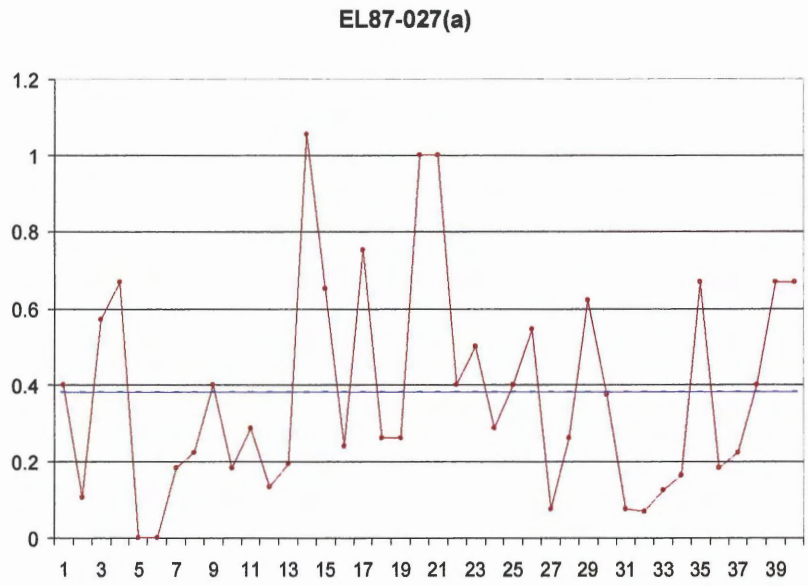
Figure 4.7: Annual and mean sensitivity graphs for EL87-027. Number of growth rings plots on the *x* axis and the sensitivity values plot on the *y* axis.
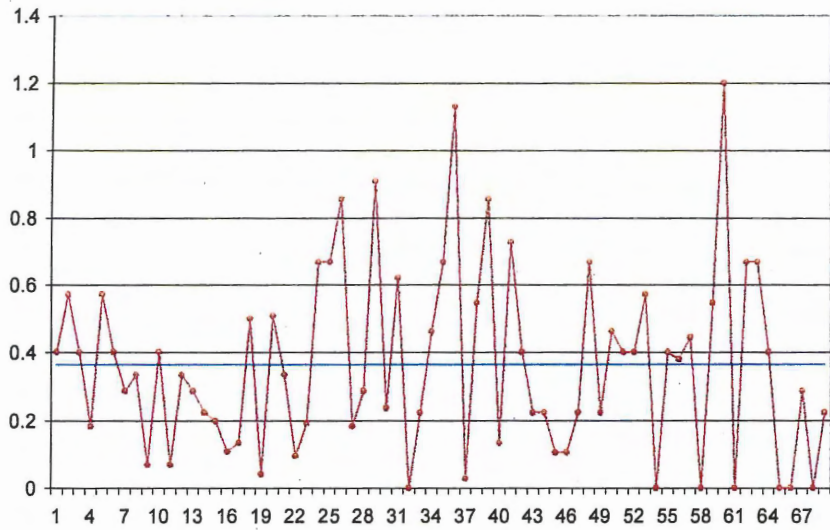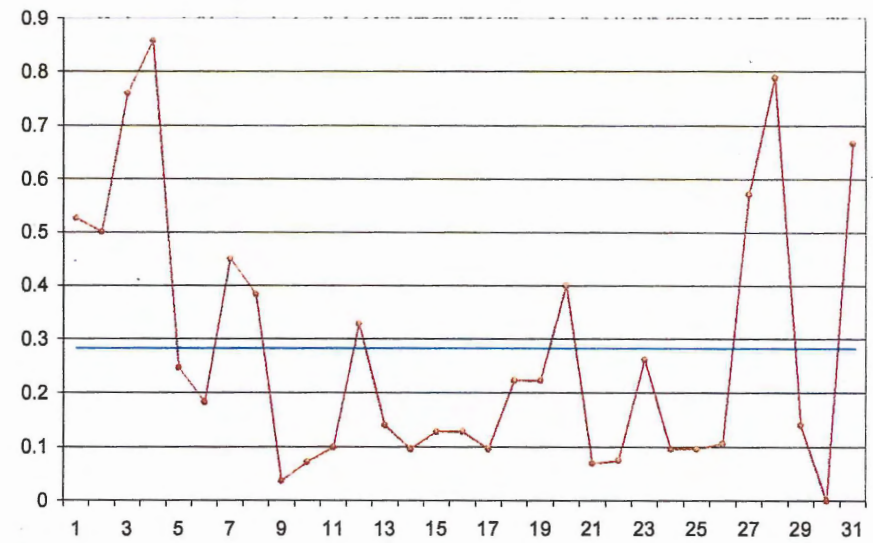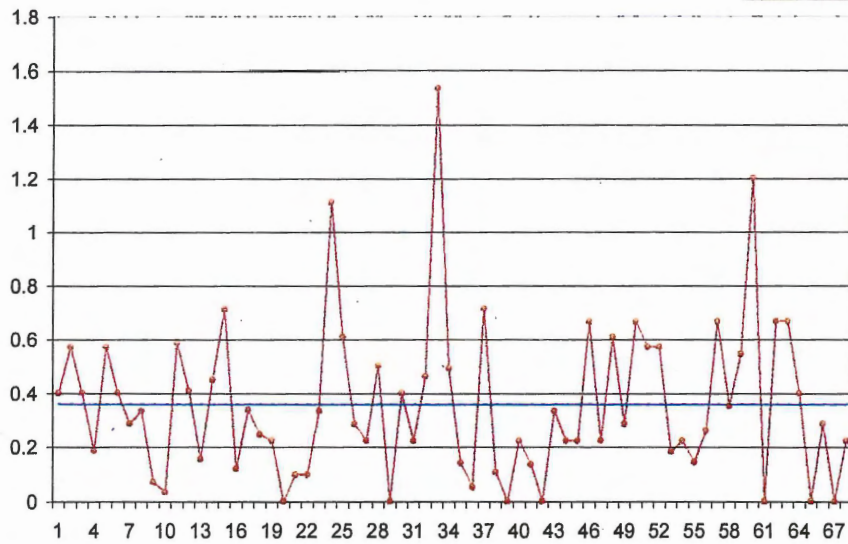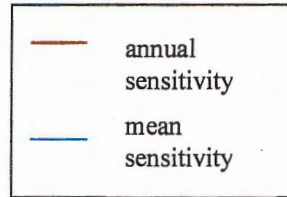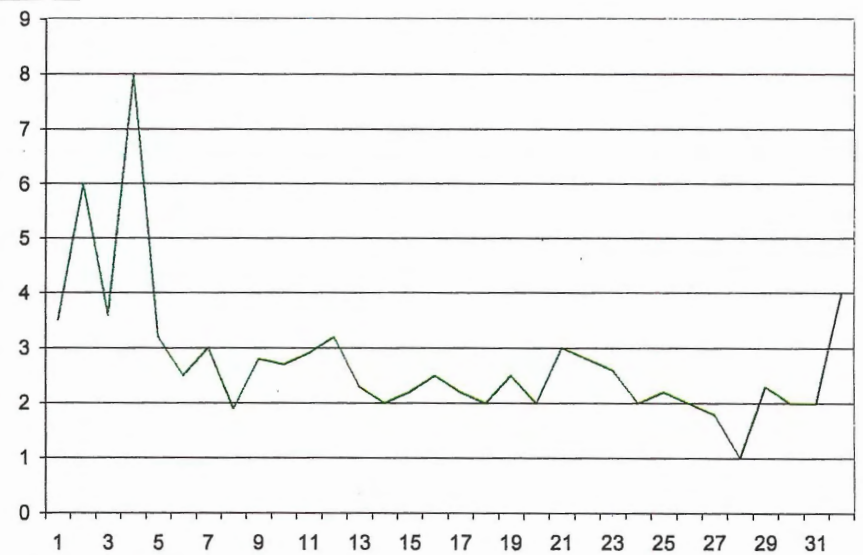
Figure 4.8: (a-c) Annual and mean sensitivity graphs for EL87-206 and EL87-257 with number of growth rings on the *x* axis and sensitivity values on the *y* axis. (d) Growth ring width graph for EL87-257, ring width in millimetres on the *y* axis and ring number on the *x* axis.

not easily discerned, such as in trees from arid environments for the cells will show smaller scale variations than the complete ring. The next step in this analysis is to find the deviation from the mean, this is the difference between each individual cell's diameter and the mean cell diameter. The deviations from the mean are then summed and when plotted on a graph known as a CSDM (for Cumulative Standard Deviation from the Mean) curve which appears similar to a bell curve (Fig. 4.10). The positive slope being where the cell diameters are higher than the mean cell diameter and the negative slope being where the diameters are lower than the mean. The degree to which this curve is skewed and in which direction, positive or negative can provide specific information about the tree and its environment. According to Falcon-Lang, (2000) this can give the measure of leaf longevity, a negatively skewed graph indicates that the tree is deciduous. Deciduous trees have a shorter growing season than evergreen trees and so throw more of their energy into growth earlier, as soon as their leaves appear. Growth ceases in deciduous trees in the autumn when their leaves die. Evergreen trees on the other hand start growing as soon as conditions become warm enough (or in our case light enough) and don't stop growing until conditions become unfavorable again thus a positively skewed graph shows that the tree is evergreen. Creber and Francis, (1999) found that fossil woods from the Antarctic show fairly symmetrical CSDM curves and that this could be an indication of the unique polar growing conditions the peak on the graph being the point where light conditions begin to decrease. Although the second explanation is valid it does not explain why some of the CSDM curves obtained in this study can have so many non-symmetrical values even though they were obtained from polar trees.
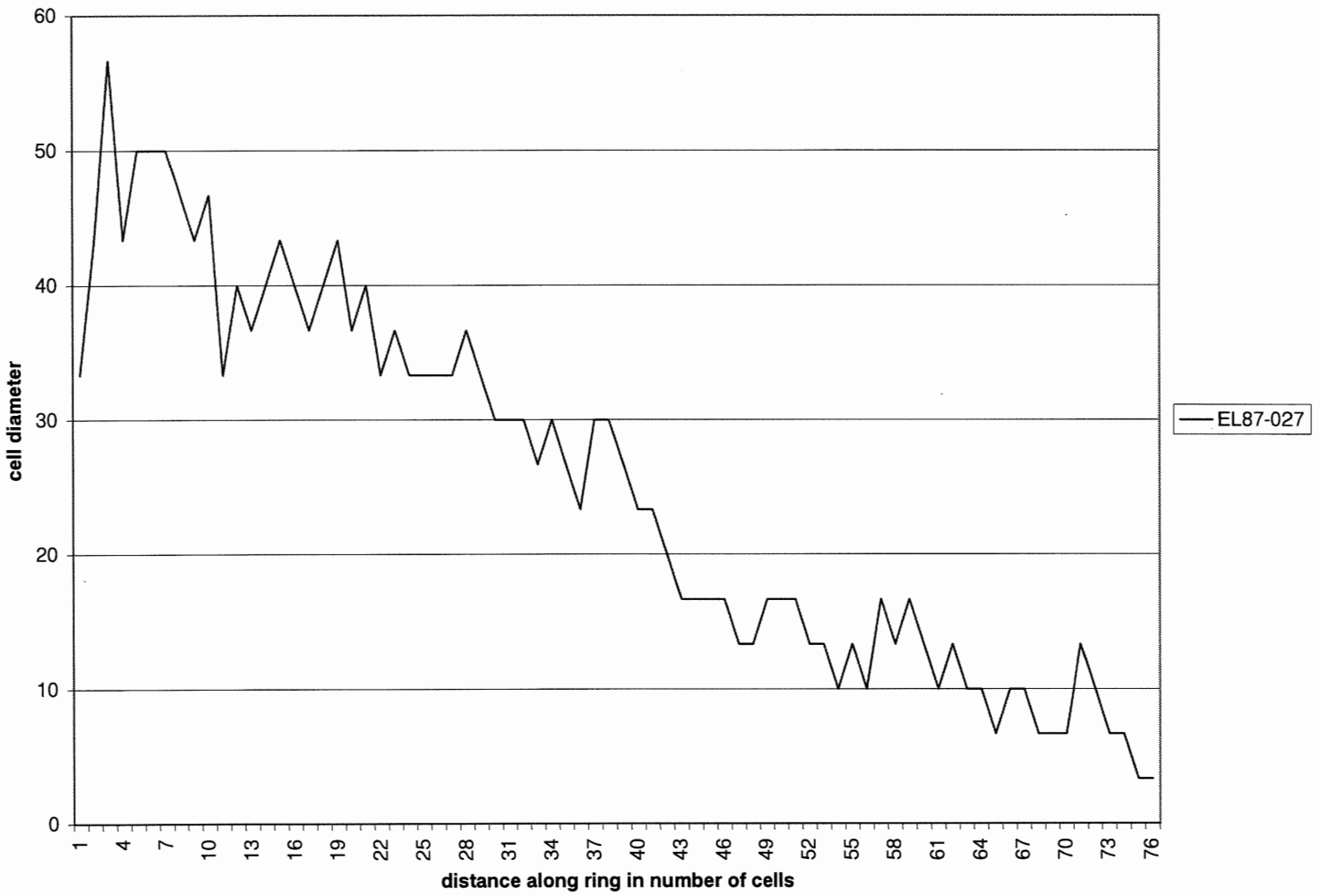
Figure 4.9: Shows how cell diameter decreases as a function of distance along a growth ring.
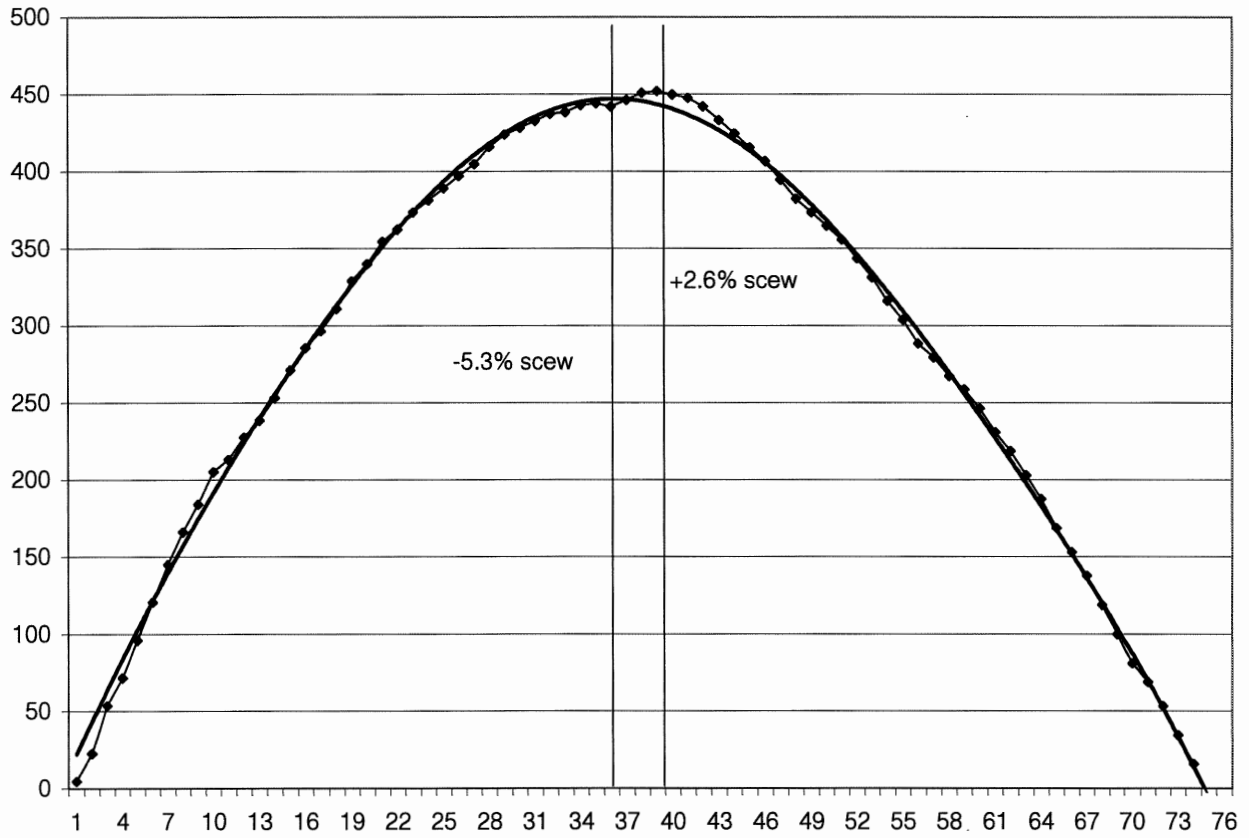
Figure 4.10: The Cumulative Stadard Deviation from the Mean curve (CSDM) you can see the bell curve like shape of the curve. The point where the slope begins to decrease is the early wood late wood boundary. the x axis is the number of cells and the y axis is the sum of the deviations from the mean cell diameter.

4.3.3.2 Results

Results for the Ellesmere Island samples are presented in Table 4.2 and Figures
4.11-4.18.

EL87-027	EL87-206	EL87-257	EL87-268	Phillips-86
-6.80%	7.50%	23.30%	0%	-22%
14%	13.60%	27.20%		-18.90%
2.60%	19%			
-18.40%				
-24.40%				
-23.50%				
Values calculated using a best fit curve				
EL87-027	EL87-206	EL87-257	EL87-268	Phillips-86
6.80%	14%	23.30%	11%	-3.80%
-11.80%	15%	27.20%		-22%
-2.60%	13.60%			
-5.60%				
-24.40%				
-6.80%				

Table 4.2: Table of percent skewness for all CSDM curves. Top table is the actual values the bottom table
lists values calculated after fitting a trend curve to the data.

Some general things to note about the data are the presence of false peaks on
some of the curves (Fig. 4.19). The first peak is probably a false ring, see section 4.5
below. When the percent skew is plotted most of the values show relatively little skew.
Figure 4.20 shows the percent skew plotted as a function of increasing leaf longevity for
all samples.
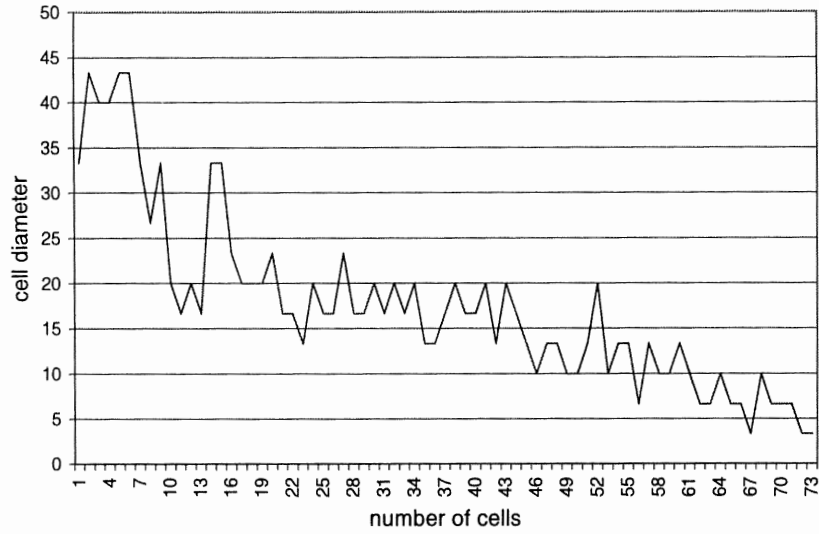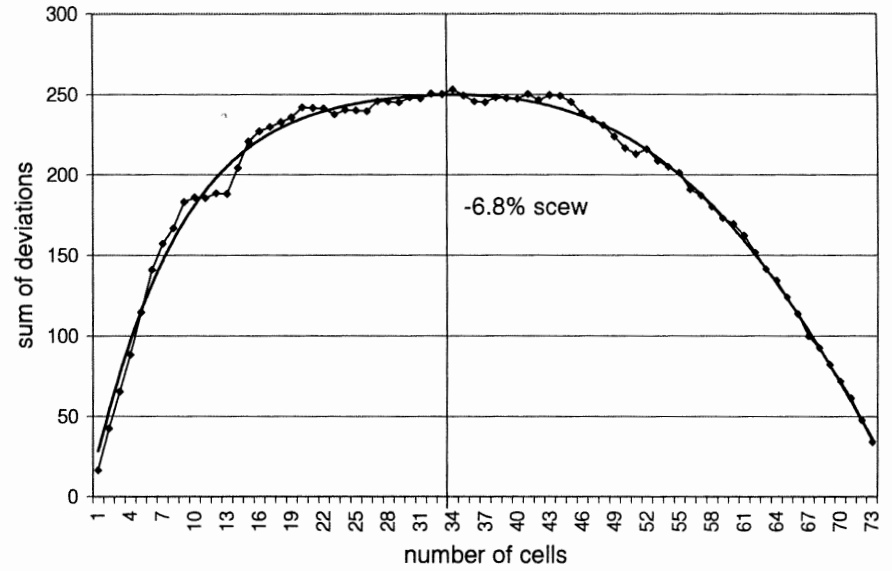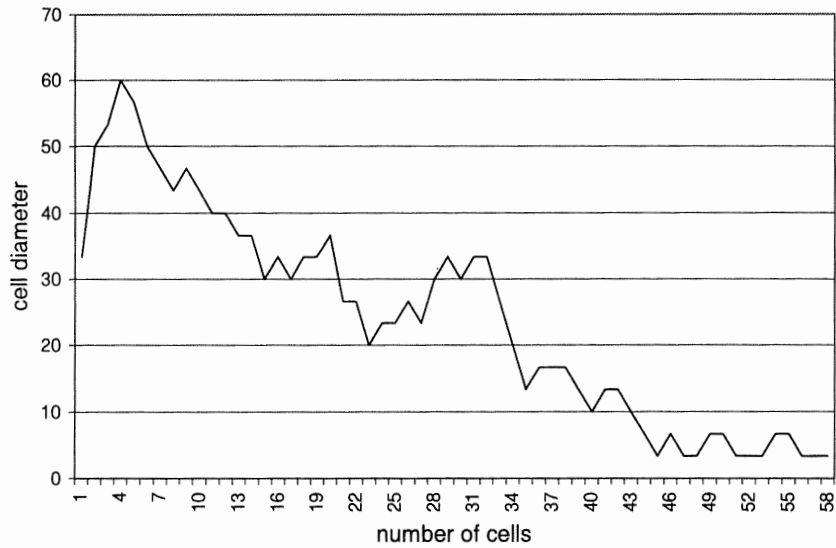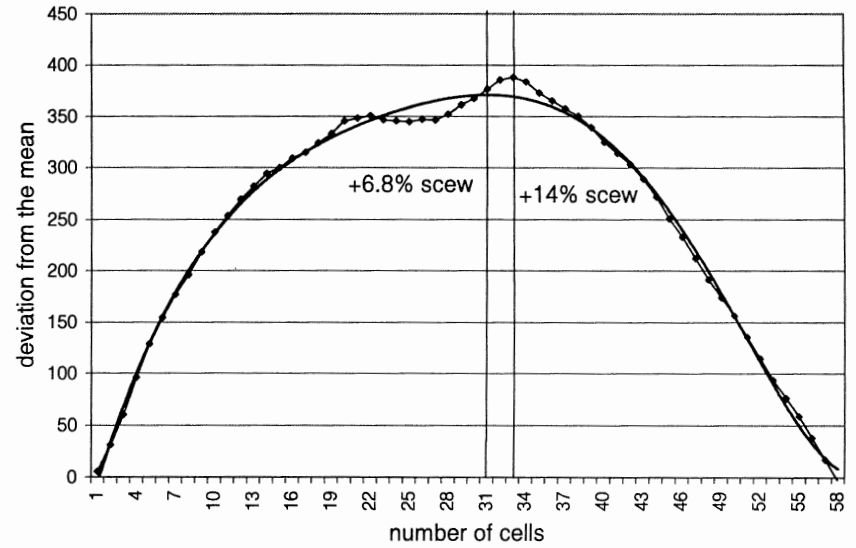
Figure 4.11: On the right are graphs of the cell diameters for two cell files measured along the width of two growth rings. On the left are the two resultant CSDM curves calculated from the cell diameters.
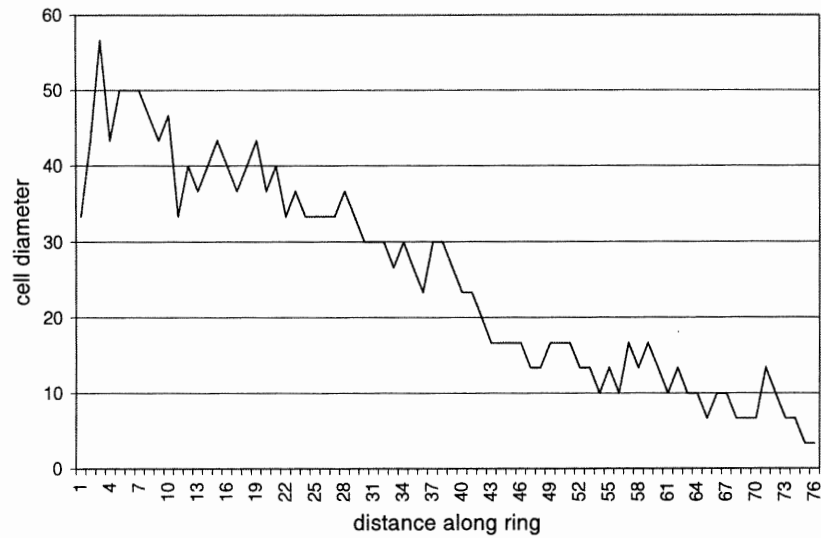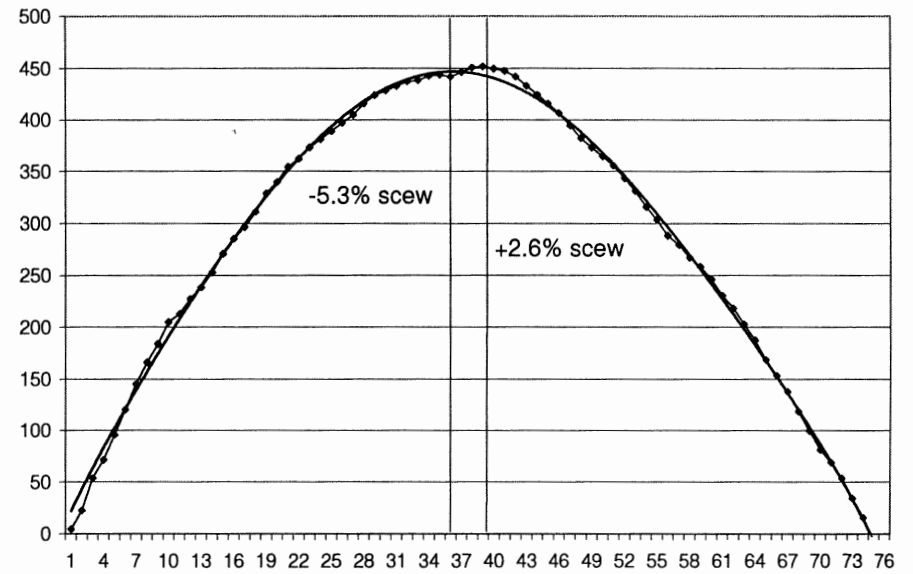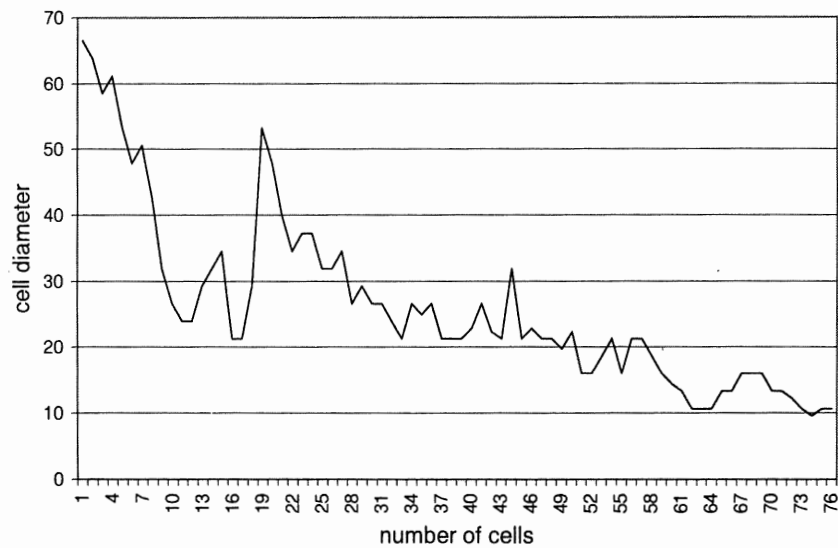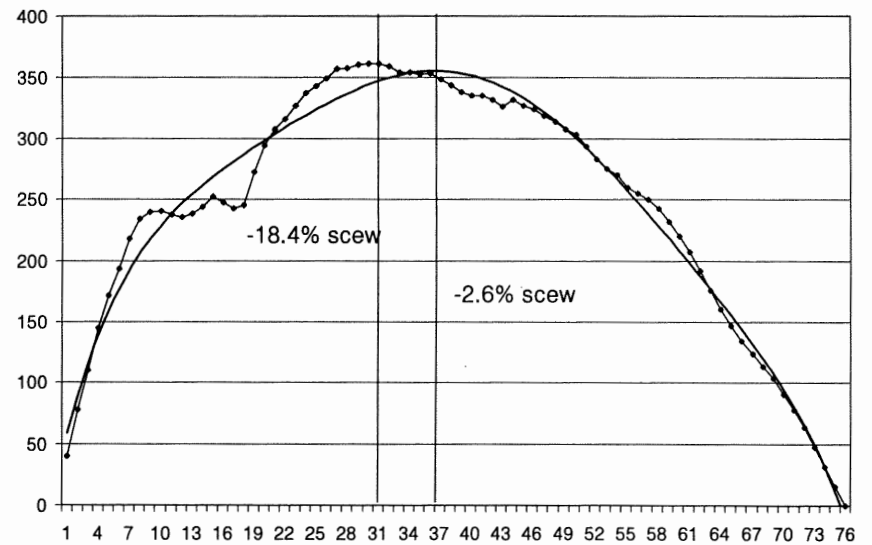
Figure 4.12: On the right are graphs of the cell diameters for two cell files measured along the width of two growth rings. On the left are the two resultant CSDM curves calculated from the cell diameters.
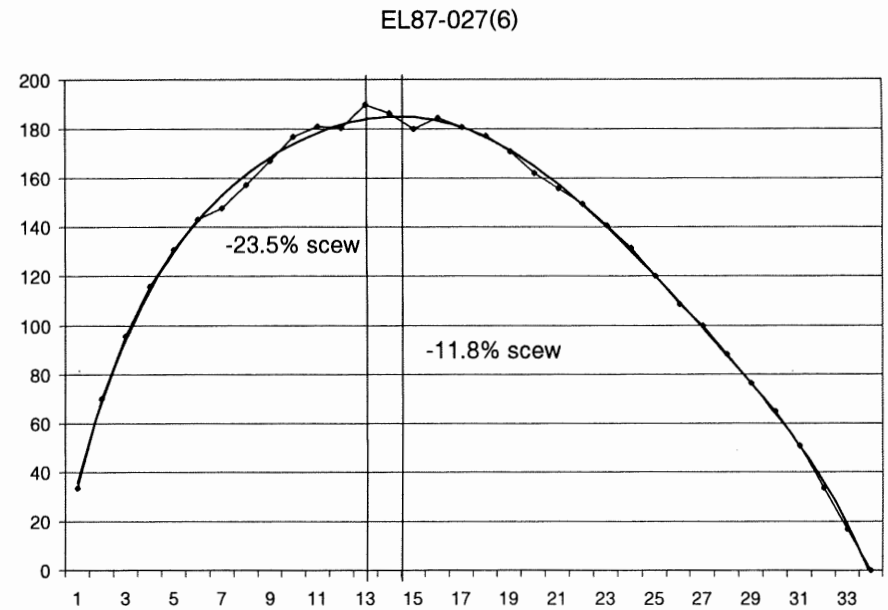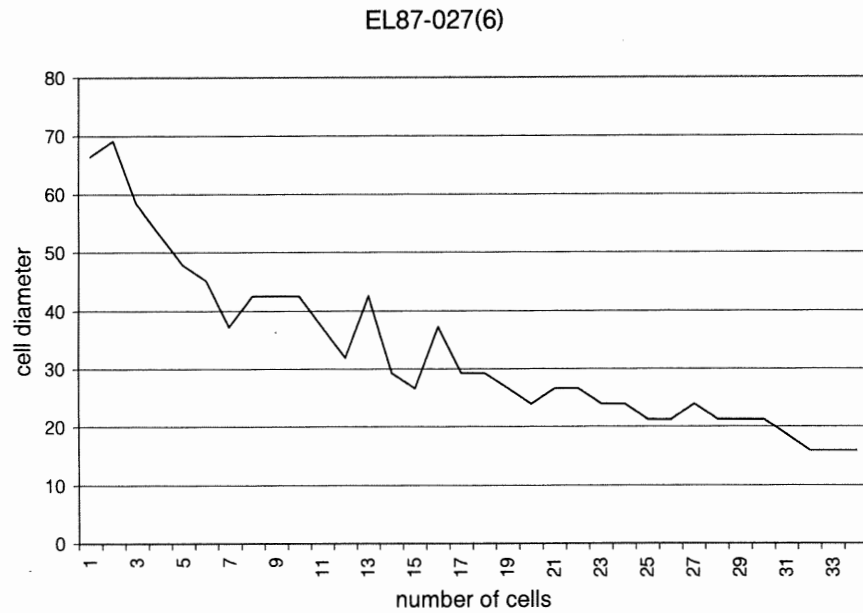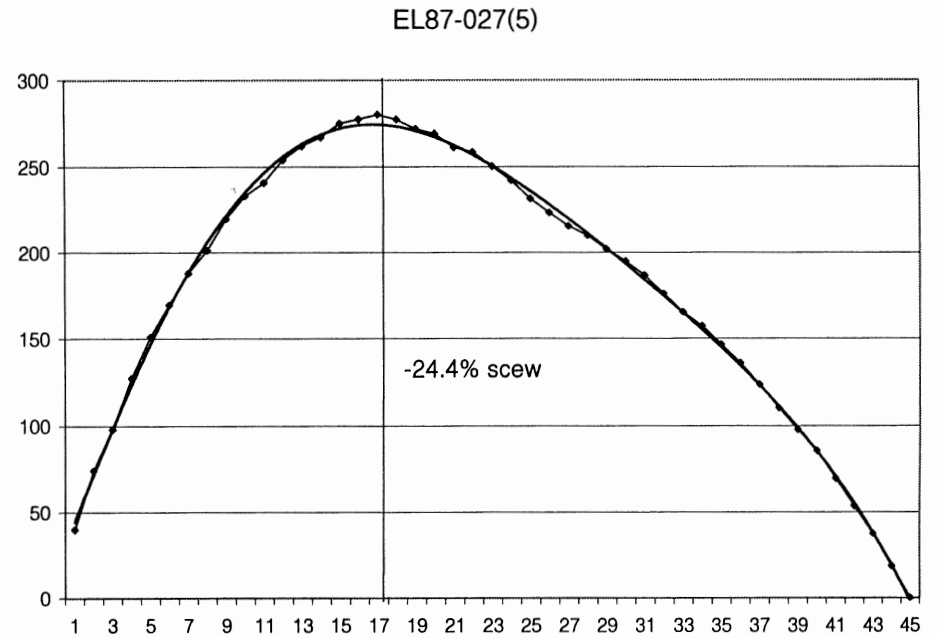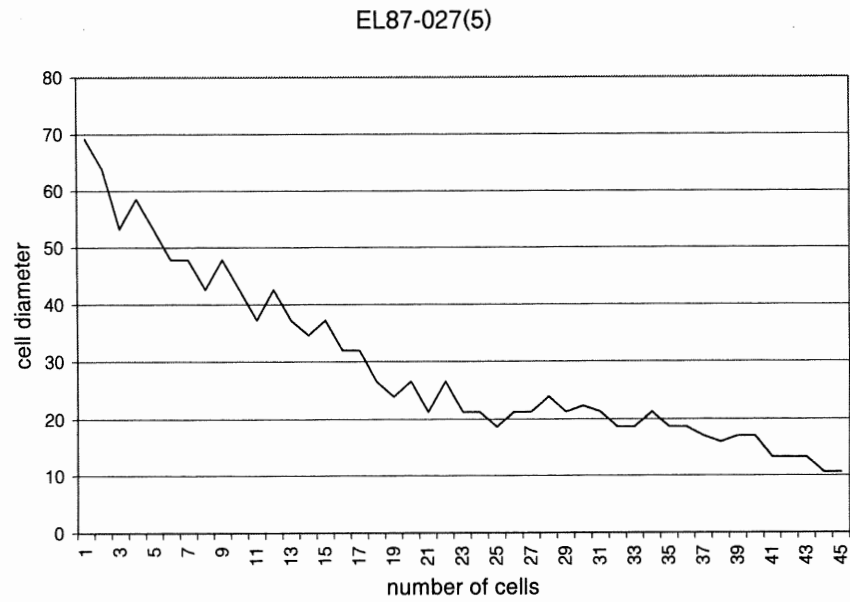
Figure 4.13: On the right are graphs of the cell diameters for two cell files measured along the width of two growth rings. On the left are the two resultant CSDM curves calculated from the cell diameters.
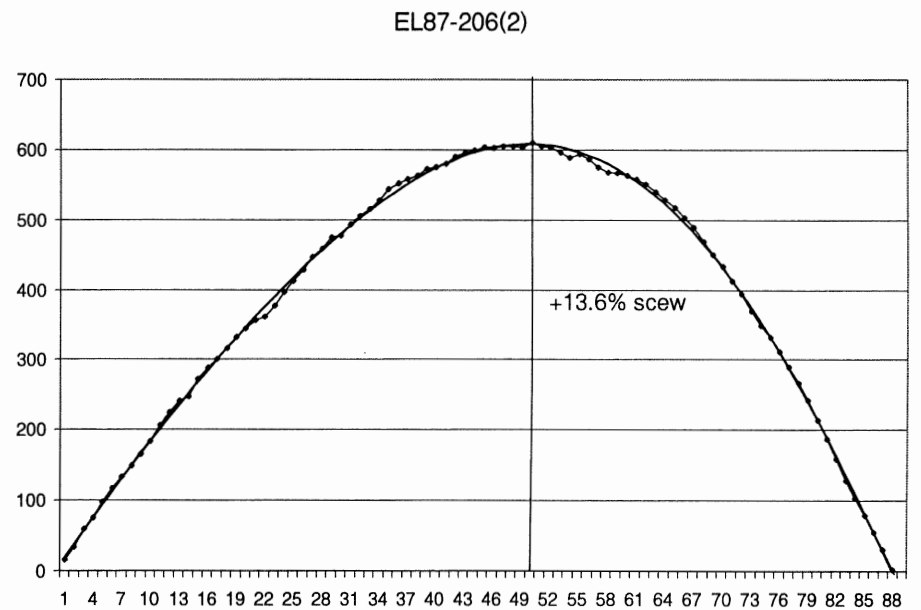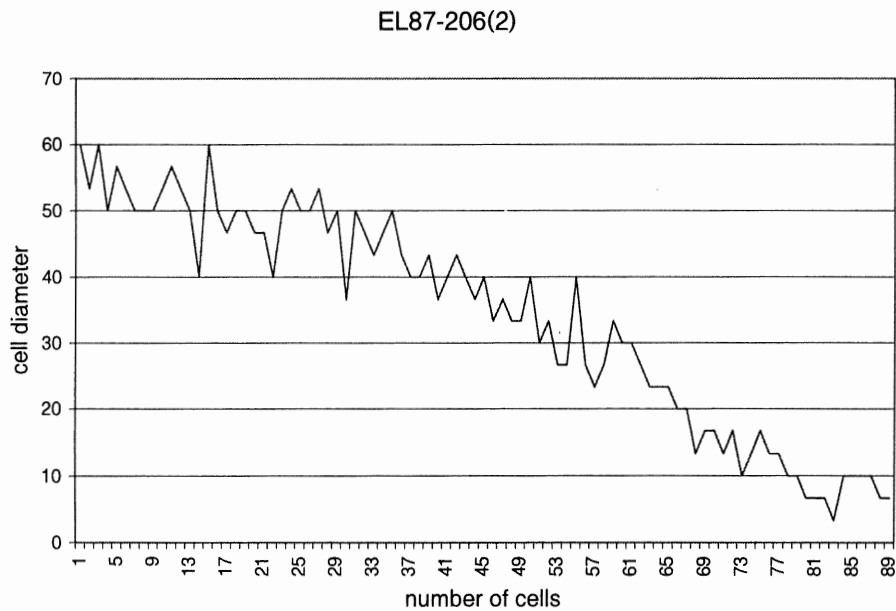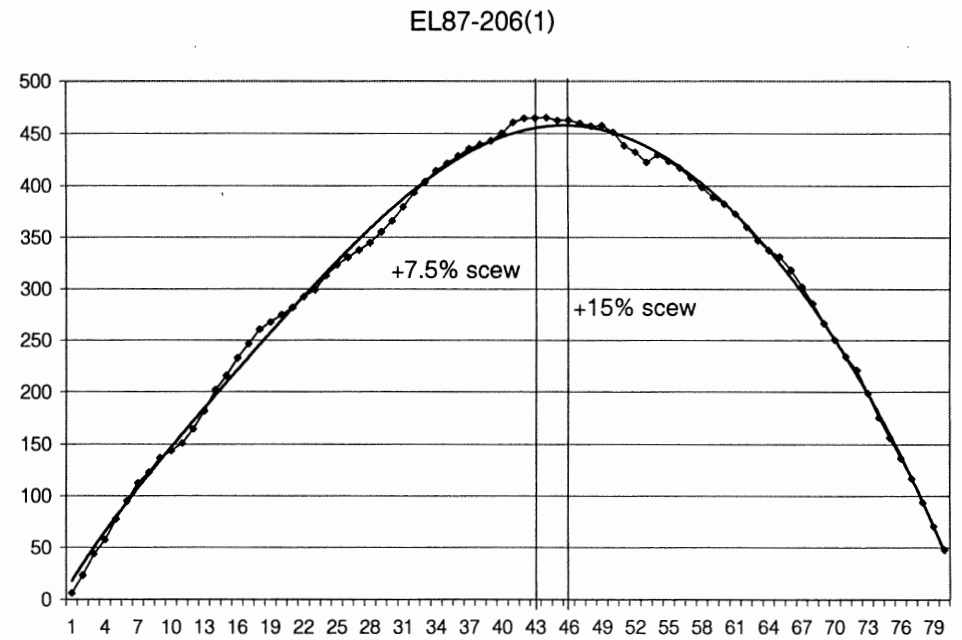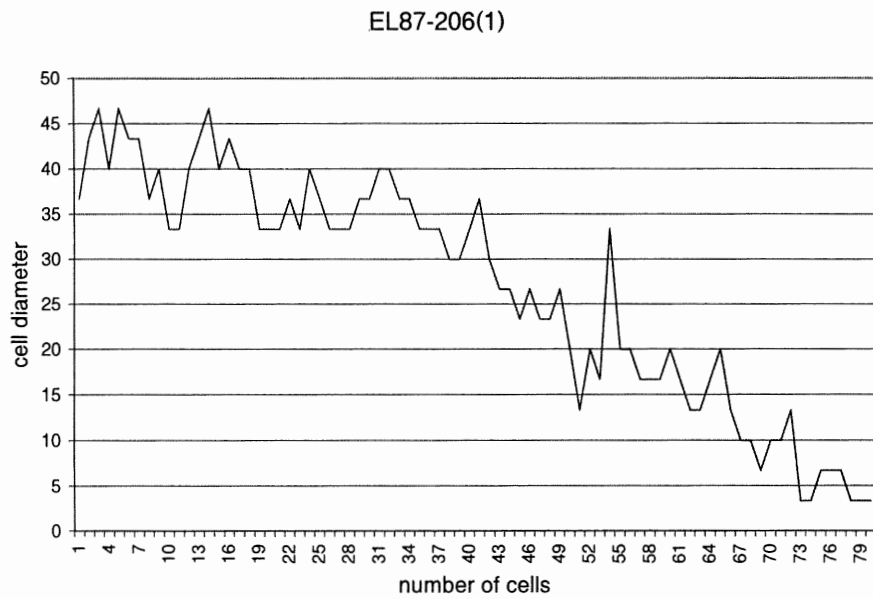
Figure 4.14: On the right are graphs of the cell diameters for two cell files measured along the width of two growth rings in sample EL87-206. On the left are the two resultant CSDM curves calculated from the cell diameters.
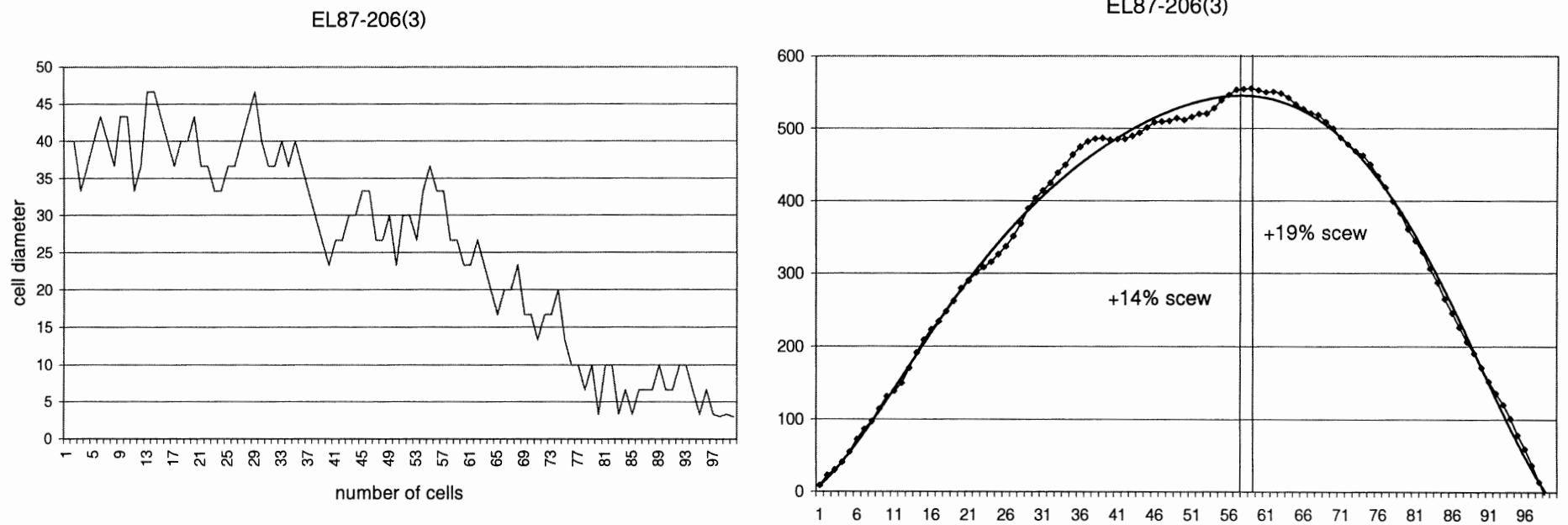
Figure 4.15: On the right are graphs of the cell diameters for two cell files measured along the width of two growth rings in sample EL87-206. On the left are the two resultant CSDM curves calculated from the cell diameters.
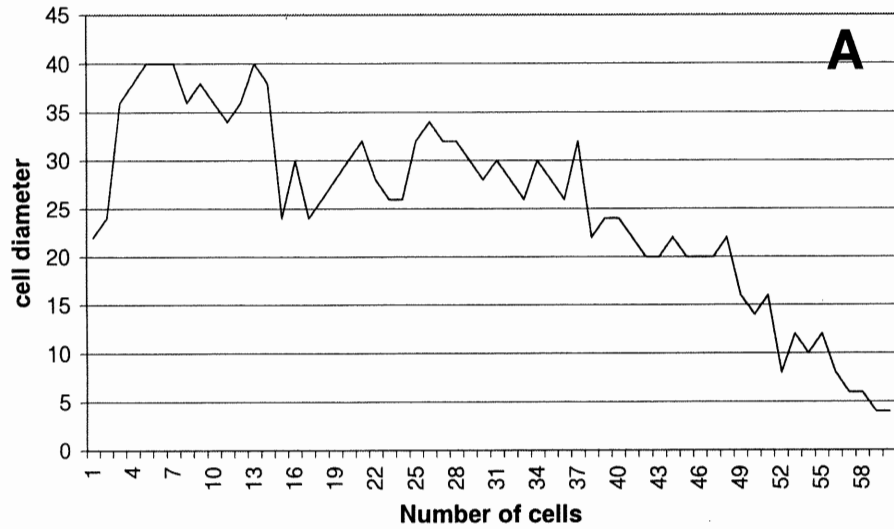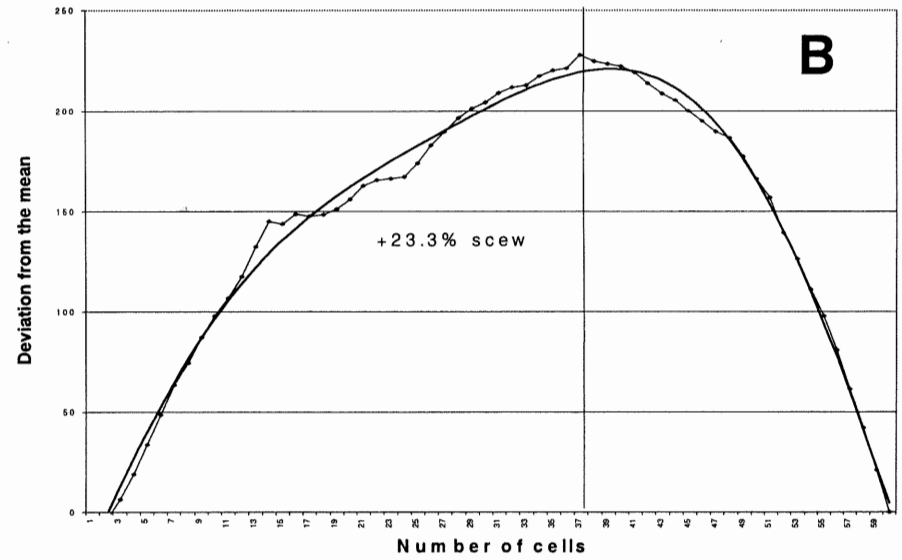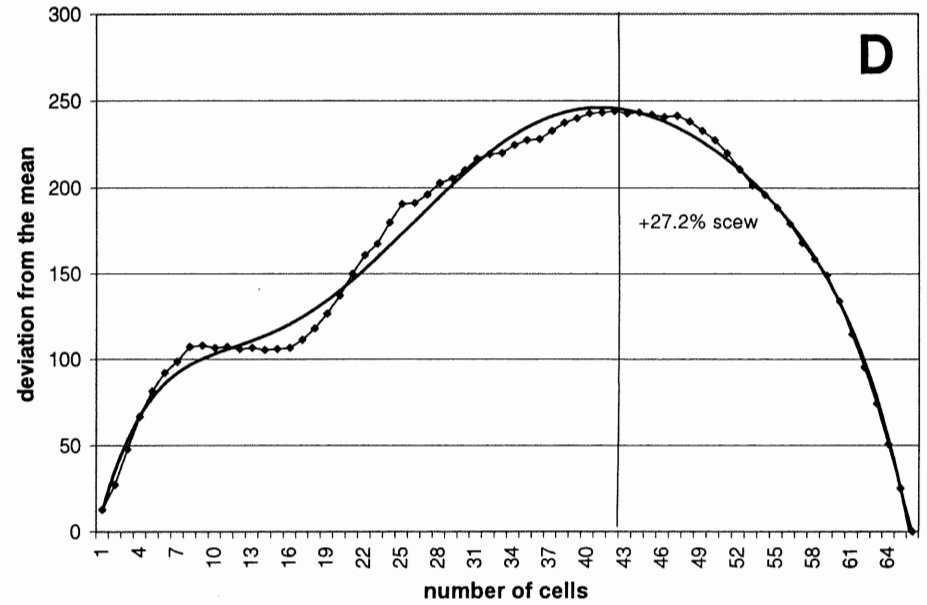
Figure 4.16: On the right (A, C) are graphs of the cell diameters for two cell files measured along the width of two growth rings in sample EL87-257. On the left (B, D) are the two resultant CSDM curves calculated from the cell diameters.
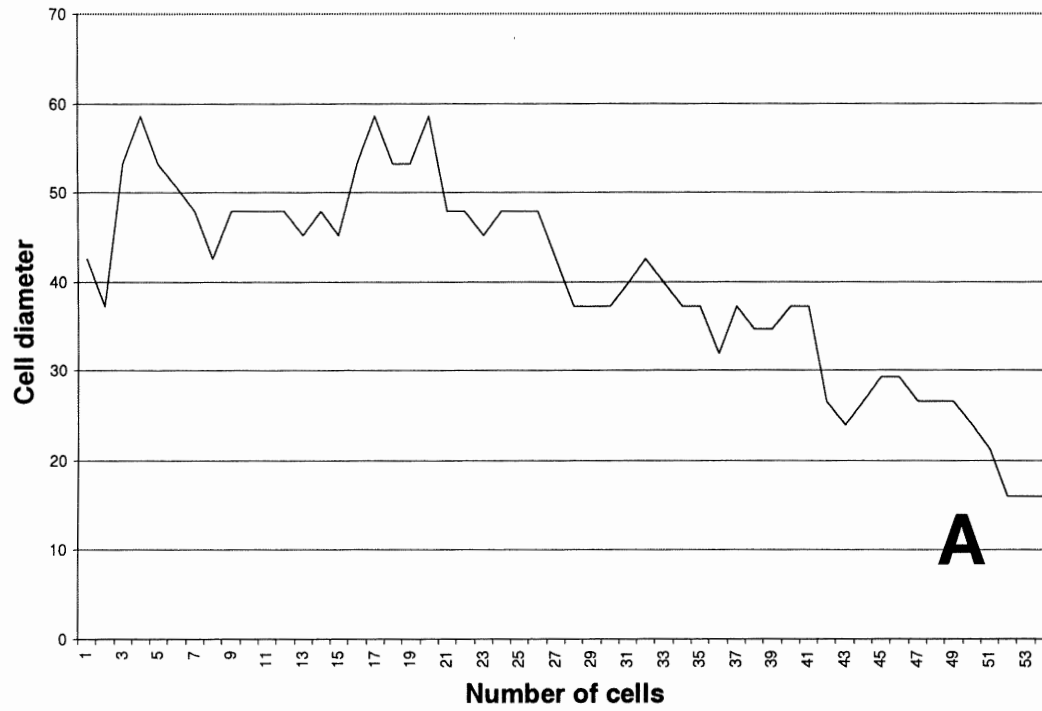
EL87-268
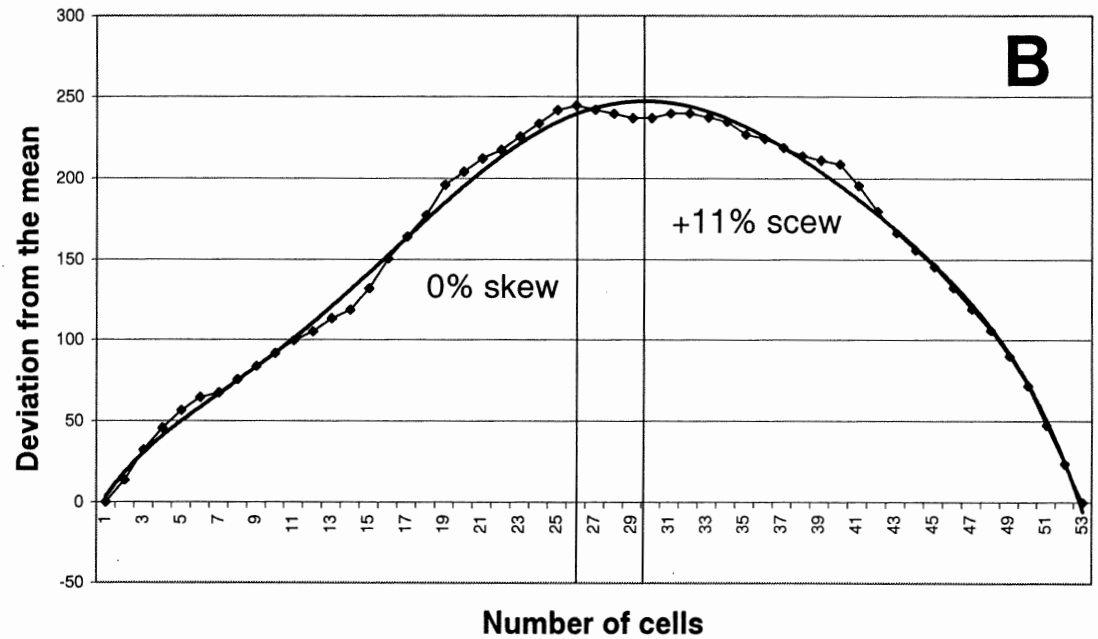
Figure 4.17: CSDM curve for sample EL87-268. (A) is a plot of cell diameter with increasing distance along the growth ring. (B) is the resultant CSDM curve calculated from the cell diameters.
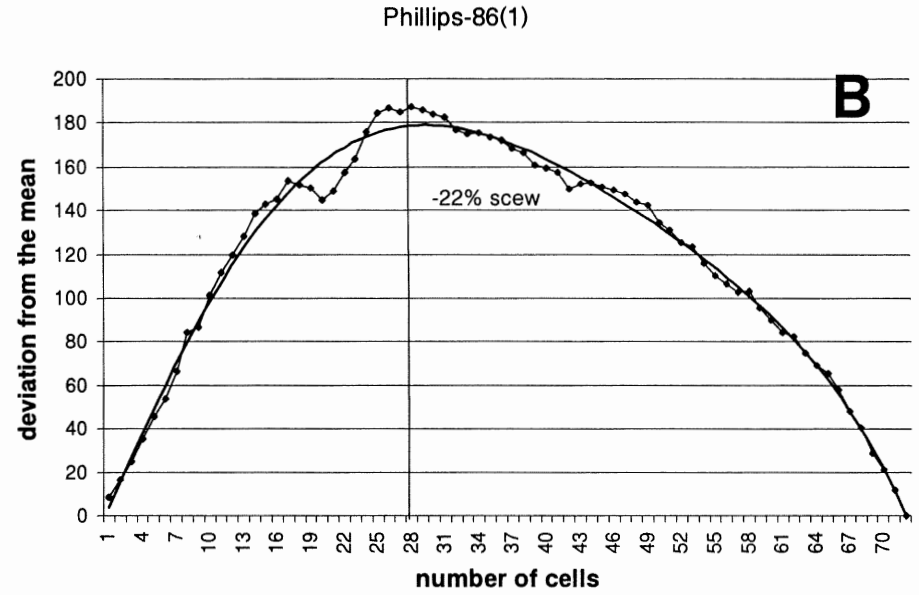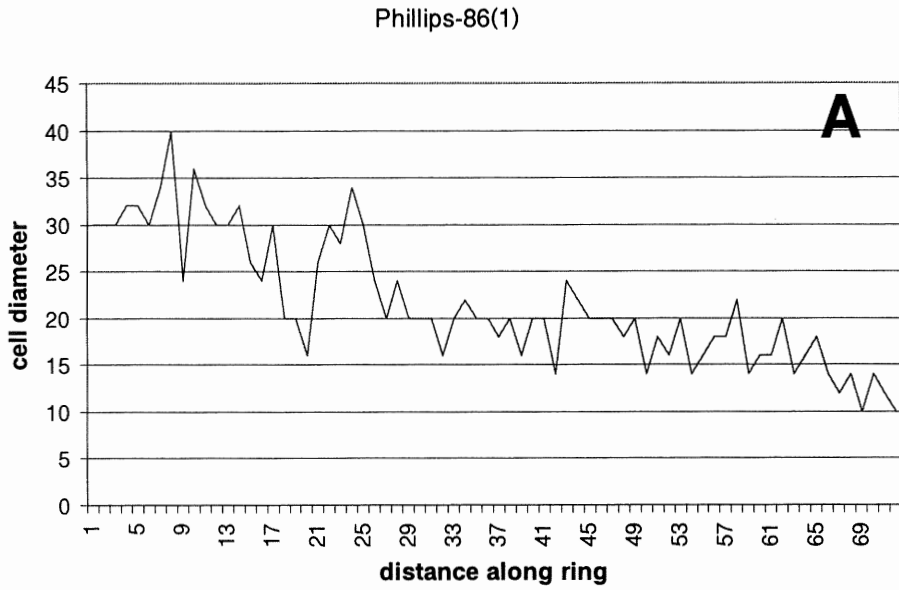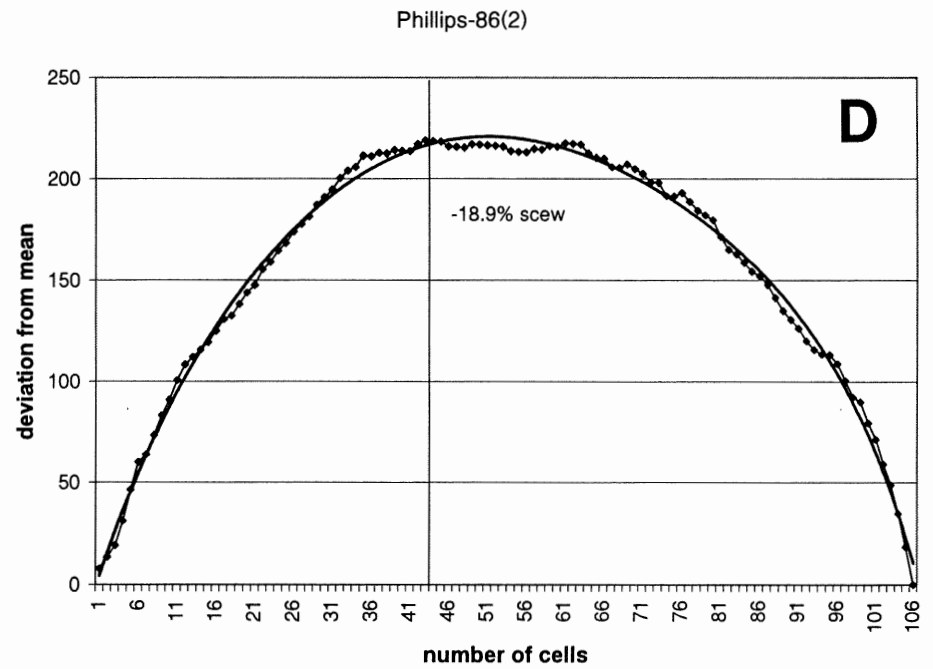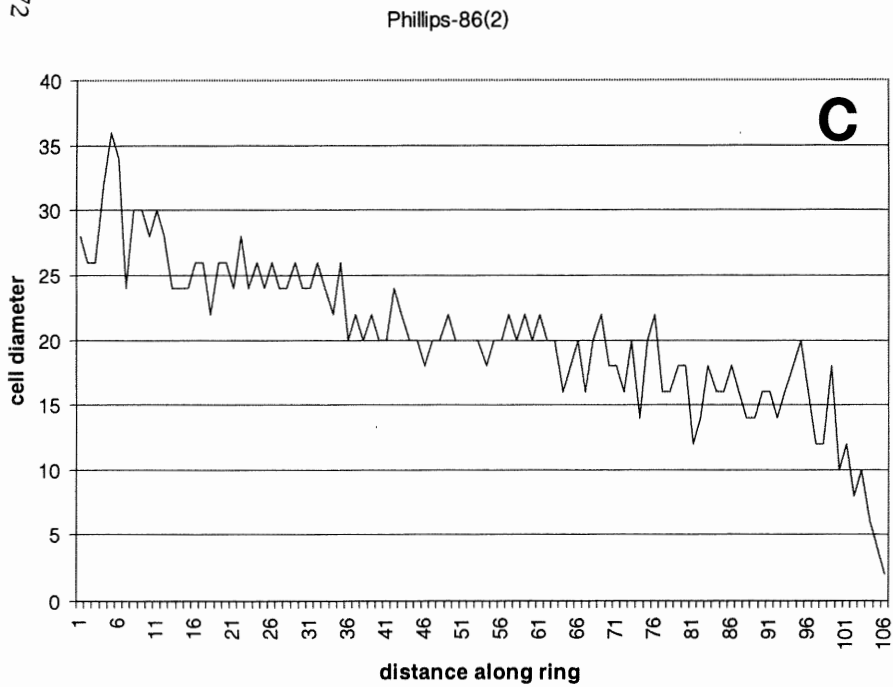
Figure 4.18: On the right (A, C) are graphs of the cell diameters for two cell files measured along the width of two growth rings in sample Phillips-86. On the left (B, D) are the two resultant CSDM curves calculated from the cell diameters.
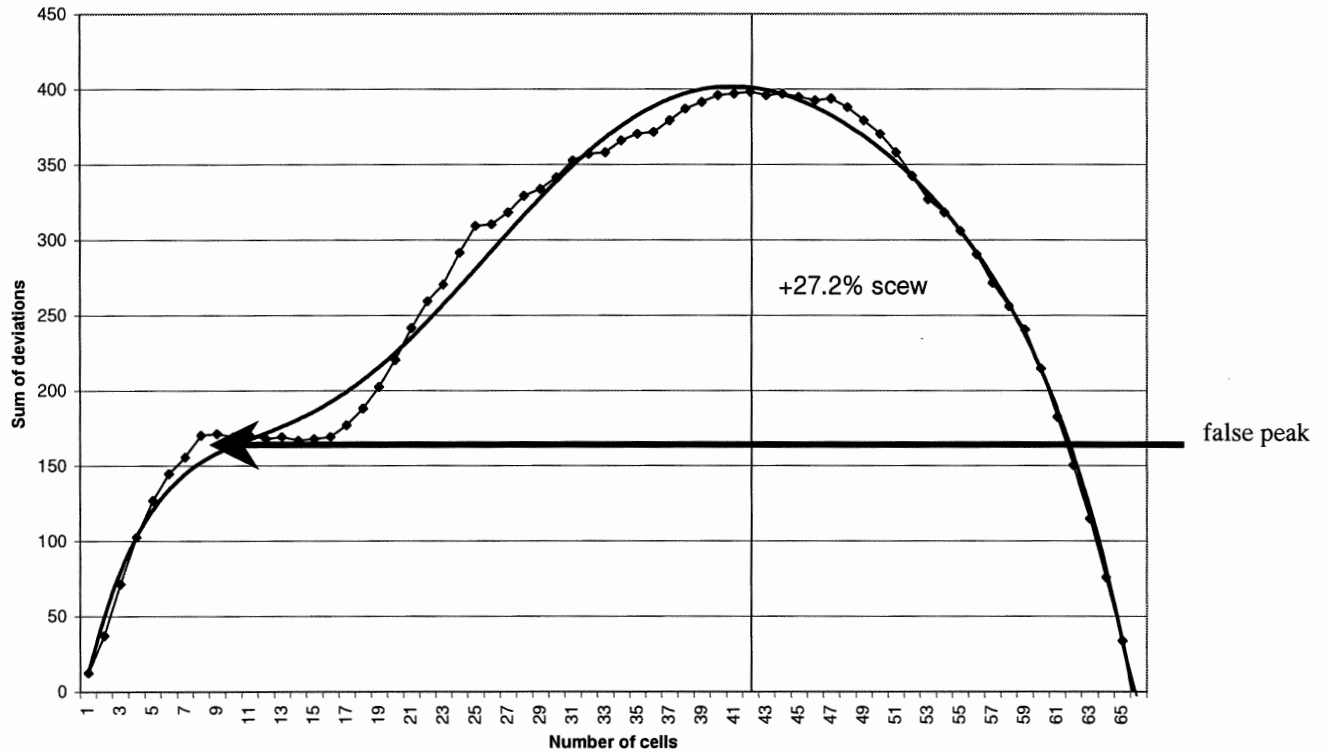
Figure 4.17: The arrow points out a false peak on the CSDM curve, which represents a false ring. You can see where growth stopped before continuing as usual. The Y axis represents the sum of the deviations from the mean and the X axis is the number of cells in the growth ring.
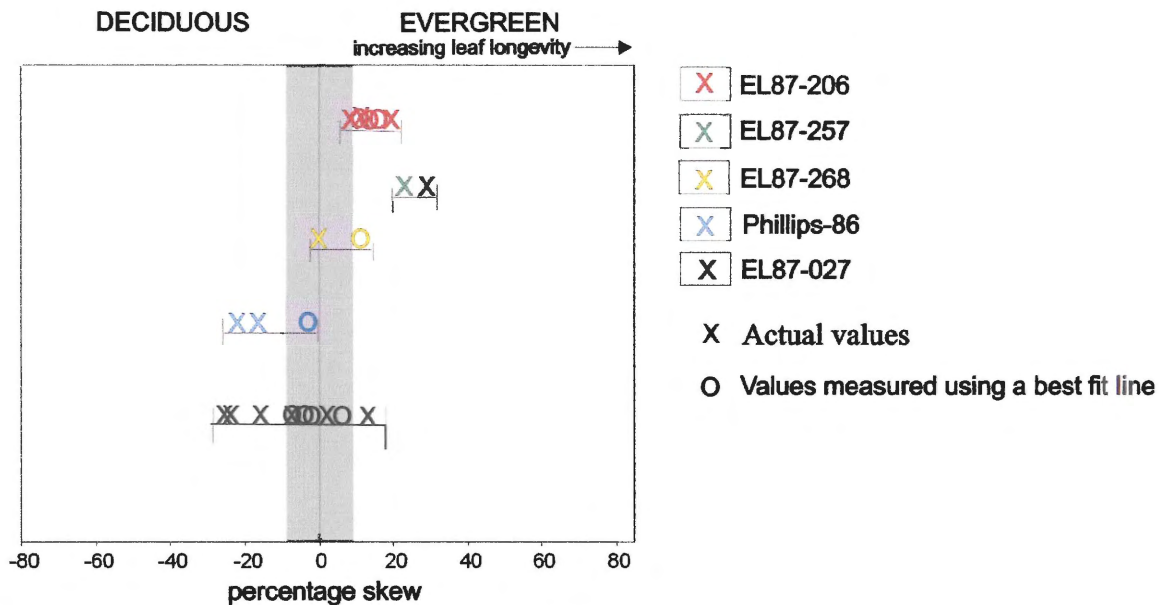
Figure 4.20: Plot of CSDM curve skewness as a function of leaf longevity.

4.3.4 Traumatic rings: false rings and frost rings

False rings form when for some reason growth is interrupted in the tree before continuing on to the end of the year. This could be caused by several factors such as drought in the summer or an early cold period in the autumn or a late cold period in the spring. Frost rings form after a tree has begun its growth for the season when ice crystals form inside the vascular cambium damaging this growth layer (Glerum *et al.*, 1966) After temperatures rise again the vascular cambium begins growing again but can only grow in areas where the cambium is undamaged, thus larger than normal cells are produced to fill the gaps created by the damaged tissue. Figure 4.21 shows some frost rings. Samples EL87-027, EL87-257 and EL87-206 contained false rings. Only EL87-206 had frost rings and that sample contained 8 frost rings in total.
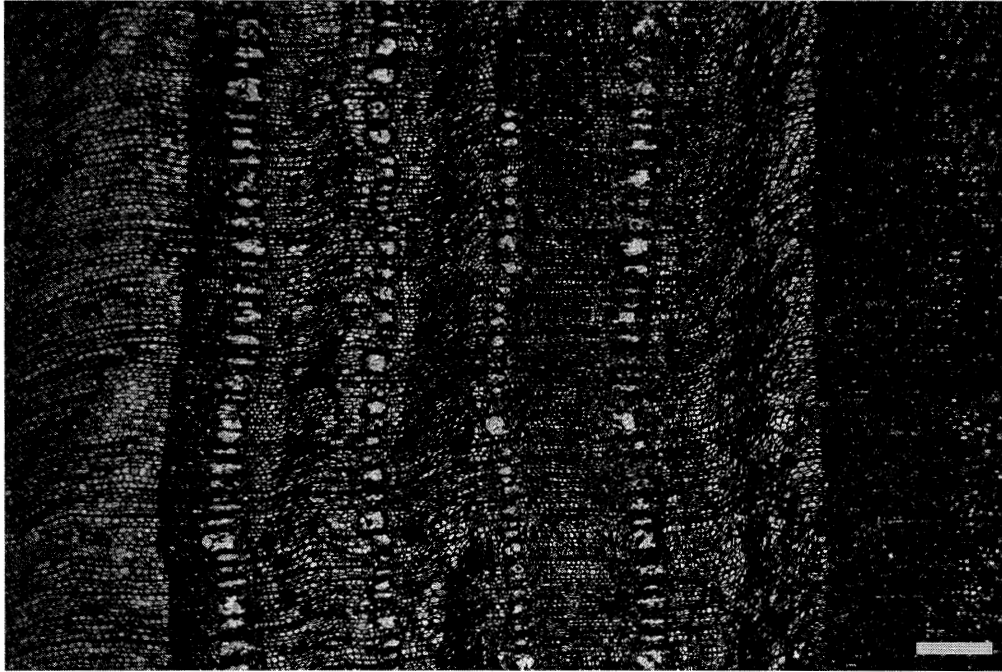
Figure 4.19: Frost rings in sample EL87-206. Scale bar is equal to 200 μm.

4.3.5 Interpretation of tree rings

Growth ring widths for the Ellesmere forest were on average 1-2 mm in diameter. Trees growing in tropical settings tend to not to have growth rings or if they do to have very faint rings. Temperate trees have moderate ring widths with the cooler temperate zones having narrower rings than trees growing in warm temperate or subtropical zones. Even when the seasonal polar light conditions are taken into account tropical trees would still have wider rings since their tracheid cells would maintain a constant size throughout the entire growing season. Other growth ring studies (Creber and Chaloner, 1985) (Table 4.1) suggest that values of 1-2 mm average growth ring widths, like those measured in this study, would indicate temperate growing conditions.

With mean sensitivity values almost all above 0.3 (only one fell below at 0.28) values fall into the disturbed or sensitive category. Falcon-Lang *et al.* (2001) showed that sensitive values tend to occur in braided river settings where tree growth is affected by flooding. This resulted in a short term increase in growth rate followed by a long term decline resulting in irregular growth. Other factors which could lead to high mean sensitivity values would be disturbances such as abundant wildfires. Studies by Falcon-Lang *et al.*, (unpubl. subm.) found abundant charcoal in the Emma Fiord lignite beds indicating that wildfires were not uncommon in the region. Also, as evidenced by the basaltic units, this forest existed in a volcanic environment. Volcanoes can cause short term climate variations by ejecting dust into the atmosphere and blocking solar radiation. This short term cooling, as we will see later in this section, is detectable in the tree ring record. Volcanic eruptions could also be the cause of wildfires resulting in further disturbance. All of these factors could cause disturbances in the forest, however, volcanic eruptions are too infrequent to cause much change in mean sensitivity values. Mean sensitivity values recorded in braided river settings by Falcon-Lang *et al.* (2001) are in the same range as the values recorded in this study. Also, sedimentology for the area (Ch. 2) indicates a alluvial floodplain setting for the fossils, this data suggests that the mean sensitivity values are probably related to flood events.

Features such as false rings and frost rings provide further evidence of disturbance in the environment. False rings form when tree growth is briefly interrupted during

growth. This could be caused by a drop in temperature, a fire or a flood (Falcon-Lang *et al*, 2001). All of these are possible in our environment, however, the flood explanation is probably most likely given the mean sensitivity values discussed above. Frost rings present in sample EL87-206 provide evidence for low temperatures after the growing season has started. The shear abundance of the frost rings (8) in EL87-206 suggests that it was a regular occurrence to have freezing temperatures after growth had started. Trees contain a natural version of anti-freeze in their resin, this natural anti-freeze is different for each species and can withstand different temperatures depending on the species. taxodiaceous conifers, like EL87-206, can withstand temperatures as low as -10 $^{\circ}$C depending on the species. While Pinaceous conifers can withstand temperatures from -20 to –70 $^{\circ}$C. This means that the prevalence of frost rings in EL87-206 is simply a species difference rather than an environmental effect (Sakai and Larcher, 1987). That the frost rings only occur in the Taxodiaceous conifer indicates that temperatures probably went down below -10° C and the lack of frost rings in the Pinaceous conifers tells us that the temperature during these cold spells didn't go below -20° C during frost ring formation (Sakai and Larcher, 1987). This was perhaps caused by warm but short days followed by long nights where temperatures would have had a chance to drop well below zero, such conditions would have existed during the polar spring. Another possibility is that frost rings formed because of the volcanic environment these forests were growing in. Immediately preceding volcanic eruptions there is often a cold spell caused by the volcanic ash and dust ejected into the atmosphere blocking solar radiation from reaching the local area and causing a local cooling effect (LaMarche and Hirschboeck, 1984). These eruptions could be the cause of the frost rings present in our sample.

The CSDM curves indicate that our samples were for the most part deciduous (Fig. 4.20). This is what we would expect from a Northern Hemisphere polar forest (Axelrod, 1984). Read and Francis (1992) noted that when trees are subjected to lack of light for three months, as the Ellesmere forests would have been, they fair better at certain temperatures. Evergreen trees need colder temperatures to cope with the lack of light than deciduous trees. This is because under normal circumstances evergreen trees photosynthesize all year round and do not shut down all growth until it becomes too cold for growth. Deciduous trees on the other hand shut down all growth and go into a kind of

77

hibernation once they drop their leaves until the time comes to start growing new leaves. This means that if winter conditions were relatively warm and dark deciduous trees would have an advantage over evergreen trees. A tree's phenology is determined by its carbon balance: evergreen trees growing under warm dark conditions would respire and lose carbon, deciduous forms would be dormant and would therefore not lose carbon (Beerling and Osborne, 2002). Winter conditions on Ellesmere were probably warm and dark.

5. Discussion

5.1 Palaeoecology of Northwest Ellesmere Island

As we have seen in Chapter 3 wood preserved from the Late Cretaceous-Early Tertiary forests of Ellesmere Island show three distinct genera present in 5 samples and all but one of them Pinaceous. Palynologic data (MacRae unpubl. BSc. thesis, 1989) show that the forests were dominated by taxodiaceous pollen and the leaf litter is comprised predominantly of taxodiaceous foliage (Falcon-Lang, pers. com.). The difference between the wood species, the foliage and the pollen could be because of a provincialism in the plants. The pollen samples and the foliage samples all come from the Emma Fiord locality which is a more mire-like environment and would favor taxodiaceous conifers, while Phillips Inlet is more fluvial in setting, and may have had better soil drainage favoring pinaceous conifers (Fig. 5.1). The fluvial situation may have meant pinaceous trunks were carried down from further upstream during a flood and deposited in a basin along with the local leaf litter. Or, on the other hand, the leaves could have been carried down from upstream to join the local trunks to make up the deposit. Mire settings would also favor the degradation of plants rather than preservation, while a fluvial setting is more favorable to preservation. This flood plain/ peat mire setting is supported by the presence of lignites, cross-bedded sandstones with fining upward sequences and Mean Sensitivity data which indicates a sensitive environment possibly caused by flooding (Falcon-Lang *et al.*, 2001). Both locations are separated in time as well as space and the dominance of pinaceous conifers at Phillips Inlet could have resulted by a shift in vegetation from the Campanian/Maastrichtian of Emma Fiord to the Maastrichtian/Danian of Phillips Inlet. This vegetation shift could have been caused by the warming trend in the Paleocene or possibly by the K/T event.

Even with foliage and palynologic data included the species diversity is quite low a fact which excludes a tropical setting for this forest. It is, however, comparable to other Cretaceous and Tertiary high-latitude forests which also show low species diversity compared with lower latitude forests both modern and ancient (Christie and McMillan,

1991; Falcon-Lang *et al.*, 2001; Spicer and Parish, 1990a; Axelrod, 1984; Creber and Chaloner, 1985; Wolfe, 1979).
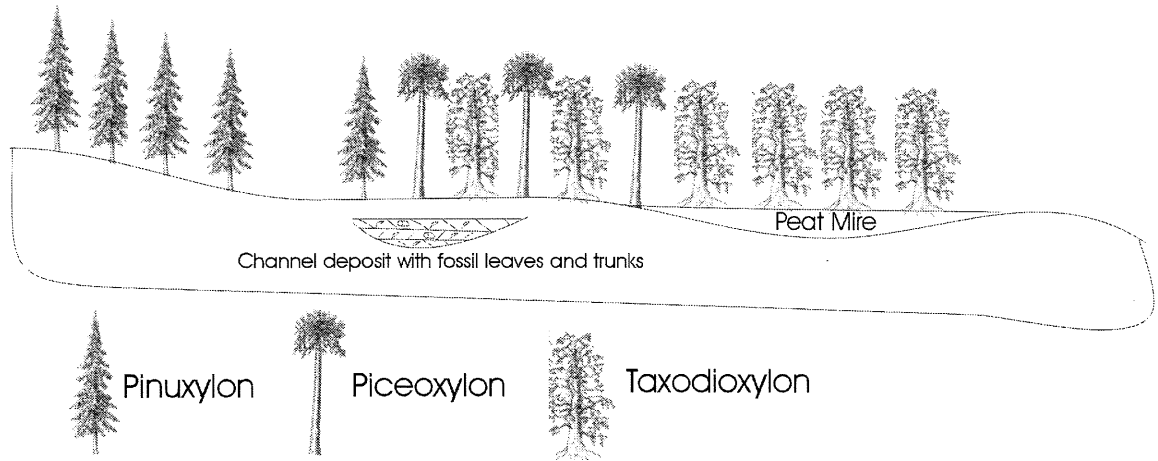
Figure 5.1: A schematic representation of the probable vegetation distribution in the ancient Ellesmere forests.

5.2 Comparison with modern boreal forests

When compared with several different types of modern boreal forests the fossil forests of Ellesmere show similarities with many of the more southerly forests of North America. The most similar modern forests are those of the Pacific Northwest of North America. These forests are known as Low Montane Mixed Coniferous Forest following the classification scheme of Wolfe (1979). The Low Montane Mixed Coniferous Forest, hereafter refered to as the mixed coniferous forest, is dominated by *Pseudotsuga, Tsuga, Pinus, Thuja, Abies, Larix, Sequoia* and *Sequoiadendron* with the similar Asian Mixed Coniferous Forest (Wolfe, 1979) adding *Metasequoia, Glyptostrobus, Taxodium*, and *Taiwania* to the list of conifers. *Picea* and *Abies* dominate true boreal forests with no Taxodiaceous or other deciduous conifers at all and very little *Pinus* and *Cedrus*. Under the classification scheme of the Canadian Forest Service the fossil Ellesmere forest fits into the Pacific Maritime Ecozone (Environment Canada, 2002). The temperature ranges for both these zones indicate a mean annual temperature of approximately 9 ° C and mean winter temperatures of 1-3 °C dropping as low as -15 °C (Environment Canada,

2002). This climate would be quite appropriate to our forest given the growth ring data (Fig.5.2).

5.3 Palaeoclimate implications

Frost rings present at fairly frequent intervals in the Taxodiaceous conifer suggest that this tree was in a climate much cooler than ideal. CSDM data indicates that our trees had fairly low leaf longevity (Fig 4.18). Read and Francis (1992) found that in dark conditions, such as those that would have existed in our forest, deciduous trees cope better than evergreen trees especially if temperatures remain warm during the winter months. Growth ring widths suggest that the Ellesmere forests had a climate that was quite amenable to tree growth as demonstrated by Creber and Chaloner (1985). The presence of frost rings in EL87-206 suggests that temperatures dropped below -10 °C during the growing season, which could be related to local volcanic events. Wood shows a distinct pattern of decreasing tracheid diameter through the course of each growth ring indicating that light, although important, was not the only factor contributing to the sharp growth ring boundaries. The earlywood/latewood transition in the fossil trees is quite abrupt suggesting a strong seasonality for the region much like modern temperate forests. The species that are present while not an absolute indication of paleoclimate does suggest that the climate was temperate. Paleoclimate results based on growth ring data suggests a cool temperate climate much like the climate of southern Canada today.

5.4 Comparison with other Cretaceous polar forests

Polar forests have been found in numerous regions around the world both in the Southern Hemisphere and the Northern Hemisphere. The following two sections will look at these forests and compare them with the forests of Ellesmere Island.

5.4.1 Southern Hemisphere

In the Southern Hemisphere studies have been conducted on the fossil forests of Australia (Douglas and Williams, 1982; Pole, 1999; Pole and Douglas, 1999a; Pole, 2000), New Zealand (Pole and Douglas, 1999b; Thorn, 2001) and Antarctica (Jefferson, 1982; Cantrill, 2000; Falcon-Lang and Cantrill, 2000; Poole *et al.*, 2001).

The polar forests of Australia were located at between 70-85°S paleolatitude in the Cretaceous (Douglas and Williams, 1982). Vegetation in these forests was dominated by conifers consiting of Araucariaceae, Podocarpaceae and some Taxodiaceae (Pole, 2000). Benettitales, Ginkgoales and Filicales (Pole and Douglas, 1999a) are the other dominant species present in the area (Douglas and Williams, 1982). Climates for the region as suggested by Douglas and Williams (1982), based on a nearest living relative (NLR) approach, and Pole (2000), based on foliage are temperate for the duration of the Cretaceous. Climate for the Australian forests was similar to the climate of the Ellesmere forests, which existed at similar latitudes. Differences consist in the types of plants, although both Ellesmerian and Australian forests seem to have had a similar species diversity. Present in the Australian forests were araucarian, podocarp and taxodiaceous conifers while the Ellesmere forests were entirely taxodiaceous and pinaceous. This vegetation difference is partly hemispheric in origin since pinaceous conifers are not found in the Southern Hemisphere and araucarian and podocarp conifers are exclusively Southern Hemisphere varieties. Australian forests contain mostly evergreen species while the Ellesmere forests contain a more deciduous flora. This is perhaps because the Southern Hemisphere may have had a more continental climate with much cooler winters and hotter summers than the Northern Hemisphere forests. In the polar winter forests would have to be able to survive for 3 months with no light. Under normal light conditions trees respire when it is dark. For deciduous trees three months of darkness would present no great challenge for once they drop their leaves deciduous trees hibernate for the winter to conserve energy. If temperatures are warm evergreen trees do not go dormant and so would continue to respire for the entire three month period and use up all their stored energy, just like a solar battery. If temperatures are cold evergreen trees will go dormant conserving their energy until it is warm and light again and since they do

not have to regrow their leaves evergreen trees can begin to photosynthesize immediately, giving them an advantage over deciduous trees. Average ring width in the Australian forests ranged from 0.34 to 4.53 mm, with an overall mean of 2.23 mm (Frakes and Francis, 1990). Mean sensitivities for these woods fell, for the most part, into the complacent category with values ranging from 0.104 to 0.366 (Frakes and Francis, 1990). Frakes and Francis (1990) found two different populations of trees in Australia. One population had very narrow tree rings (0.34-0.92 mm) and were interpreted as having grown in a cold-temperate setting. The other population had moderate growth ring widths (1.17-4.53 mm) indicating a warm-cool temperate setting for these trees. Frakes and Francis (1990) also found that both populations occurred in the same stratigraphic unit indicating that trunks and branches from the smaller ringed population may have been transported downstream from cooler high latitudes. The low mean sensitivity values indicate that there was little disturbance in this environment, climatic or otherwise (Frakes and Francis, 1990). The forests of Ellesmere Island had average ring widths between 1-3 mm suggesting that they grew under similar climatic conditions to the second Australian population under a warm-cool temperate setting. Higher mean sensitivity values suggest that the Ellesmere forests grew under much more variable conditions than the Australian forests.

In New Zealand the fossil forests are similar to those found in Australia and existed at paleolatitudes of 75-78 °S (Thorn, 2001). New Zealand forests are dominated by Araucariaceae, Podocarpaceae and Taxodiaceae (Pole and Douglas, 1999b). Climate in the Middle Jurassic of New Zealand as suggested by Thorn (2001) was interpreted as a humid warm temperate climate. Since the Mid Jurassic is similar in mean temperatures to the Cretaceous it is not unreasonable to make comparisons (Spicer and Chapman, 1990). Vegetation for the Middle Jurassic forests of New Zealand is similar to the Cretaceous vegetation of Australia, Antarctica and New Zealand, other than a lack of angiosperms, and is made up of Araucariaceae, Podocarpaceae and Taxodiaceae and like the forests of Australia is mostly evergreen. Cretaceous forests of New Zealand have been identified by Pole and Douglas (1999b) and contain the same conifer types as the Mid Jurassic forests, however, the Cretaceous forests have begun to be taken over by angiosperms. Conifers are still dominant even in the Late Cretaceous of New Zealand as

83

well as Ginkgoales and the conifers of the New Zealand forests like those of Australia and unlike the forests of North America are dominantly evergreen (Pole and Douglas, 1999b). Forests in New Zealand in the Late Cretaceous have much more in the way of angiosperms than the forests of Ellesmere Island.

The forests of Antarctica are found mostly on the peninsula that stretches out towards the tip of South America. These forests existed at paleolatitudes of 70-75°S and enjoyed a cool temperate climate much like the modern Southern Hemisphere forests of New Zealand (Falcon-Lang and Cantril, 2001; Cantrill, 2001). Vegetation in the Antarctic forests consisted of araucariaceous, podocarpaceous and taxodiaceous conifers like the polar forests of Australia and New Zealand and like those forests were dominantly evergreen (Falcon-Lang and Cantrill, 2000). Polar forests continued to thrive in Antarctica in the Eocene with little change in the dominant vegetation other than the addition of more angiosperm species (Poole *et al*., 2001). Growth rings of conifers growing in Antarctica had maximum ring widths between high as 1.12 and 7.78 mm with mean rings widths between 0.401 mm and 3.58 (Jefferson, 1982). Ring widths on Ellesmere Island had maximum widths between 5.3 and 8 mm with mean widths between 1.2 and 2.8 mm. Mean sensitivity values for the Antarctic forests range from 0.029 to 0.739 with most values falling between 0.3 and 0.5 (Jefferson, 1982). These values, especially those from Jefferson's (1982) Titan Nunatak sites are quite similar to the values of 0.28-0.46 recorded for the fossil wood of Ellesmere Island.

In general the Southern Hemisphere polar forests existed in a temperate climate and were dominated by evergreen araucariaceous, podocarpaceous and taxodiaceous conifers. Vegetation in our Northen Hemisphere Ellesmere Isand forest was taxodiaceous and pinaceous in composition. Modern pinaceous conifers are an exclusively Northern Hemisphere species just as Podocarps and Araucarians are Southern Hemisphere conifers thus the Cretaceous forest vegetation reflects the situation that exists today. One difference that cannot be explained by the simple Southern Hemisphere/Northern Hemisphere dichotomy is the dominance of evergreen vegetation in the Southern Hemisphere as opposed to deciduous vegetation in the north. Read and Francis (1992) proved that trees can survive the 2.5 months of darkness which would have been winter conditions for these polar forests. They also demonstrated that deciduous trees coped

better with the dark months than evergreen trees did. This information suggests that deciduous trees should be more competitive in the polar biome than evergreen trees. Falcon-Lang and Cantrill (2001) suggest that the proximity of the Gondwanan supercontinent would have dropped temperatures well below 0°C initiating winter dormancy in the trees. Also high CO_2 concentrations would have aided in reducing dark respiration in trees enabling the evergreens to cope better with the dark winters. Even so under warm dark conditions such as those that would have existed in the Cretaceous and Tertiary winters of Ellesmere Island evergreens would respire more and lose carbon. In the colder more continental Southern Hemisphere temperatures would have dropped enough to stop dark respiration in evergreens negating any advantage of being deciduous (Beerling and Osborne, 2002).

5.4.2 Northern Hemisphere

In the Northern Hemisphere polar forests have been found in Russia (Herman and Spicer, 1995), Alaska (Parrish and Spicer, 1988b; Spicer and Parrish 1990a; Spicer and Parrish, 1990b; Spicer and Herman, 2001), Greenland (Boyd, 1992), and the Canadian Arctic (Christie and McMillan, 1991; LePage and Basinger, 1991a,b; Francis and McMillan, 1987; Kumagai *et al.*, 1995; Francis, 1988; Jahren and Sternberg, 2002).

The Koryak flora of northeastern Russia is dated as being from the Middle Maastrichtian and shows vegetation as consisting of taxodioid and cupressoid conifers with some Pinacioid as well as abundant angiosperm flora (Herman and Spicer, 1995). While seldom dominant, conifers are mostly *Metasequoia*. Compared with the Ellesmere Island locality the Russian forests have a more diverse flora and contain considerably fewer conifers. Trees in the Russian forests were dominantly deciduous which is similar to the Ellesmere forests (Herman and Spicer, 1995). The higher diversity and lesser numbers of conifers suggest a climate for the Russian forests much warmer than that of Northwest Ellesmere. Abundant mollusc beds in the strata of the Koryak Subformation along with the plant fossils hint at a coastal setting for the Russian forests (Herman and Spicer, 1995). Perhaps the temperature regulation provided by the nearby ocean provided a warmer climate for the Russian forests resulting in the higher diversity.

Cretaceous Alaska was located at 75-85° N paleolatitude and was probably the closest landmass to the North Pole (Parrish and Spicer, 1988b). During the Albian-Cenomanian period taxodiaceous conifers dominated the Alaskan forests along with Ginkgoales and ferns (Spicer and Herman, 2001) with rare angiosperms these forests were also dominantly deciduous. Fossils from the Latest Cretaceous of Alaska are also dominantly taxodiaceous with and mostly deciduous (Spicer and Parrish, 1990a). The widest growth rings in trees from Alaska was measured at 5.88 mm with mean rings widths as high as 3.51 mm with mean sensitivities for the forests ranged from 0.10 to 0.77 with a mean of 0.4 (Spicer and Parrish, 1990a). Spicer and Parrish (1990a) also suggest that the high mean sensitivities are the result of river proximity and flooding. Based on fossil leaf data Spicer and Parrish (1990a) estimate a mean annual temperature of 2-6° C this is within the cool temperate range and well within the estimates for Northwest Ellesmere. Growth ring data compares well with the data for Ellesmere Island as does the climatic data obtained by Spicer and Parrish (1990a). Species diversity, at least from the Kogosukruk Tongue, is similarly low and the abundance of taxodiaceous conifers and deciduousness of the forest compares quite well to the Emma Fiord locality.

Fossil forests have been identified from western Greenland that would have existed at a paleolatitude of 65° N and contain a diverse flora consisting of all types of coniferales, mostly taxodioid and cupressoid, Ginkgoales and some Cycadales (Boyd, 1992). Taxodiaceous conifers are most similar to modern *Sequoia* and *Sequoiadendron* and most conifer species are deciduous this compares well with our data from Ellesmere Island. Paleoclimatic data, based mostly on species present, indicates an environment much warmer than that of our Ellesmere Island forests (Boyd, 1992); the lower latitude could play a role in this milder climate as well as the nearness of the Greenland forests to the ocean.

Fossil forests of the Canadian Arctic have been given sporadic attention since they were first identified on Ellesmere Island in 1883 by the ill fated Greely expedition of which only 15 of the original 24 members made it back alive. Other than the odd paper on fossil wood there has been no detailed studies conducted on the fossil forests of the Canadian Arctic other than work conducted by the GSC and others on the Eocene forests of Axel Heiberg Island. Paleolatitudes for the Cretaceous and Early Tertiary of the

Canadian forests are between 74-82° N (Irving and Wynne, 1991). During the Late
Cretaceous taxodiaceous and cupressaceous conifers dominate the Canadian Arctic fossil
forests with rare pinaceous conifers (Bannon and Fry, 1957). In the Tertiary pinaceous
conifers begin to become more abundant with species like *Larix* and a *Pseudotsuga* like
species found in the Axel Heiberg forests (Christie and McMillan, 1991), both the
Cretaceous and Tertiary forests are dominated by deciduous species. Mean ring widths
for trees from Strathcona Fiord (Southern Ellesmere Island) are between 0.44 and 3.06
mm with a maximum ring width of 5.89 mm comparable to numbers obtained for our
Ellesmere Island forest (Kumagai *et al.*, 1995). Kumagai *et al.* (1995) found mean
sensitivity values range from 0.2-0.4 with an average of 0.3 falling into the sensitive
category, although, they interpret the sensitivity as being climate influenced.
Paleoclimate estimates for the Canadian polar forests put them in a warm-cool temperate
environment according to Francis (1988). Other Canadian Arctic fossil forests compare
quite well with the forests from our Ellesmere Island sites.

In general Northern Hemisphere forests are more deciduous, contain more
angiosperms and much more taxodiaceous conifers than the Southern Hemisphere.
Climates for the two Hemispheres appear to have both been temperate, although the
Southern Hemisphere does appear to have been slightly cooler than those of the north
perhaps because the Southern Hemisphere forests were more continental in their climates.
The fossil forests of Northwest Ellesmere Island are quite similar to those of Alaska and
the rest of the Canadian Arctic, however they differ quite a bit from those of Russia and
Greenland, the later two probably having warmer climates since they have a higher
diversity and many more angiosperms. One interesting thing to note is that although false
rings are common there is no mention of frost rings appearing in any of the other
Northern Hemisphere forests we have compared our forests to. This could be climatic in
nature, though this is unlikely as the Alaskan forests were growing at a higher
paleolatitude than our forests. The more probable explanation is that some local effect
dropped the temperature briefly at our location but was not widespread enough to affect
the other fossil forest sites. With the proximity of the basalt flows the most likely cause
would have been a volcanic eruption that would have thrown ash into the air reducing the
incoming solar radiation and producing a local cooling effect.

5.5 Present-day global change: "the past is the key to the future"

Everyday in the news we hear some story about global warming or climate change, but what does all this mean really? There is no doubt that climate is indeed changing and that CO_2 levels have increased in recent years, but this is not a new thing. During the Cretaceous and Tertiary greenhouse periods CO_2 levels were 1000-2000ppm (Retallack, 2001) well above current levels and as a result temperatures were higher. Evidence of this is present in Northwestern Ellesmere Island where fossil forests remind us of a time when the poles were lush temperate rainforests teaming with life instead of the frozen Tundra of today, but why is this important to know? Predictions by the Intergovernmental Panel on Climate Change indicate an atmospheric CO_2 concentration of 450-800ppm by the year 2100 (Beerling, 1998). The high end of this estimate is only 200ppm less than the minimum estimate for CO_2 during the Cretaceous and Early Tertiary. This means that things will be getting warmer in the Arctic pushing the tree line further north and causing further warming as the albedo effect is reduced. We know from studies of fossil polar forests that trees can indeed cope with low polar light levels, that higher CO_2 levels enable trees to survive colder temperatures and prolonged darkness. We also know what sorts of conditions used to exist in earth's history and what we can expect in the future if current trends continue. In short the past is indeed the key to the future for we may find polar forests are no longer a thing of the past.

6. Conclusions

6.1 Conclusions

- Five samples of fossil wood from Northwestern Ellesmere Island were examined. Of the five, two samples from Emma Fiord consisted of a taxodiaceous conifer (*Taxodioxylon albertense*) and a pinaceous conifer (*Piceoxylon ellesmerensis*).
- The three fossil woods from Phillips Inlet consisted entirely of pinaceous conifers, *Pinuxylon woolardi* and *Pinuxylon gemenii*.
- CSDM curves indicate that trees were mostly deciduous probably in response to the warm dark winter months.
- Ring width data suggests a temperate climate much like that of British Columbia today.
- This interpretation is further supported by a comparison of the composition of the fossil forest with modern forests, which indicates that the Ellesmere Island fossil forests were similar to those forests growing in NW British Columbia today.
- Mean Sensitivity data suggest a moderately disturbed environment, perhaps relating to a river flood plain, wildfires or volcanic disturbences.
- The river flood plain interpretation is supported by sedimentological data.
- Frost rings and false rings suggest that growing conditions in the fossil forests were periodically interrupted.
- False rings are probably the result of occasional floods, frost rings on the other hand probably are formed in response to local cooling caused by nearby volcanic eruptions.

6.2 Future work

Many questions have been answered by this work both on the palaeobotany and the palaeoclimatology of the area. Many questions have also been raised by this work: are

the wood types present different from the foliage and pollen? Does the mean sensitivity data truly reflect periodic flooding? Further work is also needed to answer the broader climatic questions posed by this work. It is impossible to form a true climatic picture of the Arctic with samples from such a relatively small area. According to the GSC Memoir of Fortier *et al.* (1963) the Canadian Arctic Archipelago contains numerous fossil forests sites not just limited to a few isolated localities. These forests range from the Triassic to the Eocene spanning almost the entire range of time that fossil forests existed. In the NW Ellesmere Island region alone work that needs to be done includes: A detailed sedimentological study of the Hansen Point Volcanics. It would be useful to collect fossil woods from throughout the region and from many difference ages to give us a broader understanding of the climate and vegetation changes, which have occurred. Detailed foliage work and palynology would add to the data that should be collected. Further palynological studies and further whole rock $^{40}Ar/^{39}Ar$ could help us resolve the Campaninan vs. Maastrichtian age conflict discussed by MacRae (1989, unpubl. BSc. thesis). In the rest of the Canadian Arctic work which could be done would be a comprehensive study of fossil plant material for the entire Canadian Arctic providing a picture of the entire Triassic-Eocene ecology of the region. Climatologic studies could increase our understanding not only of the palaeoclimate of the Arctic, but of the entire Greenhouse World period. In short there is much work to do if we wish to truly understand what may become the Greenhouse World of tomorrow.

References

Alaska Climate Research Center. (2002, March, 19). *Instrumental Climate History for Alaska*. [wwwdocument] URL. http://climate.gi.alaska.edu/history/History.html

Arne, D.C., Zentilli, M., Grist, A.M., Collins, M. 1998. Constraints on the timing of thrusting during the Eurekan orogeny, Canadian Arctic Archipelago: an integrated approach to thermal history analysis. Canadian Journal of Earth Sciences, **35**: 30-38.

Arne, D.C., Grist, A.M., Zentilli, M., Collins, M., Embry, A., Gentzis, T. 2002. Denudation of the Sverdrup Basin during the Tertiary Eurekan Orogeny: implications for hydrocarbon prospectivity. Basin Research, in press (June 2002).

Axelrod, D.I. 1984. An interpretation of Cretaceous and Tertiary biota in polar regions. Paleogeography, Paleoclimatology, Paleoecology, **45**: 105-147.

Bannon, M.W., Fry, W.L. 1957. Three Cretaceous woods from the Canadian Arctic. Canadian Journal of Botany, **35**: 327-337.

Barnola, J.M., Raynaud, D., Korotkevich, Y.S., Lorius, C. 1987. Vostock ice core provides 160,000-year record of atmospheric CO_2. Nature, **329**: 408-414.

Barron, E.J. 1983. A warm, equable Cretaceous: the nature of the problem. Earth Sci. Rev. **19**: 305-338.

Basinger, J. F. 1991. The fossil forests of the Buchanan Lake Formation (Early Tertiary), Axel Heiberg Island, Canadian Arctic Archipelago: preliminary floristics and paleoclimate. *In* Christie, R.L., McMillan, N.J. *editors* Tertiary Fossil Forests of the Geodetic Hills Axel Heiberg Island, Arctic Archipelago. Geological Survey of Canada Bulletin, **403** pp. 39-65.

Beerling, D.J. 1998. The future as the key to the past for paleobotany?. Trends in Ecology and Evolution, **13** (8): 311-316.

Beerling, D.J. 1999. Long-term responses of boreal vegetation to global change: an experimental and modelling investigation. Global Change Biology, **5**: 55-74.

Beerling, D.J., and Osborne, C.P. 2002. Physiological ecology of Mesozoic polar forests in a high CO_2 environment. Annals of Botany, in press (March 2002).

Betts, R.A. 2000. Offset of the potential carbon sink from boreal forestation by decreases in surface albedo. Nature, **408** (6809): 187-190.

Boyd, A. 1992. Revision of the Late Cretaceous Pautut flora from West Greenland: Gymnospermopsida (Cycadales, Cycadeoidales, Caytoniales, Ginkgoales, Coniferales). Palaeontographica, **225**: 105-172.

Cameron, B.I., Muecke, G.K. 1996. Permian alkaline basalts associated with formation of the Sverdrup Basin, Canadian Arctic. Canadian Journal of Earth Sciences, **33**: 1462-1473.

Cantrill, D.J. 2000. A petrified cycad trunk from the Late Cretaceous of the Larsen Basin, Antarctica. Alcheringa, **24**: 307-318.

Cantrill, D.J. 2001. Cretaceous high-latitude terrestrial ecosystems: an example from Alexander Island, Antarctica. Asociacion Paleontologica Argentina. Publicacion Especial, **7**: 39-44.

Chen, Z., Osadetz, K.G., Embry, A.F., Gao, H., Hannigan, P.K. 2000. Petroleum potential in western Sverdrup Basin, Canadian Arctic Archipelago. Bulletin of Canadian Petroleum Geology, **48**: 323-338.

Chongyang, C., Jianhua, J., Chuangjian, Z., Runquan, L., Heqing, L. 1996. On the occurrence of fossil wood in Dongguan, Guangdong. Zongshan Daxue Xuebao, **35**: 90-95.

Christie, R.L., McMillan, N.J. 1991. *editors* Tertiary Fossil Forests of the Geodetic Hills Axel Heiberg Island, Arctic Archipelago. Geological Survey of Canada, Bulletin, **403**.

Creber, G.T. 1975. The effects of gravity and the Earth's rotation on the growth of wood. *In* Rosenberg, G.D., Runcorn, S.K. *editors* Growth rhythms and the history of the Earth's rotation. John Wiley & sons, pp. 75-87.

Creber, G.T. 1977. Tree rings: a natural data-storage system. Biological Review, **52**: 349-383.

Creber, G.T., Chaloner, W.G. 1985. Tree growth in the Mesozoic and Early Tertiary and the reconstruction of paleoclimates. Palaeogeography, Palaeoclimatology, Palaeoecology, **52**: 35-60.

Creber, G.T., Francis, J.E. 1999. Fossil tree-ring analysis: palaeodendrology. *In* Jones, T.P., Rowe, N.P. *editors* Fossil plants and spores: modern techniques. Geological Society, London, pp. 245-250.

Dawson, M.R. 2001. Early Eocene rodents (Mammalia) from the Eureka Sound Group of Ellesmere Island, Canada. Canadian Journal of Earth Sciences, **38**: 1107-1116.

Douglas, J.G., Williams, G.E. 1982. Southern polar forests: the Early Cretaceous floras of Victoria and their paleoclimatic significance. Palaeogeography, Palaeoclimatology, Palaeoecology, **39**: 171-185.

Douglass, A.E. 1928. Climatic cycles and tree growth. Carnegie Institution of Washington D.C. **289** (2).

Embry, A.F., Osadetz, K.G. 1988. Stratigraphy and tectonic significance of Cretaceous volcanism in the Queen Elizabeth Islands, Canadian Arctic Archipelago. Canadian Journal of Earth Sciences, **25**: 1209-1219.

Environment Canada. (2002, April, 7th). *Narrative descriptions of terrestrial ecozones and ecoregions of Canada.* [wwwdocument] URL: http://www.ec.gc.ca/soer-ree/English/Framework/NarDesc/canada_e.cfm

Falcon-Lang, H.J. 2000. A method to distinguish between woods produced by evergreen and deciduous coniferopsids on the basis of growth ring anatomy: a new palaeoecological tool. Palaeontology, **43** (4): 785-793.

Falcon-Lang, H.J., Cantrill, D.J. 2000. Cretaceous (Late Albian) coniferales of Alexander Island, Antarctica. 1: Wood taxonomy: a quantitative approach. Review of Palaeobotany and Palynology, **111**: 1-17.

Falcon-Lang, H.J., Cantrill, D.J. 2001. Gymnosperm woods from the Cretaceous (mid-Aptian) Cerro Negro Formation, Byers Peninsula, Livingston Island, Antarctica: the arborescent vegetation of a volcanic arc. Cretaceous Research, **22**: 277-293.

Falcon-Lang, H.J., Cantrill, D.J., Nichols, G.J. 2001. Biodiversity and terrestrial ecology of a mid-Cretaceous, high-latitude floodplain, Alexander Island, Antarctica. Journal of the Geological Society, London, **158**: 709-724.

Falcon-Lang, H.J., MacRae, R.A., Csank, A.Z. Composition and ecology of Late Cretaceous polar vegetation in a volcanically disturbed, alluvial plain/peat mire setting, NW Ellesmere Island, Arctic Canada. *submitted* (April, 2002), Canadian Journal of Earth Sciences.

Fortier, Y.O., Blackadar, R.G., Glenister, B.F., Greiner, H.R., McLaren, D.J., McMillan, N.J., Norris, A.W., Roots, E.F., Souther, J.G., Thorsteinsson, R., Tozer, E.T. 1963. Geology of the north-central part of the Arctic Archipelago, Northwest Territories (Operation Franklin). Geological Survey of Canada, Memoir **320**: 257-518.

Francis, J.E. 1988. A 50-million-year-old fossil forest from Strathcona Fiord, Ellesmere Island, Arctic Canada: evidence for a warm polar climate. Arctic, **41**: 314-318.

Francis, J.E., Frakes, L.A. 1993. Cretaceous climates. *In* Sedimentology Review **1**: 17-30.

Francis, J.E., McMillan, N.J. 1987. Fossil forests in the far north mummified tree stumps give scientists a glimpse of an ancient landscape in the High Arctic. GEOS, **1**: 6-9.

Frakes L.A., Francis, J.E. 1988. A guide to Phanerozoic cold polar climates from high-latitude ice-rafting in the Cretaceous. Nature, **333**: 547-549.

Frakes, L.A., Francis, J.E. 1990. Cretaceous Palaeoclimates. *In* Ginsburg, R.N., Beaudoin, B. *editors*, Cretaceous Resources, Events and Rhythms. Kluwer Academic Publishers, Neatherlands, pp. 273-287.

Glerum, C., and Farrar, J.L. 1966. Frost ring formation in the stems of some coniferous species. Canadian Journal of Botany, 44: 879-886.

Gothan, W. 1905. Sur anatomic lebender und fossile Gymnospermenholzer. Preuss. Geol. Landesanst. Abh., New Ser. **44**: 1-108.

Greguss, P. 1955. Identification of living gymnosperms on the basis of xylotomy. Akadémiai Kaidó, Budapest.

Greguss, P. 1967. Fossil gymnosperm woods in Hungary from the Permian to the Pliocene. Akadémiai Kaidó, Budapest.

Harrison, J.C., Mayr, U., McNeil, D.H., Sweet, A.R., McIntyre, D.J., Eberle, J.J., Harington, C.R., Chalmers, J.A., Dam, G., and Nøhr-Hansen, H. 1999. Correlation of Cenozoic sequences of the Canadian Arctic region and Greenland; implications for the tectonic history of northern North America. Bulletin of Canadian Petroleum Geology, **47**: 223-254.

Herman, A.B., Spicer, R.A. 1995. The Koryak flora: Did the Early Tertiary deciduous flora begin in the Late Maastrichtian of northeastern Russia? *In* Proceedings of the 4th EPPC. 87-92.

Herman, A.B., Spicer, R.A. 1996. *Nilssoniocladus* in the Cretaceous Arctic: new species and biological insights. Review of Paleobotany and Palynology, **92**: 229-243.

Houghton, J.T., Meira-Filho, L.G., Callander, B.A., Harris, N., Kattenberg, A., Maskell, K. 1996. Climate change 1995 - the science of climate change: the second assessment report of the Intergovernmental Panel on Climate Change. Cambridge University Press.

Irving, E., Wynne, P.J. 1991. The paleolatitude of the Eocene fossil forests of Arctic Canada. *In* Christie, R.L., McMillan, N.J. *editors* Tertiary Fossil Forests of the Geodetic Hills Axel Heiberg Island, Arctic Archipelago. Geological Survey of Canada, Bulletin, **403**.

Jahren, A.H., Sternberg, L.S.L. 2002. Eocene meridional weather patterns reflected in the oxygen isotopes of Arctic fossil wood. GSA Today, **12**(1): 4-9.

Jane, F.W. 1970. The structure of wood. Adam & Charles Black, London.

Jefferson, T.H. 1982. Fossil forests from the Lower Cretaceous of Alexander Island, Antarctica. Palaeontology, **25**: 681-708.

Kraüsel, R. 1949. Die fossilen Koniferenholzer. Palaeontographica, **89B**: 83-203. *translated from german* by Hill, C.R.

Krüssmann, G. 1991. Manual of Cultivated Conifers. Timber Press, Portland.

Kumagai, H., Sweda, T., Hayashi, K., Kojima S., Basinger, J.F., Shibuya, M., Fukaoa, Y. 1995. Growth-ring analysis of Early Tertiary conifer woods from the Canadian High Arctic and its paleoclimatic interpretation. Palaeogeography, Palaeoclimatology, Palaeoecology, **116**: 247-262.

LaMarche, V.C. Jr., Hirschboeck, K.K. 1984. Frost rings in trees as records of major volcanic eruptions. Nature, **307**:121-126.

Lehmann, T.M., Wheeler, E.A. 2001. A fossil dicotyledonous woodland/forest from the Upper Cretaceous of Big Bend National Park, Texas. Palaios, **16**: 102-108.

LePage, B.A., Basinger, J.F. 1991a. Early Tertiary *Larix* from the Buchanan Lake Formation, Canadian Arctic Archipelago, and a consideration of the phytogeography of the genus. *In* Christie, R.L., McMillan, N.J. *editors* Tertiary Fossil Forests of the Geodetic Hills Axel Heiberg Island, Arctic Archipelago. Geological Survey of Canada, Bulletin, **403:** pp. 67-81.

LePage, B.A., Basinger, J.F. 1991b. A new species of *Larix* (Pinaceae) from the early Tertiary of Axel Heiberg Island, Arctic Canada. Review of Palaeobotany and Palynology, **70**: 89-111.

MacRae, R.A. 1987. RAM field notes 1987: Ellesmere Island. (unpublished field notes). Located at (Atlantic Geoscience Institute, Bedford Institute of Oceanography, Dartmouth, Nova Scotia).

MacRae, R.A. 1989. Palynology and Stratigraphy of an Upper Cretaceous Sedimentary-Volcanic Sequence, Emma Fiord, Northwest Ellesmere Island, N.W.T, Canada. BSc. thesis, Dalhousie University, Halifax, N.S., 169 p.

MacRae, R.A., Muecke, G.K., Reynolds, P.H. 1990. Palynology, Stratigraphy, and radiometric age of an Upper Cretaceous sedimentary-volcanic sequence, Emma Fiord, NW Ellesmere Island, Canadian Arctic. Geological Association of Canada Program with Abstracts, A81.

Meijer, J.J.F. 2000. Fossil woods from the Late Cretaceous Aachen Formation. Review of Palaeobotany and Palynology, **112**: 297-336.

Meylan, B.A. 1972. Three-dimensional structure of wood: a scanning electron microscope study. Chapman and Hall, London.

Miall, A.D., 1986. The Eureka Sound Group (Upper Cretaceous-Oligocene), Canadian Arctic Islands. Bulletin of Canadian Petroleum Geology, **34**: 240-270.

Muecke, G.K., Reynolds, P.H., Avison, H.A. 1990. ^{40}Ar/^{39}Ar geochronology of episodic magmatism during the late phases of Sverdrup Basin development, Canadian Arctic Islands. Geological Association of Canada Program with Abstracts, A93.

National Atlas of Canada. (2002, May, 7th). *Canada: coastline, boundaries.* [wwwdocument] URL: http://atlas.gc.ca/site/english/maps/reference/outlinecanada/canada01

Niklas, K.J. 1994. Predicting the height of fossil plant remains: an allometric approach to an old problem. American Journal of Botany, **81** (10): 1235-1242.

Obst, J.R., McMillan, N.J., Blanchette, R.A., Christensen, D.J., Faix, O., Han, J.S., Kuster, T.A., Landucci, L.L., Newman, R.H., Pettersen, R.C., Schwandt, V.H., Wesolowski, M.F. 1991. Characterization of Canadian Arctic fossil woods. *In* Christie, R.L., McMillan, N.J. *editors* Tertiary Fossil Forests of the Geodetic Hills Axel Heiberg Island, Arctic Archipelago. Geological Survey of Canada, Bulletin, **403**: pp. 123-144.

Parrish, J.T., Spicer, R.A. 1988a. Late Cretaceous terrestrial vegetation: A near-polar temperature curve. Geology, **16**: 22-25.

Parrish, J.T., Spicer, R.A. 1988b. Middle Cretaceous wood from the Nanushuk Group, Central North Slope Alaska. Palaeontology, **31**:19-34.

Penhallow, D.P. 1908. Report on a collection of fossil woods from the Cretaceous of Alberta. Ottawa Naturalist, **22**: 82-88.

Pole, M. 2000. Mid-Cretaceous conifers from the Eromanga Basin, Australia. Australian Systematic Botany, **13**: 153-197.

Pole, M. 1999. Latest Albian-earliest Cenomanian monocotyledonous leaves from Australia. Botanical Journal of the Linnean Society, **129**: 177-186.

Pole, M., Douglas, J.G. 1999a. Bennettitales, Cycadales, and Ginkgoales from the mid Cretaceous of the Eromanga Basin, Queensland, Australia. Cretaceous Research, **20**: 523-538.

Pole, M., Douglas, B. 1999b. Plant macrofossils of the Upper Cretaceous Kaitangata Coalfield, New Zealand. Australian Systematic Botany, **12**: 331-364.

Poole, I., Cantrill, D.J. 2001. Forests of the polar night. Geoscientist, **11** (9): 4-6.

Poole, I., Hunt, R.J., Cantrill, D.J. 2001. A fossil wood flora from King George Island: Ecological Implications for an Antarctic Eocene vegetation. Annals of Botany, **88**: 33-54.

Ramanujam, C.G.K., Stewart, W.N. 1969. Fossil woods of Taxodiaceae from the Edmonton Formation (Upper Cretaceous) of Alberta. Canadian Journal of Botany, **47**: 115-124.

Read, J., Francis, J. 1992. Responses of some Southern Hemisphere tree species to a prolonged dark period and their implications for high-latitude Cretaceous and Tertiary floras. Palaeogeography, Palaeoclimatology, Palaeoecology, **99**: 271-290.

Retallack, G.J. 2001. A 300-million-year record of atmospheric carbon dioxide from fossil plant cuticles. Nature, **411**: 287-290.

Ricketts, B.D., 1991. Delta evolution in the Eureka Sound Group, western Axel Heiberg Island: the transition from wave-dominated to fluvial-dominated deltas. Geological Survey of Canada Bulletin 402, 72 p.

Ricketts, B.D., Stephenson, R.A. 1994. The demise of the Sverdrup Basin: Late Cretaceous-Paleogene sequence stratigraphy and forward modeling. Journal of Sedimentary Research, **B64** (4): 516-530.

Rossler, W. 1937. Pliozane koniferenholzer der Umgebund von Gleichenberg in Steiermark. Mitt. Naturwiss. Ver. Steiermark, **74**. (In German)

Roy, S.K., Hills, L.V. 1972. Fossil woods of the Beufort Formation (Tertiary) northwestern Banks Island, Canada. Canadian Journal of Botany, **50**: 2637-2648.

Ruddiman, W.F. 2001. Earth's Climate Past and Future. W.H. Freeman and company, pp. 414-418.

Sakai, A., and Larcher, W. 1987. Frost survival in plants. Ecostudies 62, Springer-Verlag, Berlin, 221 pp.

Shimakura, M. 1937. Studies on fossil woods from Japan and adjacent lands, Contribution 2. Scientific Report of Tokoku Imperial University, Series 2 Geology, **19**(1): 1-73.

Spicer, R.A., Chapman, J.L. 1990. Climate Change and the Evolution of High-latitude Terrestrial Vegetation and Floras. Trends in Ecology and Evolution, **5** (9): 279-284.

Spicer, R.A., Herman, A.B. 2001. The Albian-Cenomanian flora of the Kukpowruk River, western North Slope, Alaska: stratigraphy, palaeofloristics, and plant

comunities. Cretaceous Research, **22**: 1-40.

Spicer, R.A., Parrish, J.T. 1986. Paleobotanical evidence for cool north polar climates in middle Cretaceous (Albian-Cenomanian) time. Geology, **14**: 703-706.

Spicer, R.A., Parrish, J.T. 1990a. Latest Cretaceous woods of the central North Slope, Alaska. Palaeontology, **33**: 225-242.

Spicer, R.A., Parrish, J.T. 1990b. Late Cretaceous-early Tertiary paleoclimates of the northern high latitudes: a quantitative view. Journal of the Geological Society of London, **147**: 329-341.

Tarduno, J.A., Brinkman, D.B, Renne, P.R, Cottrell, R.D, Scher, H., Castillo, P. 1998. Evidence for extreme climatic warmth from Late Cretaceous Arctic vertebrates. Science, **282**: 2241-2244.

Thorn, V. 2001. Vegetation communities of a high palaeolatitude Middle Jurassic forest in New Zealand. Palaeogeography, Palaeoclimatology, Palaeoecology, **168**: 273-289.

Thorsteinsson, R., Trettin, H.P. 1972. Geology Map 1305A: Cape Stalworthy Map Area, District of Franklin. GSC Surveys and Mapping Branch.

Tidwell, W.D., Parker, L.R., Folkman, V.K. 1986. *Pinuxylon woolardii* sp. nov., a new petrified taxon of Pinaceae from the Miocene basalts of Eastern Oregon. American Journal of Botany. **73** (11): 1517-1524.

UNFCCC. (1998, March 16th). *Kyoto Protocol to the United Nations Framework Convention on Climate Change.* [wwwdocument] URL: http://unfccc.int/resource/docs/convkp/kpeng.pdf

Wall, A. & Hytönen, J. 1996. Painomaan vaikutus metsitetyn turvepellon ravinnemääriin (Summary: Effect of mineral soil admixture on the nutrient amounts of afforested peat fields). Suo **47** (3): 73-83. (In Finnish)

Wolfe, J.A. 1979. Temperature parameters of humid to mesic forests of Eastern Asia and relation to forests of other regions of the Northern Hemisphere and Australasia. US Dept. of Interior, Geological Survey Professional Paper. **1106**.

Wynne, P.J., Irving, E., and Osadetz, K.G. 1988. Paleomagnetism of Cretaceous volcanic rocks of Sverdrup Basin - magnetostratigraphy, paleolatitudes, and rotations. Canadian Journal of Earth Sciences, **25**: 1220-1239.

Appendix A:

Thin section analysis data

EL87-027

Bordered pitting

	EW	LW
uniseriate	47	60
biseriate	43	0
triseriate	15	0
blank	27	43
alternate	4	N/A
opposite	96	N/A
Number of contiguous bordered pits		
equal to 1	0	2
equal to 2	3	2
equal to 3	8	5
equal to 4	7	4
equal to 5	10	8
equal to 6	15	16
equal to 7	23	27
equal to 8	38	9
equal to 9	20	0
equal to 10	13	0
equal to 11	6	0

Cross-field pitting

number of cross-field pits per field				
with # cross-fields = 1	2	3	4	
18	41	57	6	

Ray type

Ray type	
uniseriate	80
biseriate	15
fusiform	8

Ray lengths in mm
1.98
1.87
1.95
2.16
2.05
1.91
1.75
2.12
1.88
1.73

Ray cell dimensions	
height	21.28 µm
width	15.96 µm
length	63.84 µm

Rays / Cross-field pitting / Resin ducts

ray heights in number of ray cells high	number of rays per linear mm	cross-field pit type	Axial – number of epitheleal cells	Horizontal – number of epitheleal cells
35	15	taxodioid		
13	10	taxodioid	9	8
13	14	cupressoid	12	9
14	15	taxodioid	10	13
30	14	piceoid	11	14
29	16	taxodioid	11	12
4	14	taxodioid	10	11
12	14	taxodioid	11	9
4	10	cupressoid	9	9
24	14	cupressoid	9	10
16	12	piceoid	9	8
16	13	piceoid	8	13
11	13	taxodioid	10	13
15	15	taxodioid	11	12
16	17	piceoid	11	10
18	16	piceoid	12	11
17	13	piceoid	9	11
24	15	cupressoid	9	8
21	14	taxodioid	10	13
10	15	piceoid	11	10
16		piceoid	12	9
12		cupressoid	10	9
18		taxodioid	12	9
22		piceoid	9	8
11		piceoid	9	10
15		cupressoid	8	11
9		cupressoid	8	10
2		piceoid	8	13
13		piceoid	11	12
18		taxodioid	dimensions of a representative duct	dimensions of a representative duct
18		taxodioid	width 47.88 µm	width 23.94 µm
22		piceoid	height 42.56 µm	height 23.94 µm
14		piceoid	epithelial cell thickness	epithelial cell thickness
20		taxodioid	7.98 µm	4.25 µm
2		cupressoid		
2		taxodioid		
6		taxodioid		
8		piceoid		
26		cupressoid		
20		piceoid		
4		taxodioid		
2		piceoid		
3		piceoid		
24		piceoid		
6		cupressoid		
22		cupressoid		
11		cupressoid		
15		piceoid		
25		taxodioid		
4		taxodioid		
4		piceoid		
6				
10				
23				
14				
12				
15				

ray heights in number of ray cells high
9
11
6
7
8
17
16
26
27
16
4
6
10
17
35
9
10
15
20
5
13
13
10
21
12
17
15
24
27
7
22
19
10
5
2
3
14
17
9
17
30
11

EL87-206	Bordered pitting		Ray type		Rays — ray heights in number of ray cells high	number of rays per linear mm	Cross-field pitting — cross-field pit type
uniseriate	49		uniseriate	90	15	16	taxodioid
biseriate	40		biseriate	13	19	17	taxodioid
triseriate	5		fusiform	0	10	12	taxodioid
blank	22				11	18	taxodioid
alternate	2		Ray lengths in mm		20	12	taxodioid
opposite	46		1.26		15	14	taxodioid
Number of contiguous			1.32		15	12	taxodioid
bordered pits			1.14		8	14	taxodioid
equal to 1	1		1.22		7	14	taxodioid
equal to 2	3		1.15		16	13	taxodioid
equal to 3	4		1.3		11	14	taxodioid
equal to 4	1		1.28		7	16	taxodioid
equal to 5	10		1.23		11	14	taxodioid
equal to 6	12		1.35		7	13	taxodioid
equal to 7	13		1.25		11	14	taxodioid
equal to 8	19		Ray cell dimensions		4	16	taxodioid
equal to 9	8		height	12.24 µm	16	11	
equal to 10	3		width	10.64 µm	10	14	
equal to 11	0		length	63.84 µm	9	14	
Cross-field pitting					33	12	
number of cross-field pits per field					7		
with # cross-fields = 1	2	3	4		25		
16	19	3	0		20		
					4		
					9		
					10		
					5		
					4		
					9		
					16		
					8		
					12		
					21		
					9		
					29		
					34		
					10		
					11		
					30		
					3		
					11		
					18		
					7		
					3		
					15		
					11		
					7		
					12		
					6		

ray heights in number of ray cells high
10
11
18
20
8
10
4
22
9
20
9
7
8
20
3
10
4
18
6
16
16
12
9
20
9
13
10
8
13
10
16
12
8
23
9
16
7
5
13
9
10
15
9
8
16
40
6
18
5
20
11

EL87-257

Bordered pitting

uniseriate	42
biseriate	70
triseriate	3
blank	19
alternate	2
opposite	98

Number of contiguous bordered pits

equal to 1	2
equal to 2	0
equal to 3	6
equal to 4	30
equal to 5	40
equal to 6	18
equal to 7	13
equal to 8	2
equal to 9	4
equal to 10	0
equal to 11	0

Cross-field pitting
number of cross-field pits per field

with # cross-fields = 1	2	3	4
10	71	5	6

Rays

Ray type	
uniseriate	94
biseriate	21
fusiform	10

Ray lengths in mm

2.22
2.46
2.28
2.55
2.32
2.36
2.41
2.42
2.49
2.39

Ray cell dimensions

height	10.64 μm
width	15.96 μm
length	79.8 μm

ray heights in number of ray cells high	number of rays per linear mm
11	17
8	23
4	16
10	22
10	19
8	15
11	17
19	18
9	17
7	13
10	20
7	14
11	15
10	13
15	12
18	16
17	11
11	15
15	14
13	15
17	
13	
6	
4	
4	
22	
12	
12	
7	
8	
7	
15	
17	
8	
12	
11	
7	
8	
25	
6	
6	
9	
7	
14	
8	
7	
11	
15	
7	
37	
20	
10	
3	
16	
8	
13	

Cross-field pitting / Resin ducts

cross-field pit type	Axial number of epitheleal cells	Horizontal number of epitheleal cells
piceoid	14	8
taxodioid	12	10
piceoid	13	10
taxodioid	15	12
piceoid	14	6
piceoid	14	6
taxodioid	12	6
piceoid	13	7
piceoid	13	9
piceoid	14	9
taxodioid	15	10
piceoid	15	8
piceoid	15	11
taxodioid	12	11
piceoid	12	8
piceoid	13	12
piceoid	13	9
piceoid	14	9
piceoid	14	9
taxodioid	12	7
taxodioid	15	6
piceoid	13	12
piceoid	13	12
piceoid	12	10
piceoid	12	8
piceoid	15	11
taxodioid	14	11
taxodioid		
piceoid		

dimensions of a representative duct		dimensions of a representative duct	
width	111.7 μm	width	34.58 μm
height	95.76 μm	height	37.24 μm

epithelial cell thickness	epithelial cell thickness
26.6 μm	7.98 μm

ray heights in number of ray cells high
9
9
17
11
5
13
10
11
11
6
11
11
12
12
12
6
7
14
19
9
10
13
8
5
7
9
5
23
9
10
17
10
12
10
5
26
9
11
15
15
8
15
13
15

EL87-268

Bordered pitting

	EW	LW
uniseriate	45	61
biseriate	76	5
triseriate	0	0
blank	25	71
alternate	0	0
opposite	100	5
Number of contiguous bordered pits		
equal to 1	0	0
equal to 2	5	2
equal to 3	27	33
equal to 4	44	53
equal to 5	22	15
equal to 6	15	13
equal to 7	9	5
equal to 8	3	1
equal to 9	0	0
equal to 10	0	0
equal to 11	0	0

Cross-field pitting

number of cross-field pits per field

with # cross-fields = 1	2	3	4
36	59	20	7

Rays

Ray type

uniseriate	75
biseriate	15
fusiform	10

Ray lengths in mm

1.95, 1.98, 2.29, 2.11, 1.93, 1.99, 1.9, 2.12, 2, 2.14

Ray cell dimensions

height	15.96 μm
width	13.3 μm
length	85.12 μm

ray heights in number of ray cells high

12, 12, 4, 23, 10, 5, 6, 12, 10, 9, 19, 5, 5, 6, 7, 10, 12, 19, 8, 9, 7, 8, 8, 11, 15, 3, 13, 12, 11, 10, 9, 8, 9, 7, 6, 13, 11, 6, 11, 10, 10, 19, 5, 7, 9, 10, 10, 18, 8, 4, 13, 8, 8, 20, 13, 9, 18

number of rays per linear mm

18, 16, 17, 17, 16, 20, 18, 19, 17, 15, 16, 16, 14, 19, 16, 17, 16, 15, 20, 16

Cross-field pitting

cross-field pit type

taxodioid, taxodioid, piceoid, taxodioid, piceoid, taxodioid, taxodioid, taxodioid, taxodioid, piceoid, piceoid, piceoid, taxodioid, taxodioid, piceoid, piceoid, piceoid, piceoid, taxodioid, piceoid, piceoid, taxodioid, piceoid, piceoid, piceoid, piceoid, piceoid, piceoid, taxodioid, taxodioid, piceoid, piceoid, taxodioid, taxodioid, piceoid, piceoid, taxodioid, taxodioid, piceoid, piceoid, piceoid, taxodioid, piceoid, piceoid, piceoid, taxodioid, piceoid, taxodioid, taxodioid, piceoid

Resin ducts

Axial — number of epitheleal cells	Horizontal — number of epitheleal cells
14	7
12	7
12	7
12	8
10	6
10	7
11	6
14	6
13	8
10	7
14	7
12	8
12	6
11	6
11	8
11	8
11	7
13	7
14	7
10	6
12	6
11	6
13	6
13	8
13	7
12	8
12	7

dimensions of a representative duct (Axial)

width	85.12 μm
height	79.8 μm

epithelial cell thickness: 18.62 μm

dimensions of a representative duct (Horizontal)

width	39.9 μm
height	42.56 μm

epithelial cell thickness: 6.92 μm

A-8

ray heights in number of ray cells high
17
7
9
8
11
12
4
11
5
8
13
16
6
5
11
10
15
4
4
5
5
9
14
5
20
7
5
20
8
14
7
10
3
6
8
5
6
9
8
11
10
14
8

Phillips-86

Bordered pitting		Ray type		ray heights in number of ray cells high	number of rays per linear mm	cross-field pit type	Resin ducts — Axial (number of epitheleal cells)	Resin ducts — Horizontal (number of epitheleal cells)
uniseriate	45	uniseriate	83	7	20	piceoid	9	8
biseriate	77	biseriate	41	9	22	taxodioid	10	8
triseriate	3	fusiform	25	12	25	taxodioid	8	8
blank	25			10	26	taxodioid	8	8
alternate	1	Ray lengths in mm		5	19	piceoid	8	9
opposite	99	1.64		6	18	taxodioid	9	9
Number of contiguous		1.55		5	20	piceoid	10	7
bordered pits		1.57		6	20	piceoid	10	12
equal to 1	0	1.59		5	19	taxodioid	8	10
equal to 2	2	1.62		7	23	taxodioid	9	10
equal to 3	7	1.63		7	18	piceoid	9	10
equal to 4	27	1.56		13	24	piceoid	9	11
equal to 5	55	1.53		7	20	piceoid	8	11
equal to 6	11	1.68		9	17	piceoid	10	9
equal to 7	3	1.53		23	16	piceoid	10	9
equal to 8	2	Ray cell dimensions		18	18	taxodioid	9	8
equal to 9	0	height	15.96 μm	8	19	taxodioid	8	11
equal to 10	0	width	21.28 μm	13	20	piceoid	8	11
equal to 11	0	length	53.2 μm	11	19	piceoid	8	8
Cross-field pitting				10	18	piceoid	8	8
number of cross-field pits per field				6		piceoid	10	11
with # cross-fields = 1 / 2 / 3 / 4 / 5				5		taxodioid	10	12
24 / 73 / 2 / 5				14		taxodioid	9	7
				8		piceoid	10	11
				4		piceoid	8	9
				7		taxodioid	9	10
				8		taxodioid	10	12
				11		piceoid	10	11
				10		piceoid	8	11
				11		piceoid	dimensions of a representative duct: width 101.1 μm; height 106.4 μm	dimensions of a representative duct: width 42.57 μm; height 37.24 μm
				7		taxodioid	epithelial cell thickness 21.28 μm	epithelial cell thickness 10.62 μm
				7		piceoid		
				8		piceoid		
				5		piceoid		
				6		taxodioid		
				4		taxodioid		
				10		piceoid		
				10		piceoid		
				20		piceoid		
				14		taxodioid		
				10				
				7				
				5				
				8				
				8				
				6				
				5				
				14				
				9				
				15				
				8				
				5				
				10				
				15				
				7				
				11				
				13				

A-11

ray heights in number of ray cells high
7
12
12
3
6
11
6
9
7
10
9
6
10
11
16
12
9
13
9
17
7
8
6
12
9
5
6
7
29
7
17
13
3
9
8
14
6
7
12
8
7
15
10
7

Appendix B:

Growth ring width and Mean Sensitivity data

EL87-027					
(a axis)					
growth ring diameter (mm)	year to year differences [Xt-X(t+1)]	sum of both rings [Xt+X(t+1)]	differences X2 2[Xt-X(t+1)]	Annual sensitivity [2(Xt-X(t+1))]/[Xt+X(t+1)]	mean sensitivity [Sum of Annual sensitivity/(n-1)]
1.5					
1	0.5	2.5	1	0.4	0.381393859
0.9	0.1	1.9	0.2	0.105263158	0.381393859
0.5	0.4	1.4	0.8	0.571428571	0.381393859
1	0.5	1.5	1	0.666666667	0.381393859
1	0	2	0	0	0.381393859
1	0	2	0	0	0.381393859
1.2	0.2	2.2	0.4	0.181818182	0.381393859
1.5	0.3	2.7	0.6	0.222222222	0.381393859
1	0.5	2.5	1	0.4	0.381393859
1.2	0.2	2.2	0.4	0.181818182	0.381393859
1.6	0.4	2.8	0.8	0.285714286	0.381393859
1.4	0.2	3	0.4	0.133333333	0.381393859
1.7	0.3	3.1	0.6	0.193548387	0.381393859
5.5	3.8	7.2	7.6	1.055555556	0.381393859
2.8	2.7	8.3	5.4	0.65060241	0.381393859
2.2	0.6	5	1.2	0.24	0.381393859
1	1.2	3.2	2.4	0.75	0.381393859
1.3	0.3	2.3	0.6	0.260869565	0.381393859
1	0.3	2.3	0.6	0.260869565	0.381393859
3	2	4	4	1	0.381393859
1	2	4	4	1	0.381393859
1.5	0.5	2.5	1	0.4	0.381393859
0.9	0.6	2.4	1.2	0.5	0.381393859
1.2	0.3	2.1	0.6	0.285714286	0.381393859
0.8	0.4	2	0.8	0.4	0.381393859
1.4	0.6	2.2	1.2	0.545454545	0.381393859
1.3	0.1	2.7	0.2	0.074074074	0.381393859
1	0.3	2.3	0.6	0.260869565	0.381393859
1.9	0.9	2.9	1.8	0.620689655	0.381393859
1.3	0.6	3.2	1.2	0.375	0.381393859
1.4	0.1	2.7	0.2	0.074074074	0.381393859
1.5	0.1	2.9	0.2	0.068965517	0.381393859
1.7	0.2	3.2	0.4	0.125	0.381393859
2	0.3	3.7	0.6	0.162162162	0.381393859
1	1	3	2	0.666666667	0.381393859
1.2	0.2	2.2	0.4	0.181818182	0.381393859
1.5	0.3	2.7	0.6	0.222222222	0.381393859
1	0.5	2.5	1	0.4	0.381393859
0.5	0.5	1.5	1	0.666666667	0.381393859
1	0.5	1.5	1	0.666666667	0.381393859

EL87-027	(b axis)				
ring diameter	year to year differences [At-A(t+1)]	sum of both rings [At+A(t+1)]	differences *2	Annual sensitivity [Xt-X(t+1)*2]/[Xt+X(t+1)]	mean sensitivity [Sum of Annual sensitivity/(n-1)]
0					
1	1	3	2	0.666666667	0.435455841
2	1.6	2.4	3.2	1.333333333	0.435455841
0.4	0.2	1	0.4	0.4	0.435455841
0.6	0.5	1.7	1	0.588235294	0.435455841
1.1	0.1	2.1	0.2	0.095238095	0.435455841
1	0.8	1.2	1.6	1.333333333	0.435455841
0.2	0.8	1.2	1.6	1.333333333	0.435455841
1	0.3	1.7	0.6	0.352941176	0.435455841
0.7	0.5	1.9	1	0.526315789	0.435455841
1.2	0.2	2.2	0.4	0.181818182	0.435455841
1	0.3	1.7	0.6	0.352941176	0.435455841
0.7	0.1	1.5	0.2	0.133333333	0.435455841
0.8	0.2	1.8	0.4	0.222222222	0.435455841
1	0.1	2.1	0.2	0.095238095	0.435455841
1.1	0.1	2.1	0.2	0.095238095	0.435455841
1	0.9	2.9	1.8	0.620689655	0.435455841
1.9	0.9	2.9	1.8	0.620689655	0.435455841
1	1.2	3.2	2.4	0.75	0.435455841
2.2	0.4	4	0.8	0.2	0.435455841
1.8	0.3	3.3	0.6	0.181818182	0.435455841
1.5	0.1	3.1	0.2	0.064516129	0.435455841
1.6	0.9	4.1	1.8	0.43902439	0.435455841
2.5	0.5	4.5	1	0.222222222	0.435455841
2	1	3	2	0.666666667	0.435455841
1	0.3	1.7	0.6	0.352941176	0.435455841
0.7	0.2	1.2	0.4	0.333333333	0.435455841
0.5	0.5	1.5	1	0.666666667	0.435455841
1	0	2	0	0	0.435455841
1	0	2	0	0	0.435455841
1	0.2	2.2	0.4	0.181818182	0.435455841
1.2	0.2	2.2	0.4	0.181818182	0.435455841
1	0.5	2.5	1	0.4	0.435455841
1.5	0.2	2.8	0.4	0.142857143	0.435455841
1.3	0.1	2.7	0.2	0.074074074	0.435455841
1.4	0.6	3.4	1.2	0.352941176	0.435455841
2	1	3	2	0.666666667	0.435455841
1	0	2	0	0	0.435455841
1	0.7	1.3	1.4	1.076923077	0.435455841
0.3	0.7	1.3	1.4	1.076923077	0.435455841
1					

EL87-027	(c axis)				
growth ring diameter (mm)	year to year differences [Xt-X(t+1)]	sum of both rings [Xt+X(t+1)]	differences X2 2[Xt-X(t+1)]	Annual sensitivity [2(Xt-X(t+1))]/[Xt+X(t+1)]	mean sensitivity [Sum of Annual sensitivity/(n-1)]
1.3					
1	0.3	2.3	0.6	0.260869565	0.347707562
1	0	2	0	0	0.347707562
0.8	0.2	1.8	0.4	0.222222222	0.347707562
1.5	0.7	2.3	1.4	0.608695652	0.347707562
1.7	0.2	3.2	0.4	0.125	0.347707562
1	0.7	2.7	1.4	0.518518519	0.347707562
1.8	0.8	2.8	1.6	0.571428571	0.347707562
1.5	0.3	3.3	0.6	0.181818182	0.347707562
0.9	0.6	2.4	1.2	0.5	0.347707562
1.8	0.9	2.7	1.8	0.666666667	0.347707562
3.2	1.4	5	2.8	0.56	0.347707562
1.2	2	4.4	4	0.909090909	0.347707562
1.8	0.6	3	1.2	0.4	0.347707562
1.3	0.5	3.1	1	0.322580645	0.347707562
1.3	0	2.6	0	0	0.347707562
1.5	0.2	2.8	0.4	0.142857143	0.347707562
1.2	0.3	2.7	0.6	0.222222222	0.347707562
1	0.2	2.2	0.4	0.181818182	0.347707562
0.5	0.5	1.5	1	0.666666667	0.347707562
1	0.5	1.5	1	0.666666667	0.347707562
1	0	2	0	0	0.347707562
1.2	0.2	2.2	0.4	0.181818182	0.347707562
1	0.2	2.2	0.4	0.181818182	0.347707562
1	0	2	0	0	0.347707562
1.3	0.3	2.3	0.6	0.260869565	0.347707562
1	0.3	2.3	0.6	0.260869565	0.347707562
1	0	2	0	0	0.347707562
1	0	2	0	0	0.347707562
1.3	0.3	2.3	0.6	0.260869565	0.347707562
1	0.3	2.3	0.6	0.260869565	0.347707562
1.8	0.8	2.8	1.6	0.571428571	0.347707562
0.8	1	2.6	2	0.769230769	0.347707562
1	0.2	1.8	0.4	0.222222222	0.347707562
1.5	0.5	2.5	1	0.4	0.347707562
2	0.5	3.5	1	0.285714286	0.347707562
1	1	3	2	0.666666667	0.347707562
1.8	0.8	2.8	1.6	0.571428571	0.347707562
1.2	0.6	3	1.2	0.4	0.347707562
0.8	0.4	2	0.8	0.4	0.347707562
1	0.2	1.8	0.4	0.222222222	0.347707562
0.5	0.5	1.5	1	0.666666667	0.347707562

EL87-027	(d axis)				
growth ring diameter (mm)	year to year differences [Xt-X(t+1)]	sum of both rings [Xt+X(t+1)]	differences X2 2[Xt-X(t+1)]	Annual sensitivity [2(Xt-X(t+1))]/[Xt+X(t+1)]	mean sensitivity [Sum of Annual sensitivity/(n-1)]
1.2					
0.9	0.3	2.1	0.6	0.285714286	0.456362189
0.4	0.5	1.3	1	0.769230769	0.456362189
0.6	0.2	1	0.4	0.4	0.456362189
2.2	1.6	2.8	3.2	1.142857143	0.456362189
1.4	0.8	3.6	1.6	0.444444444	0.456362189
2	0.6	3.4	1.2	0.352941176	0.456362189
0.8	1.2	2.8	2.4	0.857142857	0.456362189
1.8	1	2.6	2	0.769230769	0.456362189
1.1	0.7	2.9	1.4	0.482758621	0.456362189
0.7	0.4	1.8	0.8	0.444444444	0.456362189
1.5	0.8	2.2	1.6	0.727272727	0.456362189
1	0.5	2.5	1	0.4	0.456362189
1	0	2	0	0	0.456362189
0.5	0.5	1.5	1	0.666666667	0.456362189
1	0.5	1.5	1	0.666666667	0.456362189
0.6	0.4	1.6	0.8	0.5	0.456362189
0.4	0.2	1	0.4	0.4	0.456362189
0.2	0.2	0.6	0.4	0.666666667	0.456362189
0.3	0.1	0.5	0.2	0.4	0.456362189
0.6	0.3	0.9	0.6	0.666666667	0.456362189
1	0.4	1.6	0.8	0.5	0.456362189
1	0	2	0	0	0.456362189
1	0	2	0	0	0.456362189
1	0	2	0	0	0.456362189
1	0	2	0	0	0.456362189
0.5	0.5	1.5	1	0.666666667	0.456362189
1.5	1	2	2	1	0.456362189
0.6	0.9	2.1	1.8	0.857142857	0.456362189
0.8	0.2	1.4	0.4	0.285714286	0.456362189
1	0.2	1.8	0.4	0.222222222	0.456362189
1	0	2	0	0	0.456362189
0.7	0.3	1.7	0.6	0.352941176	0.456362189
1.2	0.5	1.9	1	0.526315789	0.456362189
1.2	0	2.4	0	0	0.456362189
0.6	0.6	1.8	1.2	0.666666667	0.456362189
1.5	0.9	2.1	1.8	0.857142857	0.456362189
1	0.5	2.5	1	0.4	0.456362189
1	0	2	0	0	0.456362189
0.5	0.5	1.5	1	0.666666667	0.456362189
1	0.5	1.5	1	0.666666667	0.456362189

EL87-027	(mean of all axis)				
growth ring diameter (mm)	year to year differences [Xt-X(t+1)]	sum of both rings [Xt+X(t+1)]	differences X2 2[Xt-X(t+1)]	Annual sensitivity [2(Xt-X(t+1))]/[Xt+X(t+1)]	mean sensitivity [Sum of Annual sensitivity/(n-1)]
1	1	1	2		
0.975	0.025	1.975	0.05	0.025316456	0.262540432
1.075	0.1	2.05	0.2	0.097560976	0.262540432
0.575	0.5	1.65	1	0.606060606	0.262540432
1.325	0.75	1.9	1.5	0.789473684	0.262540432
1.3	0.025	2.625	0.05	0.019047619	0.262540432
1.25	0.05	2.55	0.1	0.039215686	0.262540432
1	0.25	2.25	0.5	0.222222222	0.262540432
1.45	0.45	2.45	0.9	0.367346939	0.262540432
0.925	0.525	2.375	1.05	0.442105263	0.262540432
1.225	0.3	2.15	0.6	0.279069767	0.262540432
1.825	0.6	3.05	1.2	0.393442623	0.262540432
1.075	0.75	2.9	1.5	0.517241379	0.262540432
1.325	0.25	2.4	0.5	0.208333333	0.262540432
2.075	0.75	3.4	1.5	0.441176471	0.262540432
1.55	0.525	3.625	1.05	0.289655172	0.262540432
1.325	0.225	2.875	0.45	0.156521739	0.262540432
1.125	0.2	2.45	0.4	0.163265306	0.262540432
0.875	0.25	2	0.5	0.25	0.262540432
1	0.125	1.875	0.25	0.133333333	0.262540432
1.6	0.6	2.6	1.2	0.461538462	0.262540432
1.125	0.475	2.725	0.95	0.348623853	0.262540432
1.325	0.2	2.45	0.4	0.163265306	0.262540432
1.35	0.025	2.675	0.05	0.018691589	0.262540432
1.3	0.05	2.65	0.1	0.037735849	0.262540432
1.025	0.275	2.325	0.55	0.23655914	0.262540432
0.9	0.125	1.925	0.25	0.12987013	0.262540432
1.075	0.175	1.975	0.35	0.17721519	0.262540432
0.9	0.175	1.975	0.35	0.17721519	0.262540432
1.25	0.35	2.15	0.7	0.325581395	0.262540432
1.075	0.175	2.325	0.35	0.150537634	0.262540432
1.35	0.275	2.425	0.55	0.226804124	0.262540432
1	0.35	2.35	0.7	0.29787234	0.262540432
1.35	0.35	2.35	0.7	0.29787234	0.262540432
1.5	0.15	2.85	0.3	0.105263158	0.262540432
1.25	0.25	2.75	0.5	0.181818182	0.262540432
1.425	0.175	2.675	0.35	0.130841121	0.262540432
1.325	0.1	2.75	0.2	0.072727273	0.262540432
1.05	0.275	2.375	0.55	0.231578947	0.262540432
0.525	0.525	1.575	1.05	0.666666667	0.262540432
1	0.475	1.525	0.95	0.62295082	0.262540432

EL87-206	furrow				
growth ring diameter (mm)	year to year differences [Xt-X(t+1)]	sum of both rings [Xt+X(t+1)]	differences X2 2[Xt-X(t+1)]	Annual sensitivity [2(Xt-X(t+1))]/[Xt+X(t+1)]	mean sensitivity [Sum of Annual sensitivity/(n-1)]
1.2					
1.8	0.6	3	1.2	0.4	0.358698543
1	0.8	2.8	1.6	0.571428571	0.358698543
1.5	0.5	2.5	1	0.4	0.358698543
1.8	0.3	3.3	0.6	0.181818182	0.358698543
1	0.8	2.8	1.6	0.571428571	0.358698543
1.5	0.5	2.5	1	0.4	0.358698543
2	0.5	3.5	1	0.285714286	0.358698543
2.8	0.8	4.8	1.6	0.333333333	0.358698543
3	0.2	5.8	0.4	0.068965517	0.358698543
2.9	0.1	5.9	0.2	0.033898305	0.358698543
5.3	2.4	8.2	4.8	0.585365854	0.358698543
3.5	1.8	8.8	3.6	0.409090909	0.358698543
3	0.5	6.5	1	0.153846154	0.358698543
1.9	1.1	4.9	2.2	0.448979592	0.358698543
4	2.1	5.9	4.2	0.711864407	0.358698543
4.5	0.5	8.5	1	0.117647059	0.358698543
3.2	1.3	7.7	2.6	0.337662338	0.358698543
2.5	0.7	5.7	1.4	0.245614035	0.358698543
2	0.5	4.5	1	0.222222222	0.358698543
2	0	4	0	0	0.358698543
2.2	0.2	4.2	0.4	0.095238095	0.358698543
2	0.2	4.2	0.4	0.095238095	0.358698543
2.8	0.8	4.8	1.6	0.333333333	0.358698543
0.8	2	3.6	4	1.111111111	0.358698543
1.5	0.7	2.3	1.4	0.608695652	0.358698543
2	0.5	3.5	1	0.285714286	0.358698543
2.5	0.5	4.5	1	0.222222222	0.358698543
1.5	1	4	2	0.5	0.358698543
1.5	0	3	0	0	0.358698543
1	0.5	2.5	1	0.4	0.358698543
0.8	0.2	1.8	0.4	0.222222222	0.358698543
0.5	0.3	1.3	0.6	0.461538462	0.358698543
3.8	3.3	4.3	6.6	1.534883721	0.358698543
2.3	1.5	6.1	3	0.491803279	0.358698543
2	0.3	4.3	0.6	0.139534884	0.358698543
1.9	0.1	3.9	0.2	0.051282051	0.358698543
0.9	1	2.8	2	0.714285714	0.358698543
1	0.1	1.9	0.2	0.105263158	0.358698543
1	0	2	0	0	0.358698543
0.8	0.2	1.8	0.4	0.222222222	0.358698543
0.7	0.1	1.5	0.2	0.133333333	0.358698543
0.7	0	1.4	0	0	0.358698543
0.5	0.2	1.2	0.4	0.333333333	0.358698543
0.4	0.1	0.9	0.2	0.222222222	0.358698543
0.5	0.1	0.9	0.2	0.222222222	0.358698543
1	0.5	1.5	1	0.666666667	0.358698543
0.8	0.2	1.8	0.4	0.222222222	0.358698543
1.5	0.7	2.3	1.4	0.608695652	0.358698543
2	0.5	3.5	1	0.285714286	0.358698543
1	1	3	2	0.666666667	0.358698543
1.8	0.8	2.8	1.6	0.571428571	0.358698543
1	0.8	2.8	1.6	0.571428571	0.358698543
1.2	0.2	2.2	0.4	0.181818182	0.358698543
1.5	0.3	2.7	0.6	0.222222222	0.358698543
1.3	0.2	2.8	0.4	0.142857143	0.358698543
1	0.3	2.3	0.6	0.260869565	0.358698543
2	1	3	2	0.666666667	0.358698543
1.4	0.6	3.4	1.2	0.352941176	0.358698543
0.8	0.6	2.2	1.2	0.545454545	0.358698543
0.2	0.6	1	1.2	1.2	0.358698543
0.2	0	0.4	0	0	0.358698543
0.1	0.1	0.3	0.2	0.666666667	0.358698543
0.2	0.1	0.3	0.2	0.666666667	0.358698543
0.3	0.1	0.5	0.2	0.4	0.358698543
0.3	0	0.6	0	0	0.358698543
0.4	0.1	0.7	0.2	0.285714286	0.358698543
0.4	0	0.8	0	0	0.358698543
0.5	0.1	0.9	0.2	0.222222222	0.358698543

EL87-206	ridge				
growth ring diameter (mm)	year to year differences [Xt-X(t+1)]	sum of both rings [Xt+X(t+1)]	differences X2 2[Xt-X(t+1)]	Annual sensitivity [(2(Xt-X(t+1)))/(Xt+X(t+1))]	mean sensitivity [Sum of Annual sensitivity/(n-1)]
1.2					
1.8	0.6	3	1.2	0.4	0.362812952
1	0.8	2.8	1.6	0.571428571	0.362812952
1.5	0.5	2.5	1	0.4	0.362812952
1.8	0.3	3.3	0.6	0.181818182	0.362812952
1	0.8	2.8	1.6	0.571428571	0.362812952
1.5	0.5	2.5	1	0.4	0.362812952
2	0.5	3.5	1	0.285714286	0.362812952
2.8	0.8	4.8	1.6	0.333333333	0.362812952
3	0.2	5.8	0.4	0.068965517	0.362812952
4.5	1.5	7.5	3	0.4	0.362812952
4.2	0.3	8.7	0.6	0.068965517	0.362812952
3	1.2	7.2	2.4	0.333333333	0.362812952
4	1	7	2	0.285714286	0.362812952
3.2	0.8	7.2	1.6	0.222222222	0.362812952
3.9	0.7	7.1	1.4	0.197183099	0.362812952
3.5	0.4	7.4	0.8	0.108108108	0.362812952
4	0.5	7.5	1	0.133333333	0.362812952
2.4	1.6	6.4	3.2	0.5	0.362812952
2.5	0.1	4.9	0.2	0.040816327	0.362812952
4.2	1.7	6.7	3.4	0.507462687	0.362812952
3	1.2	7.2	2.4	0.333333333	0.362812952
3.3	0.3	6.3	0.6	0.095238095	0.362812952
4	0.7	7.3	1.4	0.191780822	0.362812952
2	2	6	4	0.666666667	0.362812952
1	1	3	2	0.666666667	0.362812952
2.5	1.5	3.5	3	0.857142857	0.362812952
3	0.5	5.5	1	0.181818182	0.362812952
4	1	7	2	0.285714286	0.362812952
1.5	2.5	5.5	5	0.909090909	0.362812952
1.9	0.4	3.4	0.8	0.235294118	0.362812952
1	0.9	2.9	1.8	0.620689655	0.362812952
1	0	2	0	0	0.362812952
0.8	0.2	1.8	0.4	0.222222222	0.362812952
0.5	0.3	1.3	0.6	0.461538462	0.362812952
1	0.5	1.5	1	0.666666667	0.362812952
3.6	2.6	4.6	5.2	1.130434783	0.362812952
3.5	0.1	7.1	0.2	0.028169014	0.362812952
2	1.5	5.5	3	0.545454545	0.362812952
0.8	1.2	2.8	2.4	0.857142857	0.362812952
0.7	0.1	1.5	0.2	0.133333333	0.362812952
1.5	0.8	2.2	1.6	0.727272727	0.362812952
1	0.5	2.5	1	0.4	0.362812952
0.8	0.2	1.8	0.4	0.222222222	0.362812952
1	0.2	1.8	0.4	0.222222222	0.362812952
0.9	0.1	1.9	0.2	0.105263158	0.362812952
1	0.1	1.9	0.2	0.105263158	0.362812952
0.8	0.2	1.8	0.4	0.222222222	0.362812952
0.4	0.4	1.2	0.8	0.666666667	0.362812952
0.5	0.1	0.9	0.2	0.222222222	0.362812952
0.8	0.3	1.3	0.6	0.461538462	0.362812952
1.2	0.4	2	0.8	0.4	0.362812952
1.8	0.6	3	1.2	0.4	0.362812952
1	0.8	2.8	1.6	0.571428571	0.362812952
1	0	2	0	0	0.362812952
1.5	0.5	2.5	1	0.4	0.362812952
2.2	0.7	3.7	1.4	0.378378378	0.362812952
1.4	0.8	3.6	1.6	0.444444444	0.362812952
1.4	0	2.8	0	0	0.362812952
0.8	0.6	2.2	1.2	0.545454545	0.362812952
0.2	0.6	1	1.2	1.2	0.362812952
0.2	0	0.4	0	0	0.362812952
0.1	0.1	0.3	0.2	0.666666667	0.362812952
0.2	0.1	0.3	0.2	0.666666667	0.362812952
0.3	0.1	0.5	0.2	0.4	0.362812952
0.3	0	0.6	0	0	0.362812952
0.3	0	0.6	0	0	0.362812952
0.4	0.1	0.7	0.2	0.285714286	0.362812952
0.4	0	0.8	0	0	0.362812952
0.5	0.1	0.9	0.2	0.222222222	0.362812952

EL87-257					
growth ring diameter (mm)	year to year differences [Xt-X(t+1)]	sum of both rings [Xt+X(t+1)]	differences X2 2[Xt-X(t+1)]	Annual sensitivity [2(Xt-X(t+1))]/[Xt+X(t+1)]	mean sensitivity [Sum of Annual sensitivity/(n-1)]
3.5					
6	2.5	9.5	5	0.526315789	0.28160734
3.6	2.4	9.6	4.8	0.5	0.28160734
8	4.4	11.6	8.8	0.75862069	0.28160734
3.2	4.8	11.2	9.6	0.857142857	0.28160734
2.5	0.7	5.7	1.4	0.245614035	0.28160734
3	0.5	5.5	1	0.181818182	0.28160734
1.9	1.1	4.9	2.2	0.448979592	0.28160734
2.8	0.9	4.7	1.8	0.382978723	0.28160734
2.7	0.1	5.5	0.2	0.036363636	0.28160734
2.9	0.2	5.6	0.4	0.071428571	0.28160734
3.2	0.3	6.1	0.6	0.098360656	0.28160734
2.3	0.9	5.5	1.8	0.327272727	0.28160734
2	0.3	4.3	0.6	0.139534884	0.28160734
2.2	0.2	4.2	0.4	0.095238095	0.28160734
2.5	0.3	4.7	0.6	0.127659574	0.28160734
2.2	0.3	4.7	0.6	0.127659574	0.28160734
2	0.2	4.2	0.4	0.095238095	0.28160734
2.5	0.5	4.5	1	0.222222222	0.28160734
2	0.5	4.5	1	0.222222222	0.28160734
3	1	5	2	0.4	0.28160734
2.8	0.2	5.8	0.4	0.068965517	0.28160734
2.6	0.2	5.4	0.4	0.074074074	0.28160734
2	0.6	4.6	1.2	0.260869565	0.28160734
2.2	0.2	4.2	0.4	0.095238095	0.28160734
2	0.2	4.2	0.4	0.095238095	0.28160734
1.8	0.2	3.8	0.4	0.105263158	0.28160734
1	0.8	2.8	1.6	0.571428571	0.28160734
2.3	1.3	3.3	2.6	0.787878788	0.28160734
2	0.3	4.3	0.6	0.139534884	0.28160734
2	0	4	0	0	0.28160734
4	2	6	4	0.666666667	0.28160734

Appendix C:

Cell-by-Cell measurment and CSDM data

EL87-027					
cell diameter (D) (μm)	distance along growth ring (μm)	mean diameter (md)	D - md	deviation from the mean [Σ(D - md)]	diameter in microscope scale bar units
33.3333333	0	17.06666665	16.2666667	16.26666665	1
43.33333329	33.3333333	17.06666665	26.2666666	42.53333329	1.3
39.99999996	76.66666659	17.06666665	22.9333333	65.4666666	1.2
39.99999996	116.6666666	17.06666665	22.9333333	88.39999991	1.2
43.33333329	156.6666665	17.06666665	26.2666666	114.6666666	1.3
43.33333329	199.9999998	17.06666665	26.2666666	140.9333332	1.3
33.3333333	243.3333331	17.06666665	16.2666667	157.1999998	1
26.66666664	276.6666664	17.06666665	9.59999999	166.7999998	0.8
33.3333333	303.333333	17.06666665	16.2666667	183.0666665	1
19.99999998	336.6666663	17.06666665	2.93333333	185.9999998	0.6
16.66666665	356.6666663	17.06666665	-0.4	185.5999998	0.5
19.99999998	373.333333	17.06666665	2.93333333	188.5333331	0.6
16.66666665	393.3333329	17.06666665	-0.4	188.1333331	0.5
33.3333333	409.9999996	17.06666665	16.2666667	204.3999998	1
33.3333333	443.3333329	17.06666665	16.2666667	220.6666664	1
23.33333331	476.6666662	17.06666665	6.26666666	226.9333331	0.7
19.99999998	499.9999995	17.06666665	2.93333333	229.8666664	0.6
19.99999998	519.9999995	17.06666665	2.93333333	232.7999998	0.6
19.99999998	539.9999995	17.06666665	2.93333333	235.7333331	0.6
23.33333331	559.9999994	17.06666665	6.26666666	241.9999998	0.7
16.66666665	583.3333328	17.06666665	-0.4	241.5999998	0.5
16.66666665	599.9999994	17.06666665	-0.4	241.1999998	0.5
13.33333332	616.6666661	17.06666665	-3.73333333	237.4666664	0.4
19.99999998	629.9999994	17.06666665	2.93333333	240.3999998	0.6
16.66666665	649.9999994	17.06666665	-0.4	239.9999998	0.5
16.66666665	666.666666	17.06666665	-0.4	239.5999998	0.5
23.33333331	683.3333327	17.06666665	6.26666666	245.8666664	0.7
16.66666665	706.666666	17.06666665	-0.4	245.4666664	0.5
16.66666665	723.3333326	17.06666665	-0.4	245.0666664	0.5
19.99999998	739.9999993	17.06666665	2.93333333	247.9999998	0.6
16.66666665	759.9999992	17.06666665	-0.4	247.5999998	0.5
19.99999998	776.6666659	17.06666665	2.93333333	250.5333331	0.6
16.66666665	796.6666659	17.06666665	-0.4	250.1333331	0.5
19.99999998	813.3333325	17.06666665	2.93333333	253.0666664	0.6
13.33333332	833.3333325	17.06666665	-3.73333333	249.3333331	0.4
13.33333332	846.6666658	17.06666665	-3.73333333	245.5999998	0.4
16.66666665	859.9999991	17.06666665	-0.4	245.1999998	0.5
19.99999998	876.6666658	17.06666665	2.93333333	248.1333331	0.6
16.66666665	896.6666658	17.06666665	-0.4	247.7333331	0.5
16.66666665	913.3333324	17.06666665	-0.4	247.3333331	0.5
19.99999998	929.9999991	17.06666665	2.93333333	250.2666664	0.6
13.33333332	949.9999991	17.06666665	-3.73333333	246.5333331	0.4

C-2

EL87-027					
cell diameter (D) (μm)	distance along growth ring (μm)	mean diameter (md)	D - md	deviation from the mean [Σ(D - md)]	diameter in microscope scale bar units
19.99999998	963.3333324	17.06666665	2.93333333	249.4666664	0.6
16.66666665	983.3333324	17.06666665	-0.4	249.0666664	0.5
13.33333332	999.999999	17.06666665	-3.73333333	245.3333331	0.4
9.99999999	1013.333332	17.06666665	-7.06666666	238.2666664	0.3
13.33333332	1023.333332	17.06666665	-3.73333333	234.5333331	0.4
13.33333332	1036.666666	17.06666665	-3.73333333	230.7999998	0.4
9.99999999	1049.999999	17.06666665	-7.06666666	223.7333331	0.3
9.99999999	1059.999999	17.06666665	-7.06666666	216.6666665	0.3
13.33333332	1069.999999	17.06666665	-3.73333333	212.9333331	0.4
19.99999998	1083.333332	17.06666665	2.93333333	215.8666665	0.6
9.99999999	1103.333332	17.06666665	-7.06666666	208.7999998	0.3
13.33333332	1113.333332	17.06666665	-3.73333333	205.0666665	0.4
13.33333332	1126.666666	17.06666665	-3.73333333	201.3333331	0.4
6.66666666	1139.999999	17.06666665	-10.4	190.9333331	0.2
13.33333332	1146.666666	17.06666665	-3.73333333	187.1999998	0.4
9.99999999	1159.999999	17.06666665	-7.06666666	180.1333332	0.3
9.99999999	1169.999999	17.06666665	-7.06666666	173.0666665	0.3
13.33333332	1179.999999	17.06666665	-3.73333333	169.3333332	0.4
9.99999999	1193.333332	17.06666665	-7.06666666	162.2666665	0.3
6.66666666	1203.333332	17.06666665	-10.4	151.8666665	0.2
6.66666666	1209.999999	17.06666665	-10.4	141.4666665	0.2
9.99999999	1216.666665	17.06666665	-7.06666666	134.3999999	0.3
6.66666666	1226.666665	17.06666665	-10.4	123.9999999	0.2
6.66666666	1233.333332	17.06666665	-10.4	113.5999999	0.2
3.33333333	1239.999999	17.06666665	-13.7333333	99.86666657	0.1
9.99999999	1243.333332	17.06666665	-7.06666666	92.79999991	0.3
6.66666666	1253.333332	17.06666665	-10.4	82.39999992	0.2
6.66666666	1259.999999	17.06666665	-10.4	71.99999993	0.2
6.66666666	1266.666665	17.06666665	-10.4	61.59999994	0.2
3.33333333	1273.333332	17.06666665	-13.7333333	47.86666662	0.1
3.33333333	1276.666665	17.06666665	-13.7333333	34.1333333	0.1

EL87-027(2)

cell diameter (D) (μm)	distance along growth ring (μm)	mean diameter (md)	D - md	deviation from the mean [Σ(D - md)]	diameter in scale bar units
33.3333333	0	24.19540227	9.13793103	5.48275862	1
49.99999995	33.3333333	24.19540227	25.8045977	31.2873563	1.5
53.33333328	83.33333325	24.19540227	29.137931	60.4252873	1.6
59.99999994	136.6666665	24.19540227	35.8045977	96.22988497	1.8
56.66666661	196.6666665	24.19540227	32.4712643	128.7011493	1.7
49.99999995	253.3333331	24.19540227	25.8045977	154.505747	1.5
46.66666662	303.333333	24.19540227	22.4712643	176.9770113	1.4
43.33333329	349.9999997	24.19540227	19.137931	196.1149423	1.3
46.66666662	393.3333329	24.19540227	22.4712643	218.5862067	1.4
43.33333329	439.9999996	24.19540227	19.137931	237.7241377	1.3
39.99999996	483.3333329	24.19540227	15.8045977	253.5287354	1.2
39.99999996	523.3333328	24.19540227	15.8045977	269.3333331	1.2
36.66666663	563.3333328	24.19540227	12.4712644	281.8045974	1.1
36.66666663	599.9999994	24.19540227	12.4712644	294.2758618	1.1
29.99999997	636.666666	24.19540227	5.8045977	300.0804595	0.9
33.3333333	666.666666	24.19540227	9.13793103	309.2183905	1
29.99999997	699.9999993	24.19540227	5.8045977	315.0229882	0.9
33.3333333	729.9999993	24.19540227	9.13793103	324.1609192	1
33.3333333	763.3333326	24.19540227	9.13793103	333.2988502	1
36.66666663	796.6666659	24.19540227	12.4712644	345.7701146	1.1
26.66666664	833.3333325	24.19540227	2.47126437	348.241379	0.8
26.66666664	859.9999991	24.19540227	2.47126437	350.7126433	0.8
19.99999998	886.6666658	24.19540227	-4.19540229	346.517241	0.6
23.33333331	906.6666658	24.19540227	-0.86206896	345.6551721	0.7
23.33333331	929.9999991	24.19540227	-0.86206896	344.7931031	0.7
26.66666664	953.3333324	24.19540227	2.47126437	347.2643675	0.8
23.33333331	979.999999	24.19540227	-0.86206896	346.4022985	0.7
29.99999997	1003.333332	24.19540227	5.8045977	352.2068962	0.9
33.3333333	1033.333332	24.19540227	9.13793103	361.3448272	1
29.99999997	1066.666666	24.19540227	5.8045977	367.1494249	0.9
33.3333333	1096.666666	24.19540227	9.13793103	376.287356	1
33.3333333	1129.999999	24.19540227	9.13793103	385.425287	1
26.66666664	1163.333332	24.19540227	2.47126437	387.8965513	0.8
19.99999998	1189.999999	24.19540227	-4.19540229	383.701149	0.6
13.33333332	1209.999999	24.19540227	-10.862069	372.8390801	0.4
16.66666665	1223.333332	24.19540227	-7.52873562	365.3103445	0.5
16.66666665	1239.999999	24.19540227	-7.52873562	357.7816088	0.5
16.66666665	1256.666665	24.19540227	-7.52873562	350.2528732	0.5
13.33333332	1273.333332	24.19540227	-10.862069	339.3908043	0.4
9.99999999	1286.666665	24.19540227	-14.1954023	325.195402	0.3
13.33333332	1296.666665	24.19540227	-10.862069	314.333333	0.4
13.33333332	1309.999999	24.19540227	-10.862069	303.4712641	0.4
9.99999999	1323.333332	24.19540227	-14.1954023	289.2758618	0.3

C-4

EL87-027(2)

cell diameter (D) (μm)	distance along growth ring (μm)	mean diameter (md)	D - md	deviation from the mean [Σ(D - md)]	diameter in scale bar units
6.66666666	1333.333332	24.19540227	-17.5287356	271.7471262	0.2
3.33333333	1339.999999	24.19540227	-20.8620689	250.8850572	0.1
6.66666666	1343.333332	24.19540227	-17.5287356	233.3563216	0.2
3.33333333	1349.999999	24.19540227	-20.8620689	212.4942527	0.1
3.33333333	1353.333332	24.19540227	-20.8620689	191.6321837	0.1
6.66666666	1356.666665	24.19540227	-17.5287356	174.1034481	0.2
6.66666666	1363.333332	24.19540227	-17.5287356	156.5747125	0.2
3.33333333	1369.999999	24.19540227	-20.8620689	135.7126435	0.1
3.33333333	1373.333332	24.19540227	-20.8620689	114.8505746	0.1
3.33333333	1376.666665	24.19540227	-20.8620689	93.98850566	0.1
6.66666666	1379.999999	24.19540227	-17.5287356	76.45977004	0.2
6.66666666	1386.666665	24.19540227	-17.5287356	58.93103443	0.2
3.33333333	1393.333332	24.19540227	-20.8620689	38.06896548	0.1
3.33333333	1396.666665	24.19540227	-20.8620689	17.20689654	0.1
3.33333333	1399.999999	24.19540227	-20.8620689	-3.655172405	0.1

C-5

EL87-027(3)

cell diameter (D) (μm)	distance along growth ring (μm)	mean diameter (md)	D - md	deviation from the mean [Σ(D - md)]	diameter in scale bar units
33.3333333	0	25.51111109	7.82222221	4.69333333	1
43.33333329	33.3333333	25.51111109	17.8222222	22.51555553	1.3
56.66666661	76.66666659	25.51111109	31.1555555	53.67111106	1.7
43.33333329	133.3333332	25.51111109	17.8222222	71.49333326	1.3
49.99999995	176.6666665	25.51111109	24.4888889	95.98222213	1.5
49.99999995	226.6666664	25.51111109	24.4888889	120.471111	1.5
49.99999995	276.6666664	25.51111109	24.4888889	144.9599999	1.5
46.66666662	326.6666663	25.51111109	21.1555555	166.1155554	1.4
43.33333329	373.333333	25.51111109	17.8222222	183.9377776	1.3
46.66666662	416.6666663	25.51111109	21.1555555	205.0933331	1.4
33.3333333	463.3333329	25.51111109	7.82222221	212.9155553	1
39.99999996	496.6666662	25.51111109	14.4888889	227.4044442	1.2
36.66666663	536.6666661	25.51111109	11.1555555	238.5599998	1.1
39.99999996	573.3333328	25.51111109	14.4888889	253.0488886	1.2
43.33333329	613.3333327	25.51111109	17.8222222	270.8711108	1.3
39.99999996	656.666666	25.51111109	14.4888889	285.3599997	1.2
36.66666663	696.666666	25.51111109	11.1555555	296.5155553	1.1
39.99999996	733.3333326	25.51111109	14.4888889	311.0044441	1.2
43.33333329	773.3333326	25.51111109	17.8222222	328.8266663	1.3
36.66666663	816.6666659	25.51111109	11.1555555	339.9822219	1.1
39.99999996	853.3333325	25.51111109	14.4888889	354.4711108	1.2
33.3333333	893.3333324	25.51111109	7.82222221	362.293333	1
36.66666663	926.6666657	25.51111109	11.1555555	373.4488885	1.1
33.3333333	963.3333324	25.51111109	7.82222221	381.2711107	1
33.3333333	996.6666657	25.51111109	7.82222221	389.0933329	1
33.3333333	1029.999999	25.51111109	7.82222221	396.9155552	1
33.3333333	1063.333332	25.51111109	7.82222221	404.7377774	1
36.66666663	1096.666666	25.51111109	11.1555555	415.8933329	1.1
33.3333333	1133.333332	25.51111109	7.82222221	423.7155551	1
29.99999997	1166.666666	25.51111109	4.48888888	428.204444	0.9
29.99999997	1196.666665	25.51111109	4.48888888	432.6933329	0.9
29.99999997	1226.666665	25.51111109	4.48888888	437.1822218	0.9
26.66666664	1256.666665	25.51111109	1.15555555	438.3377773	0.8
29.99999997	1283.333332	25.51111109	4.48888888	442.8266662	0.9
26.66666664	1313.333332	25.51111109	1.15555555	443.9822218	0.8
23.33333331	1339.999999	25.51111109	-2.17777778	441.804444	0.7
29.99999997	1363.333332	25.51111109	4.48888888	446.2933329	0.9
29.99999997	1393.333332	25.51111109	4.48888888	450.7822218	0.9
26.66666664	1423.333332	25.51111109	1.15555555	451.9377773	0.8
23.33333331	1449.999999	25.51111109	-2.17777778	449.7599996	0.7
23.33333331	1473.333332	25.51111109	-2.17777778	447.5822218	0.7
19.99999998	1496.666665	25.51111109	-5.51111111	442.0711107	0.6
16.66666665	1516.666665	25.51111109	-8.84444444	433.2266662	0.5

EL87-027(3)

cell diameter (D) (μm)	distance along growth ring (μm)	mean diameter (md)	D - md	deviation from the mean [Σ(D - md)]	diameter in scale bar units
16.66666665	1533.333332	25.51111109	-8.84444444	424.3822218	0.5
16.66666665	1549.999998	25.51111109	-8.84444444	415.5377774	0.5
16.66666665	1566.666665	25.51111109	-8.84444444	406.6933329	0.5
13.33333332	1583.333332	25.51111109	-12.1777778	394.5155552	0.4
13.33333332	1596.666665	25.51111109	-12.1777778	382.3377774	0.4
16.66666665	1609.999998	25.51111109	-8.84444444	373.493333	0.5
16.66666665	1626.666665	25.51111109	-8.84444444	364.6488885	0.5
16.66666665	1643.333332	25.51111109	-8.84444444	355.8044441	0.5
13.33333332	1659.999998	25.51111109	-12.1777778	343.6266663	0.4
13.33333332	1673.333332	25.51111109	-12.1777778	331.4488886	0.4
9.99999999	1686.666665	25.51111109	-15.5111111	315.9377775	0.3
13.33333332	1696.666665	25.51111109	-12.1777778	303.7599997	0.4
9.99999999	1709.999998	25.51111109	-15.5111111	288.2488886	0.3
16.66666665	1719.999998	25.51111109	-8.84444444	279.4044442	0.5
13.33333332	1736.666665	25.51111109	-12.1777778	267.2266664	0.4
16.66666665	1749.999998	25.51111109	-8.84444444	258.382222	0.5
13.33333332	1766.666665	25.51111109	-12.1777778	246.2044442	0.4
9.99999999	1779.999998	25.51111109	-15.5111111	230.6933331	0.3
13.33333332	1789.999998	25.51111109	-12.1777778	218.5155553	0.4
9.99999999	1803.333332	25.51111109	-15.5111111	203.0044442	0.3
9.99999999	1813.333332	25.51111109	-15.5111111	187.4933331	0.3
6.66666666	1823.333332	25.51111109	-18.8444444	168.6488887	0.2
9.99999999	1829.999998	25.51111109	-15.5111111	153.1377776	0.3
9.99999999	1839.999998	25.51111109	-15.5111111	137.6266665	0.3
6.66666666	1849.999998	25.51111109	-18.8444444	118.7822221	0.2
6.66666666	1856.666665	25.51111109	-18.8444444	99.93777768	0.2
6.66666666	1863.333331	25.51111109	-18.8444444	81.09333325	0.2
13.33333332	1869.999998	25.51111109	-12.1777778	68.91555549	0.4
9.99999999	1883.333331	25.51111109	-15.5111111	53.40444439	0.3
6.66666666	1893.333331	25.51111109	-18.8444444	34.55999997	0.2
6.66666666	1899.999998	25.51111109	-18.8444444	15.71555554	0.2
3.33333333	1906.666665	25.51111109	-22.1777778	-6.462222214	0.1
3.33333333	1909.999998	25.51111109	-22.1777778	-28.63999997	0.1

EL87-027(4)					
cell diameter (D) (μm)	distance along growth ring (μm)	mean diameter (md)	D - md	deviation from the mean [Σ(D - md)]	diameter in scale bar units
66.5	0	26.264	40.236	40.236	12.5
63.84	66.5	26.264	37.576	77.812	12
58.52	130.34	26.264	32.256	110.068	11
61.18	188.86	26.264	34.916	144.984	11.5
53.2	250.04	26.264	26.936	171.92	10
47.88	303.24	26.264	21.616	193.536	9
50.54	351.12	26.264	24.276	217.812	9.5
42.56	401.66	26.264	16.296	234.108	8
31.92	444.22	26.264	5.656	239.764	6
26.6	476.14	26.264	0.336	240.1	5
23.94	502.74	26.264	-2.324	237.776	4.5
23.94	526.68	26.264	-2.324	235.452	4.5
29.26	550.62	26.264	2.996	238.448	5.5
31.92	579.88	26.264	5.656	244.104	6
34.58	611.8	26.264	8.316	252.42	6.5
21.28	646.38	26.264	-4.984	247.436	4
21.28	667.66	26.264	-4.984	242.452	4
29.26	688.94	26.264	2.996	245.448	5.5
53.2	718.2	26.264	26.936	272.384	10
47.88	771.4	26.264	21.616	294	9
39.9	819.28	26.264	13.636	307.636	7.5
34.58	859.18	26.264	8.316	315.952	6.5
37.24	893.76	26.264	10.976	326.928	7
37.24	931	26.264	10.976	337.904	7
31.92	968.24	26.264	5.656	343.56	6
31.92	1000.16	26.264	5.656	349.216	6
34.58	1032.08	26.264	8.316	357.532	6.5
26.6	1066.66	26.264	0.336	357.868	5
29.26	1093.26	26.264	2.996	360.864	5.5
26.6	1122.52	26.264	0.336	361.2	5
26.6	1149.12	26.264	0.336	361.536	5
23.94	1175.72	26.264	-2.324	359.212	4.5
21.28	1199.66	26.264	-4.984	354.228	4
26.6	1220.94	26.264	0.336	354.564	5
25.004	1247.54	26.264	-1.26	353.304	4.7
26.6	1272.544	26.264	0.336	353.64	5
21.28	1299.144	26.264	-4.984	348.656	4
21.28	1320.424	26.264	-4.984	343.672	4
21.28	1341.704	26.264	-4.984	338.688	4
22.876	1362.984	26.264	-3.388	335.3	4.3
26.6	1385.86	26.264	0.336	335.636	5
22.344	1412.46	26.264	-3.92	331.716	4.2
21.28	1434.804	26.264	-4.984	326.732	4

EL87-027(4)

cell diameter (µm)	distance along growth ring (µm)	mean diameter (md)	D - md	deviation from the mean [Σ(D - md)]	diameter in scale bar units
31.92	1456.084	26.264	5.656	332.388	6
21.28	1488.004	26.264	-4.984	327.404	4
22.876	1509.284	26.264	-3.388	324.016	4.3
21.28	1532.16	26.264	-4.984	319.032	4
21.28	1553.44	26.264	-4.984	314.048	4
19.684	1574.72	26.264	-6.58	307.468	3.7
22.344	1594.404	26.264	-3.92	303.548	4.2
15.96	1616.748	26.264	-10.304	293.244	3
15.96	1632.708	26.264	-10.304	282.94	3
18.62	1648.668	26.264	-7.644	275.296	3.5
21.28	1667.288	26.264	-4.984	270.312	4
15.96	1688.568	26.264	-10.304	260.008	3
21.28	1704.528	26.264	-4.984	255.024	4
21.28	1725.808	26.264	-4.984	250.04	4
18.62	1747.088	26.264	-7.644	242.396	3.5
15.96	1765.708	26.264	-10.304	232.092	3
14.364	1781.668	26.264	-11.9	220.192	2.7
13.3	1796.032	26.264	-12.964	207.228	2.5
10.64	1809.332	26.264	-15.624	191.604	2
10.64	1819.972	26.264	-15.624	175.98	2
10.64	1830.612	26.264	-15.624	160.356	2
13.3	1841.252	26.264	-12.964	147.392	2.5
13.3	1854.552	26.264	-12.964	134.428	2.5
15.96	1867.852	26.264	-10.304	124.124	3
15.96	1883.812	26.264	-10.304	113.82	3
15.96	1899.772	26.264	-10.304	103.516	3
13.3	1915.732	26.264	-12.964	90.552	2.5
13.3	1929.032	26.264	-12.964	77.588	2.5
12.236	1942.332	26.264	-14.028	63.56	2.3
10.64	1954.568	26.264	-15.624	47.936	2
9.576	1965.208	26.264	-16.688	31.248	1.8
10.64	1974.784	26.264	-15.624	15.624	2
10.64	1985.424	26.264	-15.624	3.6593E-13	2

b-9

EL87-027(5)

cell diameter (D) (μm)	distance along growth ring (μm)	mean diameter (md)	D - md	deviation from the mean [Σ(D - md)]	diameter in scale bar units
69.16	0	29.35457778	39.8054222	39.8054222	13
63.84	69.16	29.35457778	34.4854222	74.29084442	12
53.2	133	29.35457778	23.8454222	98.13626664	10
58.52	186.2	29.35457778	29.1654222	127.3016889	11
53.2	244.72	29.35457778	23.8454222	151.1471111	10
47.88	297.92	29.35457778	18.5254222	169.6725333	9
47.88	345.8	29.35457778	18.5254222	188.1979555	9
42.56	393.68	29.35457778	13.2054222	201.4033778	8
47.88	436.24	29.35457778	18.5254222	219.9288	9
42.56	484.12	29.35457778	13.2054222	233.1342222	8
37.24	526.68	29.35457778	7.88542222	241.0196444	7
42.56	563.92	29.35457778	13.2054222	254.2250666	8
37.24	606.48	29.35457778	7.88542222	262.1104889	7
34.58	643.72	29.35457778	5.22542222	267.3359111	6.5
37.24	678.3	29.35457778	7.88542222	275.2213333	7
31.92	715.54	29.35457778	2.56542222	277.7867555	6
31.92	747.46	29.35457778	2.56542222	280.3521778	6
26.6	779.38	29.35457778	-2.75457778	277.5976	5
23.94	805.98	29.35457778	-5.41457778	272.1830222	4.5
26.6	829.92	29.35457778	-2.75457778	269.4284444	5
21.28	856.52	29.35457778	-8.07457778	261.3538666	4
26.6	877.8	29.35457778	-2.75457778	258.5992889	5
21.28	904.4	29.35457778	-8.07457778	250.5247111	4
21.28	925.68	29.35457778	-8.07457778	242.4501333	4
18.62	946.96	29.35457778	-10.7345778	231.7155555	3.5
21.28	965.58	29.35457778	-8.07457778	223.6409778	4
21.28	986.86	29.35457778	-8.07457778	215.5664	4
23.94	1008.14	29.35457778	-5.41457778	210.1518222	4.5
21.28	1032.08	29.35457778	-8.07457778	202.0772444	4
22.344	1053.36	29.35457778	-7.01057778	195.0666666	4.2
21.28	1075.704	29.35457778	-8.07457778	186.9920889	4
18.62	1096.984	29.35457778	-10.7345778	176.2575111	3.5
18.62	1115.604	29.35457778	-10.7345778	165.5229333	3.5
21.28	1134.224	29.35457778	-8.07457778	157.4483555	4
18.62	1155.504	29.35457778	-10.7345778	146.7137778	3.5
18.62	1174.124	29.35457778	-10.7345778	135.9792	3.5
17.024	1192.744	29.35457778	-12.3305778	123.6486222	3.2
15.96	1209.768	29.35457778	-13.3945778	110.2540444	3
17.024	1225.728	29.35457778	-12.3305778	97.92346664	3.2
17.024	1242.752	29.35457778	-12.3305778	85.59288887	3.2
13.3	1259.776	29.35457778	-16.0545778	69.53831109	2.5
13.3	1273.076	29.35457778	-16.0545778	53.48373331	2.5
13.3	1286.376	29.35457778	-16.0545778	37.42915553	2.5
10.64	1299.676	29.35457778	-18.7145778	18.71457776	2
10.64	1310.316	29.35457778	-18.7145778	-2.22215E-08	2

EL87-027(6)

cell diameter (D) (µm)	distance along growth ring (µm)	mean diameter (md)	D - md	deviation from the mean [Σ(D - md)]	diameter in scale bar units
66.5	0	32.85882353	33.6411765	33.6411765	12.5
69.16	66.5	32.85882353	36.3011765	69.94235297	13
58.52	135.66	32.85882353	25.6611765	95.60352944	11
53.2	194.18	32.85882353	20.3411765	115.9447059	10
47.88	247.38	32.85882353	15.0211765	130.9658824	9
45.22	295.26	32.85882353	12.3611765	143.3270589	8.5
37.24	340.48	32.85882353	4.38117647	147.7082353	7
42.56	377.72	32.85882353	9.70117647	157.4094118	8
42.56	420.28	32.85882353	9.70117647	167.1105883	8
42.56	462.84	32.85882353	9.70117647	176.8117647	8
37.24	505.4	32.85882353	4.38117647	181.1929412	7
31.92	542.64	32.85882353	-0.93882353	180.2541177	6
42.56	574.56	32.85882353	9.70117647	189.9552941	8
29.26	617.12	32.85882353	-3.59882353	186.3564706	5.5
26.6	646.38	32.85882353	-6.25882353	180.0976471	5
37.24	672.98	32.85882353	4.38117647	184.4788236	7
29.26	710.22	32.85882353	-3.59882353	180.88	5.5
29.26	739.48	32.85882353	-3.59882353	177.2811765	5.5
26.6	768.74	32.85882353	-6.25882353	171.022353	5
23.94	795.34	32.85882353	-8.91882353	162.1035294	4.5
26.6	819.28	32.85882353	-6.25882353	155.8447059	5
26.6	845.88	32.85882353	-6.25882353	149.5858824	5
23.94	872.48	32.85882353	-8.91882353	140.6670589	4.5
23.94	896.42	32.85882353	-8.91882353	131.7482353	4.5
21.28	920.36	32.85882353	-11.5788235	120.1694118	4
21.28	941.64	32.85882353	-11.5788235	108.5905883	4
23.94	962.92	32.85882353	-8.91882353	99.67176474	4.5
21.28	986.86	32.85882353	-11.5788235	88.09294121	4
21.28	1008.14	32.85882353	-11.5788235	76.51411768	4
21.28	1029.42	32.85882353	-11.5788235	64.93529415	4
18.62	1050.7	32.85882353	-14.2388235	50.69647062	3.5
15.96	1069.32	32.85882353	-16.8988235	33.79764709	3
15.96	1085.28	32.85882353	-16.8988235	16.89882356	3
15.96	1101.24	32.85882353	-16.8988235	2.94118E-08	3

EL87-206

cell diameter (D) (µm)	distance along growth ring (µm)	mean diameter (md)	D - md	deviation from the mean [Σ(D - md)]	diameter in microscope scale bar units
63.33333333	0	27.11382114	36.21951219	6.268292683	1.9
60	63.33333333	26.21951219	33.7804878	40.04878049	1.8
60	123.3333333	26.21951219	33.7804878	73.82926829	1.8
56.66666667	183.3333333	26.21951219	30.44715447	104.2764228	1.7
46.66666667	240	26.21951219	20.44715447	124.7235772	1.4
43.33333333	286.6666667	26.21951219	17.11382114	141.8373984	1.3
43.33333333	330	26.21951219	17.11382114	158.9512195	1.3
36.66666667	373.3333333	26.21951219	10.44715447	169.398374	1.1
40	410	26.21951219	13.7804878	183.1788618	1.2
33.33333333	450	26.21951219	7.113821138	190.2926829	1
33.33333333	483.3333333	26.21951219	7.113821138	197.4065041	1
40	516.6666667	26.21951219	13.7804878	211.1869919	1.2
43.33333333	556.6666667	26.21951219	17.11382114	228.300813	1.3
46.66666667	600	26.21951219	20.44715447	248.7479675	1.4
40	646.6666667	26.21951219	13.7804878	262.5284553	1.2
43.33333333	686.6666667	26.21951219	17.11382114	279.6422764	1.3
40	730	26.21951219	13.7804878	293.4227642	1.2
40	770	26.21951219	13.7804878	307.203252	1.2
33.33333333	810	26.21951219	7.113821138	314.3170732	1
33.33333333	843.3333333	26.21951219	7.113821138	321.4308943	1
33.33333333	876.6666667	26.21951219	7.113821138	328.5447154	1
36.66666667	910	26.21951219	10.44715447	338.9918699	1.1
33.33333333	946.6666667	26.21951219	7.113821138	346.1056911	1
40	980	26.21951219	13.7804878	359.8861789	1.2
36.66666667	1020	26.21951219	10.44715447	370.3333333	1.1
33.33333333	1056.666667	26.21951219	7.113821138	377.4471545	1
33.33333333	1090	26.21951219	7.113821138	384.5609756	1
33.33333333	1123.333333	26.21951219	7.113821138	391.6747967	1
36.66666667	1156.666667	26.21951219	10.44715447	402.1219512	1.1
36.66666667	1193.333333	26.21951219	10.44715447	412.5691057	1.1
40	1230	26.21951219	13.7804878	426.3495935	1.2
40	1270	26.21951219	13.7804878	440.1300813	1.2
36.66666667	1310	26.21951219	10.44715447	450.5772358	1.1
36.66666667	1346.666667	26.21951219	10.44715447	461.0243902	1.1
33.33333333	1383.333333	26.21951219	7.113821138	468.1382114	1
33.33333333	1416.666667	26.21951219	7.113821138	475.2520325	1
33.33333333	1450	26.21951219	7.113821138	482.3658537	1
30	1483.333333	26.21951219	3.780487805	486.1463415	0.9
30	1513.333333	26.21951219	3.780487805	489.9268293	0.9
33.33333333	1543.333333	26.21951219	7.113821138	497.0406504	1
36.66666667	1576.666667	26.21951219	10.44715447	507.4878049	1.1

EL87-206					
cell diameter (D) (µm)	distance along growth ring (µm)	mean diameter (md)	D - md	deviation from the mean [Σ(D - md)]	diameter in microscope scale bar units
30	1613.333333	26.21951219	3.780487805	511.2682927	0.9
26.66666667	1643.333333	26.21951219	0.447154472	511.7154471	0.8
26.66666667	1670	26.21951219	0.447154472	512.1626016	0.8
23.33333333	1696.666667	26.21951219	-2.886178862	509.2764228	0.7
26.66666667	1720	26.21951219	0.447154472	509.7235772	0.8
23.33333333	1746.666667	26.21951219	-2.886178862	506.8373984	0.7
23.33333333	1770	26.21951219	-2.886178862	503.9512195	0.7
26.66666667	1793.333333	26.21951219	0.447154472	504.398374	0.8
20	1820	26.21951219	-6.219512195	498.1788618	0.6
13.33333333	1840	26.21951219	-12.88617886	485.2926829	0.4
20	1853.333333	26.21951219	-6.219512195	479.0731707	0.6
16.66666667	1873.333333	26.21951219	-9.552845528	469.5203252	0.5
33.33333333	1890	26.21951219	7.113821138	476.6341463	1
20	1923.333333	26.21951219	-6.219512195	470.4146341	0.6
20	1943.333333	26.21951219	-6.219512195	464.1951219	0.6
16.66666667	1963.333333	26.21951219	-9.552845528	454.6422764	0.5
16.66666667	1980	26.21951219	-9.552845528	445.0894309	0.5
16.66666667	1996.666667	26.21951219	-9.552845528	435.5365854	0.5
20	2013.333333	26.21951219	-6.219512195	429.3170732	0.6
16.66666667	2033.333333	26.21951219	-9.552845528	419.7642276	0.5
13.33333333	2050	26.21951219	-12.88617886	406.8780488	0.4
13.33333333	2063.333333	26.21951219	-12.88617886	393.9918699	0.4
16.66666667	2076.666667	26.21951219	-9.552845528	384.4390244	0.5
20	2093.333333	26.21951219	-6.219512195	378.2195122	0.6
13.33333333	2113.333333	26.21951219	-12.88617886	365.3333333	0.4
10	2126.666667	26.21951219	-16.21951219	349.1138211	0.3
10	2136.666667	26.21951219	-16.21951219	332.8943089	0.3
6.666666667	2146.666667	26.21951219	-19.55284553	313.3414634	0.2
10	2153.333333	26.21951219	-16.21951219	297.1219512	0.3
10	2163.333333	26.21951219	-16.21951219	280.902439	0.3
13.33333333	2173.333333	26.21951219	-12.88617886	268.0162602	0.4
3.333333333	2186.666667	26.21951219	-22.88617886	245.1300813	0.1
3.333333333	2190	26.21951219	-22.88617886	222.2439024	0.1
6.666666667	2193.333333	26.21951219	-19.55284553	202.6910569	0.2
6.666666667	2200	26.21951219	-19.55284553	183.1382114	0.2
6.666666667	2206.666667	26.21951219	-19.55284553	163.5853659	0.2
3.333333333	2213.333333	26.21951219	-22.88617886	140.699187	0.1
3.333333333	2216.666667	26.21951219	-22.88617886	117.8130081	0.1
3.333333333	2220	26.21951219	-22.88617886	94.92682927	0.1

EL87-206(2)					
cell diameter (D) (μm)	distance along growth ring (μm)	mean diameter (md)	D - md	deviation from the mean [Σ(D - md)]	diameter in microscope scale bar units
60	0	34.50757576	25.49242424	15.43181818	1.8
53.33333333	60	34.28030303	19.0530303	34.48484848	1.6
60	113.3333333	34.28030303	25.71969697	60.20454545	1.8
50	173.3333333	34.28030303	15.71969697	75.92424242	1.5
56.66666667	223.3333333	34.28030303	22.38636364	98.31060606	1.7
53.33333333	280	34.28030303	19.0530303	117.3636364	1.6
50	333.3333333	34.28030303	15.71969697	133.0833333	1.5
50	383.3333333	34.28030303	15.71969697	148.8030303	1.5
50	433.3333333	34.28030303	15.71969697	164.5227273	1.5
53.33333333	483.3333333	34.28030303	19.0530303	183.5757576	1.6
56.66666667	536.6666667	34.28030303	22.38636364	205.9621212	1.7
53.33333333	593.3333333	34.28030303	19.0530303	225.0151515	1.6
50	646.6666667	34.28030303	15.71969697	240.7348485	1.5
40	696.6666667	34.28030303	5.71969697	246.4545455	1.2
60	736.6666667	34.28030303	25.71969697	272.1742424	1.8
50	796.6666667	34.28030303	15.71969697	287.8939394	1.5
46.66666667	846.6666667	34.28030303	12.38636364	300.280303	1.4
50	893.3333333	34.28030303	15.71969697	316	1.5
50	943.3333333	34.28030303	15.71969697	331.719697	1.5
46.66666667	993.3333333	34.28030303	12.38636364	344.1060606	1.4
46.66666667	1040	34.28030303	12.38636364	356.4924242	1.4
40	1086.666667	34.28030303	5.71969697	362.2121212	1.2
50	1126.666667	34.28030303	15.71969697	377.9318182	1.5
53.33333333	1176.666667	34.28030303	19.0530303	396.9848485	1.6
50	1230	34.28030303	15.71969697	412.7045454	1.5
50	1280	34.28030303	15.71969697	428.4242424	1.5
53.33333333	1330	34.28030303	19.0530303	447.4772727	1.6
46.66666667	1383.333333	34.28030303	12.38636364	459.8636364	1.4
50	1430	34.28030303	15.71969697	475.5833333	1.5
36.66666667	1480	34.28030303	2.386363636	477.969697	1.1
50	1516.666667	34.28030303	15.71969697	493.6893939	1.5
46.66666667	1566.666667	34.28030303	12.38636364	506.0757576	1.4
43.33333333	1613.333333	34.28030303	9.053030303	515.1287879	1.3
46.66666667	1656.666667	34.28030303	12.38636364	527.5151515	1.4
50	1703.333333	34.28030303	15.71969697	543.2348485	1.5
43.33333333	1753.333333	34.28030303	9.053030303	552.2878788	1.3
40	1796.666667	34.28030303	5.71969697	558.0075758	1.2
40	1836.666667	34.28030303	5.71969697	563.7272727	1.2
43.33333333	1876.666667	34.28030303	9.053030303	572.780303	1.3
36.66666667	1920	34.28030303	2.386363636	575.1666667	1.1
40	1956.666667	34.28030303	5.71969697	580.8863636	1.2
43.33333333	1996.666667	34.28030303	9.053030303	589.9393939	1.3
40	2040	34.28030303	5.71969697	595.6590909	1.2

EL87-206(2)

cell diameter (D) (µm)	distance along growth ring (µm)	mean diameter (md)	D - md	deviation from the mean [Σ(D - md)]	diameter in microscope scale bar units
36.66666667	2080	34.28030303	2.386363636	598.0454545	1.1
40	2116.666667	34.28030303	5.71969697	603.7651515	1.2
33.33333333	2156.666667	34.28030303	-0.946969697	602.8181818	1
36.66666667	2190	34.28030303	2.386363636	605.2045454	1.1
33.33333333	2226.666667	34.28030303	-0.946969697	604.2575757	1
33.33333333	2260	34.28030303	-0.946969697	603.3106061	1
40	2293.333333	34.28030303	5.71969697	609.030303	1.2
30	2333.333333	34.28030303	-4.28030303	604.75	0.9
33.33333333	2363.333333	34.28030303	-0.946969697	603.8030303	1
26.66666667	2396.666667	34.28030303	-7.613636364	596.1893939	0.8
26.66666667	2423.333333	34.28030303	-7.613636364	588.5757576	0.8
40	2450	34.28030303	5.71969697	594.2954545	1.2
26.66666667	2490	34.28030303	-7.613636364	586.6818182	0.8
23.33333333	2516.666667	34.28030303	-10.9469697	575.7348485	0.7
26.66666667	2540	34.28030303	-7.613636364	568.1212121	0.8
33.33333333	2566.666667	34.28030303	-0.946969697	567.1742424	1
30	2600	34.28030303	-4.28030303	562.8939394	0.9
30	2630	34.28030303	-4.28030303	558.6136364	0.9
26.66666667	2660	34.28030303	-7.613636364	551	0.8
23.33333333	2686.666667	34.28030303	-10.9469697	540.0530303	0.7
23.33333333	2710	34.28030303	-10.9469697	529.1060606	0.7
23.33333333	2733.333333	34.28030303	-10.9469697	518.1590909	0.7
20	2756.666667	34.28030303	-14.28030303	503.8787879	0.6
20	2776.666667	34.28030303	-14.28030303	489.5984848	0.6
13.33333333	2796.666667	34.28030303	-20.9469697	468.6515151	0.4
16.66666667	2810	34.28030303	-17.61363636	451.0378788	0.5
16.66666667	2826.666667	34.28030303	-17.61363636	433.4242424	0.5
13.33333333	2843.333333	34.28030303	-20.9469697	412.4772727	0.4
16.66666667	2856.666667	34.28030303	-17.61363636	394.8636364	0.5
10	2873.333333	34.28030303	-24.28030303	370.5833333	0.3
13.33333333	2883.333333	34.28030303	-20.9469697	349.6363636	0.4
16.66666667	2896.666667	34.28030303	-17.61363636	332.0227273	0.5
13.33333333	2913.333333	34.28030303	-20.9469697	311.0757576	0.4
13.33333333	2926.666667	34.28030303	-20.9469697	290.1287879	0.4
10	2940	34.28030303	-24.28030303	265.8484848	0.3
10	2950	34.28030303	-24.28030303	241.5681818	0.3
6.666666667	2960	34.28030303	-27.61363636	213.9545455	0.2
6.666666667	2966.666667	34.28030303	-27.61363636	186.3409091	0.2
6.666666667	2973.333333	34.28030303	-27.61363636	158.7272727	0.2
3.333333333	2980	34.28030303	-30.9469697	127.780303	0.1
10	2983.333333	34.28030303	-24.28030303	103.5	0.3
10	2993.333333	34.28030303	-24.28030303	79.21969697	0.3
10	3003.333333	34.28030303	-24.28030303	54.93939394	0.3
10	3013.333333	34.28030303	-24.28030303	30.65909091	0.3
6.666666667	3023.333333	34.28030303	-27.61363636	3.045454544	0.2
6.666666667	3030	34.28030303	-27.61363636	-24.56818182	0.2

EL87-206(3)					
cell diameter (D) (µm)	distance along growth ring (µm)	mean diameter (md)	D - md	deviation from the mean [Σ(D - md)]	diameter in microscope scale bar units
40	0	25.91919192	14.08080808	8.448484848	1.2
40	40	25.91919192	14.08080808	22.52929293	1.2
33.33333333	73.33333333	25.91919192	7.414141414	29.94343434	1
36.66666667	110	25.91919192	10.74747475	40.69090909	1.1
40	150	25.91919192	14.08080808	54.77171717	1.2
43.33333333	193.3333333	25.91919192	17.41414141	72.18585858	1.3
40	233.3333333	25.91919192	14.08080808	86.26666667	1.2
36.66666667	270	25.91919192	10.74747475	97.01414141	1.1
43.33333333	313.3333333	25.91919192	17.41414141	114.4282828	1.3
43.33333333	356.6666667	25.91919192	17.41414141	131.8424242	1.3
33.33333333	390	25.91919192	7.414141414	139.2565657	1
36.66666667	426.6666667	25.91919192	10.74747475	150.0040404	1.1
46.66666667	473.3333333	25.91919192	20.74747475	170.7515151	1.4
46.66666667	520	25.91919192	20.74747475	191.4989899	1.4
43.33333333	563.3333333	25.91919192	17.41414141	208.9131313	1.3
40	603.3333333	25.91919192	14.08080808	222.9939394	1.2
36.66666667	640	25.91919192	10.74747475	233.7414141	1.1
40	680	25.91919192	14.08080808	247.8222222	1.2
40	720	25.91919192	14.08080808	261.9030303	1.2
43.33333333	763.3333333	25.91919192	17.41414141	279.3171717	1.3
36.66666667	800	25.91919192	10.74747475	290.0646465	1.1
36.66666667	836.6666667	25.91919192	10.74747475	300.8121212	1.1
33.33333333	870	25.91919192	7.414141414	308.2262626	1
33.33333333	903.3333333	25.91919192	7.414141414	315.640404	1
36.66666667	940	25.91919192	10.74747475	326.3878788	1.1
36.66666667	976.6666667	25.91919192	10.74747475	337.1353535	1.1
40	1016.666667	25.91919192	14.08080808	351.2161616	1.2
43.33333333	1060	25.91919192	17.41414141	368.630303	1.3
46.66666667	1106.666667	25.91919192	20.74747475	389.3777778	1.4
40	1146.666667	25.91919192	14.08080808	403.4585859	1.2
36.66666667	1183.333333	25.91919192	10.74747475	414.2060606	1.1
36.66666667	1220	25.91919192	10.74747475	424.9535353	1.1
40	1260	25.91919192	14.08080808	439.0343434	1.2
36.66666667	1296.666667	25.91919192	10.74747475	449.7818182	1.1
40	1336.666667	25.91919192	14.08080808	463.8626263	1.2
36.66666667	1373.333333	25.91919192	10.74747475	474.610101	1.1
33.33333333	1406.666667	25.91919192	7.414141414	482.0242424	1
30	1436.666667	25.91919192	4.080808081	486.1050505	0.9
26.66666667	1463.333333	25.91919192	0.747474747	486.8525252	0.8
23.33333333	1486.666667	25.91919192	-2.585858586	484.2666667	0.7
26.66666667	1513.333333	25.91919192	0.747474747	485.0141414	0.8
26.66666667	1540	25.91919192	0.747474747	485.7616162	0.8
30	1570	25.91919192	4.080808081	489.8424242	0.9
30	1600	25.91919192	4.080808081	493.9232323	0.9
33.33333333	1633.333333	25.91919192	7.414141414	501.3373737	1
33.33333333	1666.666667	25.91919192	7.414141414	508.7515151	1

EL87-206(3)

cell diameter (D) (μm)	distance along growth ring (μm)	mean diameter (md)	D - md	deviation from the mean [Σ(D - md)]	diameter in microscope scale bar units
26.66666667	1693.333333	25.91919192	0.747474747	509.4989899	0.8
26.66666667	1720	25.91919192	0.747474747	510.2464646	0.8
30	1750	25.91919192	4.080808081	514.3272727	0.9
23.33333333	1773.333333	25.91919192	-2.585858586	511.7414141	0.7
30	1803.333333	25.91919192	4.080808081	515.8222222	0.9
30	1833.333333	25.91919192	4.080808081	519.9030303	0.9
26.66666667	1860	25.91919192	0.747474747	520.650505	0.8
33.33333333	1893.333333	25.91919192	7.414141414	528.0646465	1
36.66666667	1930	25.91919192	10.74747475	538.8121212	1.1
33.33333333	1963.333333	25.91919192	7.414141414	546.2262626	1
33.33333333	1996.666667	25.91919192	7.414141414	553.640404	1
26.66666667	2023.333333	25.91919192	0.747474747	554.3878788	0.8
26.66666667	2050	25.91919192	0.747474747	555.1353535	0.8
23.33333333	2073.333333	25.91919192	-2.585858586	552.5494949	0.7
23.33333333	2096.666667	25.91919192	-2.585858586	549.9636364	0.7
26.66666667	2123.333333	25.91919192	0.747474747	550.7111111	0.8
23.33333333	2146.666667	25.91919192	-2.585858586	548.1252525	0.7
20	2166.666667	25.91919192	-5.919191919	542.2060606	0.6
16.66666667	2183.333333	25.91919192	-9.252525252	532.9535353	0.5
20	2203.333333	25.91919192	-5.919191919	527.0343434	0.6
20	2223.333333	25.91919192	-5.919191919	521.1151515	0.6
23.33333333	2246.666667	25.91919192	-2.585858586	518.5292929	0.7
16.66666667	2263.333333	25.91919192	-9.252525252	509.2767677	0.5
16.66666667	2280	25.91919192	-9.252525252	500.0242424	0.5
13.33333333	2293.333333	25.91919192	-12.58585859	487.4383838	0.4
16.66666667	2310	25.91919192	-9.252525252	478.1858586	0.5
16.66666667	2326.666667	25.91919192	-9.252525252	468.9333333	0.5
20	2346.666667	25.91919192	-5.919191919	463.0141414	0.6
13.33333333	2360	25.91919192	-12.58585859	450.4282828	0.4
10	2370	25.91919192	-15.91919192	434.5090909	0.3
10	2380	25.91919192	-15.91919192	418.589899	0.3
6.666666667	2386.666667	25.91919192	-19.25252525	399.3373737	0.2
10	2396.666667	25.91919192	-15.91919192	383.4181818	0.3
3.333333333	2400	25.91919192	-22.58585859	360.8323232	0.1
10	2410	25.91919192	-15.91919192	344.9131313	0.3
10	2420	25.91919192	-15.91919192	328.9939394	0.3
3.333333333	2423.333333	25.91919192	-22.58585859	306.4080808	0.1
6.666666667	2430	25.91919192	-19.25252525	287.1555556	0.2
3.333333333	2433.333333	25.91919192	-22.58585859	264.569697	0.1
6.666666667	2440	25.91919192	-19.25252525	245.3171717	0.2
6.666666667	2446.666667	25.91919192	-19.25252525	226.0646465	0.2
6.666666667	2453.333333	25.91919192	-19.25252525	206.8121212	0.2
10	2463.333333	25.91919192	-15.91919192	190.8929293	0.3
6.666666667	2470	25.91919192	-19.25252525	171.640404	0.2
6.666666667	2476.666667	25.91919192	-19.25252525	152.3878788	0.2
10	2486.666667	25.91919192	-15.91919192	136.4686869	0.3

C-17

EL87-206(3)					
cell diameter (D) (μm)	distance along growth ring (μm)	mean diameter (md)	D - md	deviation from the mean [Σ(D - md)]	diameter in microscope scale bar units
10	2496.666667	25.91919192	-15.91919192	120.5494949	0.3
6.666666667	2503.333333	25.91919192	-19.25252525	101.2969697	0.2
3.333333333	2506.666667	25.91919192	-22.58585859	78.7111111,1	0.1
6.666666667	· 2513.333333	25.91919192	-19.25252525	59.45858586	0.2
3.333333333	2516.666667	25.91919192	-22.58585859	36.87272727	0.1
3	2519.666667	25.91919192	-22.91919192	13.95353535	0.09
3.333333333	2523	25.91919192	-22.58585859	-8.632323233	0.1
3	2526	25.91919192	-22.91919192	-31.55151515	0.09

Phillips-86

cell diameter (D) (μm)	distance along growth ring (μm)	mean diameter (md)	D - md	deviation from the mean [Σ(D - md)]	diameter in microscope scale bar units
50	0	36.11111111	13.88888889	8.333333333	1.5
50	50	36.11111111	13.88888889	22.22222222	1.5
50	100	36.11111111	13.88888889	36.11111111	1.5
53.33333333	150	36.11111111	17.22222222	53.33333333	1.6
53.33333333	203.3333333	36.11111111	17.22222222	70.55555556	1.6
50	256.6666667	36.11111111	13.88888889	84.44444444	1.5
56.66666667	306.6666667	36.11111111	20.55555556	105	1.7
66.66666667	363.3333333	36.11111111	30.55555556	135.5555556	2
40	430	36.11111111	3.888888889	139.4444444	1.2
60	470	36.11111111	23.88888889	163.3333333	1.8
53.33333333	530	36.11111111	17.22222222	180.5555556	1.6
50	583.3333333	36.11111111	13.88888889	194.4444444	1.5
50	633.3333333	36.11111111	13.88888889	208.3333333	1.5
53.33333333	683.3333333	36.11111111	17.22222222	225.5555556	1.6
43.33333333	736.6666667	36.11111111	7.222222222	232.7777778	1.3
40	780	36.11111111	3.888888889	236.6666667	1.2
50	820	36.11111111	13.88888889	250.5555556	1.5
33.33333333	870	36.11111111	-2.777777778	247.7777778	1
33.33333333	903.3333333	36.11111111	-2.777777778	245	1
26.66666667	936.6666667	36.11111111	-9.444444444	235.5555556	0.8
43.33333333	963.3333333	36.11111111	7.222222222	242.7777778	1.3
50	1006.666667	36.11111111	13.88888889	256.6666667	1.5
46.66666667	1056.666667	36.11111111	10.55555556	267.2222222	1.4
56.66666667	1103.333333	36.11111111	20.55555556	287.7777778	1.7
50	1160	36.11111111	13.88888889	301.6666667	1.5
40	1210	36.11111111	3.888888889	305.5555556	1.2
33.33333333	1250	36.11111111	-2.777777778	302.7777778	1
40	1283.333333	36.11111111	3.888888889	306.6666667	1.2
33.33333333	1323.333333	36.11111111	-2.777777778	303.8888889	1
33.33333333	1356.666667	36.11111111	-2.777777778	301.1111111	1
33.33333333	1390	36.11111111	-2.777777778	298.3333333	1
26.66666667	1423.333333	36.11111111	-9.444444444	288.8888889	0.8
33.33333333	1450	36.11111111	-2.777777778	286.1111111	1
36.66666667	1483.333333	36.11111111	0.555555556	286.6666667	1.1
33.33333333	1520	36.11111111	-2.777777778	283.8888889	1
33.33333333	1553.333333	36.11111111	-2.777777778	281.1111111	1
30	1586.666667	36.11111111	-6.111111111	275	0.9
33.33333333	1616.666667	36.11111111	-2.777777778	272.2222222	1
26.66666667	1650	36.11111111	-9.444444444	262.7777778	0.8
33.33333333	1676.666667	36.11111111	-2.777777778	260	1
33.33333333	1710	36.11111111	-2.777777778	257.2222222	1

Phillips-86					
cell diameter (D) (μm)	distance along growth ring (μm)	mean diameter (md)	D - md	deviation from the mean [Σ(D - md)]	diameter in microscope scale bar units
23.33333333	1743.333333	36.11111111	-12.77777778	244.4444444	0.7
40	1766.666667	36.11111111	3.888888889	248.3333333	1.2
36.66666667	1806.666667	36.11111111	0.555555556	248.8888889	1.1
33.33333333	1843.333333	36.11111111	-2.777777778	246.1111111	1
33.33333333	1876.666667	36.11111111	-2.777777778	243.3333333	1
33.33333333	1910	36.11111111	-2.777777778	240.5555556	1
30	1943.333333	36.11111111	-6.111111111	234.4444444	0.9
33.33333333	1973.333333	36.11111111	-2.777777778	231.6666667	1
23.33333333	2006.666667	36.11111111	-12.77777778	218.8888889	0.7
30	2030	36.11111111	-6.111111111	212.7777778	0.9
26.66666667	2060	36.11111111	-9.444444444	203.3333333	0.8
33.33333333	2086.666667	36.11111111	-2.777777778	200.5555556	1
23.33333333	2120	36.11111111	-12.77777778	187.7777778	0.7
26.66666667	2143.333333	36.11111111	-9.444444444	178.3333333	0.8
30	2170	36.11111111	-6.111111111	172.2222222	0.9
30	2200	36.11111111	-6.111111111	166.1111111	0.9
36.66666667	2230	36.11111111	0.555555556	166.6666667	1.1
23.33333333	2266.666667	36.11111111	-12.77777778	153.8888889	0.7
26.66666667	2290	36.11111111	-9.444444444	144.4444444	0.8
26.66666667	2316.666667	36.11111111	-9.444444444	135	0.8
33.33333333	2343.333333	36.11111111	-2.777777778	132.2222222	1
23.33333333	2376.666667	36.11111111	-12.77777778	119.4444444	0.7
26.66666667	2400	36.11111111	-9.444444444	110	0.8
30	2426.666667	36.11111111	-6.111111111	103.8888889	0.9
23.33333333	2456.666667	36.11111111	-12.77777778	91.11111111	0.7
20	2480	36.11111111	-16.11111111	75	0.6
23.33333333	2500	36.11111111	-12.77777778	62.22222222	0.7
16.66666667	2523.333333	36.11111111	-19.44444444	42.77777778	0.5
23.33333333	2540	36.11111111	-12.77777778	30	0.7
20	2563.333333	36.11111111	-16.11111111	13.88888889	0.6
16.66666667	2583.333333	36.11111111	-19.44444444	-5.555555556	0.5

Phillips-86(2)

cell diameter (D) (µm)	distance along growth ring (µm)	mean diameter (md)	D - md	deviation from the mean [Σ(D - md)]	diameter in microscope scale bar units
46.66666667	0	33.83647799	12.83018868	7.698113208	1.4
43.33333333	46.66666667	33.83647799	9.496855346	17.19496855	1.3
43.33333333	90	33.83647799	9.496855346	26.6918239	1.3
53.33333333	133.3333333	33.83647799	19.49685535	46.18867925	1.6
60	186.6666667	33.83647799	26.16352201	72.35220126	1.8
56.66666667	246.6666667	33.83647799	22.83018868	95.18238994	1.7
40	303.3333333	33.83647799	6.163522013	101.345912	1.2
50	343.3333333	33.83647799	16.16352201	117.509434	1.5
50	393.3333333	33.83647799	16.16352201	133.672956	1.5
46.66666667	443.3333333	33.83647799	12.83018868	146.5031447	1.4
50	490	33.83647799	16.16352201	162.6666667	1.5
46.66666667	540	33.83647799	12.83018868	175.4968553	1.4
40	586.6666667	33.83647799	6.163522013	181.6603774	1.2
40	626.6666667	33.83647799	6.163522013	187.8238994	1.2
40	666.6666667	33.83647799	6.163522013	193.9874214	1.2
43.33333333	706.6666667	33.83647799	9.496855346	203.4842767	1.3
43.33333333	750	33.83647799	9.496855346	212.9811321	1.3
36.66666667	793.3333333	33.83647799	2.830188679	215.8113208	1.1
43.33333333	830	33.83647799	9.496855346	225.3081761	1.3
43.33333333	873.3333333	33.83647799	9.496855346	234.8050314	1.3
40	916.6666667	33.83647799	6.163522013	240.9685535	1.2
46.66666667	956.6666667	33.83647799	12.83018868	253.7987421	1.4
40	1003.333333	33.83647799	6.163522013	259.9622642	1.2
43.33333333	1043.333333	33.83647799	9.496855346	269.4591195	1.3
40	1086.666667	33.83647799	6.163522013	275.6226415	1.2
43.33333333	1126.666667	33.83647799	9.496855346	285.1194969	1.3
40	1170	33.83647799	6.163522013	291.2830189	1.2
40	1210	33.83647799	6.163522013	297.4465409	1.2
43.33333333	1250	33.83647799	9.496855346	306.9433962	1.3
40	1293.333333	33.83647799	6.163522013	313.1069182	1.2
40	1333.333333	33.83647799	6.163522013	319.2704403	1.2
43.33333333	1373.333333	33.83647799	9.496855346	328.7672956	1.3
40	1416.666667	33.83647799	6.163522013	334.9308176	1.2
36.66666667	1456.666667	33.83647799	2.830188679	337.7610063	1.1
43.33333333	1493.333333	33.83647799	9.496855346	347.2578616	1.3
33.33333333	1536.666667	33.83647799	-0.503144654	346.754717	1
36.66666667	1570	33.83647799	2.830188679	349.5849057	1.1
33.33333333	1606.666667	33.83647799	-0.503144654	349.081761	1
36.66666667	1640	33.83647799	2.830188679	351.9119497	1.1
33.33333333	1676.666667	33.83647799	-0.503144654	351.408805	1
33.33333333	1710	33.83647799	-0.503144654	350.9056604	1
40	1743.333333	33.83647799	6.163522013	357.0691824	1.2
36.66666667	1783.333333	33.83647799	2.830188679	359.8993711	1.1
33.33333333	1820	33.83647799	-0.503144654	359.3962264	1

Phillips-86(2)

cell diameter (D) (μm)	distance along growth ring (μm)	mean diameter (md)	D - md	deviation from the mean [Σ(D - md)]	diameter in microscope scale bar units
33.33333333	1853.333333	33.83647799	-0.503144654	358.8930818	1
30	1886.666667	33.83647799	-3.836477987	355.0566038	0.9
33.33333333	1916.666667	33.83647799	-0.503144654	354.5534591	1
33.33333333	1950	33.83647799	-0.503144654	354.0503145	1
36.66666667	1983.333333	33.83647799	2.830188679	356.8805031	1.1
33.33333333	2020	33.83647799	-0.503144654	356.3773585	1
33.33333333	2053.333333	33.83647799	-0.503144654	355.8742138	1
33.33333333	2086.666667	33.83647799	-0.503144654	355.3710692	1
33.33333333	2120	33.83647799	-0.503144654	354.8679245	1
30	2153.333333	33.83647799	-3.836477987	351.0314465	0.9
33.33333333	2183.333333	33.83647799	-0.503144654	350.5283019	1
33.33333333	2216.666667	33.83647799	-0.503144654	350.0251572	1
36.66666667	2250	33.83647799	2.830188679	352.8553459	1.1
33.33333333	2286.666667	33.83647799	-0.503144654	352.3522013	1
36.66666667	2320	33.83647799	2.830188679	355.1823899	1.1
33.33333333	2356.666667	33.83647799	-0.503144654	354.6792453	1
36.66666667	2390	33.83647799	2.830188679	357.509434	1.1
33.33333333	2426.666667	33.83647799	-0.503144654	357.0062893	1
33.33333333	2460	33.83647799	-0.503144654	356.5031447	1
26.66666667	2493.333333	33.83647799	-7.169811321	349.3333333	0.8
30	2520	33.83647799	-3.836477987	345.4968553	0.9
33.33333333	2550	33.83647799	-0.503144654	344.9937107	1
26.66666667	2583.333333	33.83647799	-7.169811321	337.8238994	0.8
33.33333333	2610	33.83647799	-0.503144654	337.3207547	1
36.66666667	2643.333333	33.83647799	2.830188679	340.1509434	1.1
30	2680	33.83647799	-3.836477987	336.3144654	0.9
30	2710	33.83647799	-3.836477987	332.4779874	0.9
26.66666667	2740	33.83647799	-7.169811321	325.3081761	0.8
33.33333333	2766.666667	33.83647799	-0.503144654	324.8050314	1
23.33333333	2800	33.83647799	-10.50314465	314.3018868	0.7
33.33333333	2823.333333	33.83647799	-0.503144654	313.7987421	1
36.66666667	2856.666667	33.83647799	2.830188679	316.6289308	1.1
26.66666667	2893.333333	33.83647799	-7.169811321	309.4591195	0.8
26.66666667	2920	33.83647799	-7.169811321	302.2893082	0.8
30	2946.666667	33.83647799	-3.836477987	298.4528302	0.9
30	2976.666667	33.83647799	-3.836477987	294.6163522	0.9
20	3006.666667	33.83647799	-13.83647799	280.7798742	0.6
23.33333333	3026.666667	33.83647799	-10.50314465	270.2767296	0.7
30	3050	33.83647799	-3.836477987	266.4402516	0.9
26.66666667	3080	33.83647799	-7.169811321	259.2704403	0.8
26.66666667	3106.666667	33.83647799	-7.169811321	252.1006289	0.8
30	3133.333333	33.83647799	-3.836477987	248.2641509	0.9
26.66666667	3163.333333	33.83647799	-7.169811321	241.0943396	0.8
23.33333333	3190	33.83647799	-10.50314465	230.591195	0.7

Phillips-86(2)					
cell diameter (D) (μm)	distance along growth ring (μm)	mean diameter (md)	D - md	deviation from the mean [Σ(D - md)]	diameter in microscope scale bar units
23.33333333	3213.333333	33.83647799	-10.50314465	220.0880503	0.7
26.66666667	3236.666667	33.83647799	-7.169811321	212.918239	0.8
26.66666667	3263.333333	33.83647799	-7.169811321	205.7484277	0.8
23.33333333	3290	33.83647799	-10.50314465	195.245283	0.7
26.66666667	3313.333333	33.83647799	-7.169811321	188.0754717	0.8
30	3340	33.83647799	-3.836477987	184.2389937	0.9
33.33333333	3370	33.83647799	-0.503144654	183.7358491	1
26.66666667	3403.333333	33.83647799	-7.169811321	176.5660377	0.8
20	3430	33.83647799	-13.83647799	162.7295597	0.6
20	3450	33.83647799	-13.83647799	148.8930818	0.6
30	3470	33.83647799	-3.836477987	145.0566038	0.9
16.66666667	3500	33.83647799	-17.16981132	127.8867925	0.5
20	3516.666667	33.83647799	-13.83647799	114.0503145	0.6
13.33333333	3536.666667	33.83647799	-20.50314465	93.54716981	0.4
16.66666667	3550	33.83647799	-17.16981132	76.37735849	0.5
10	3566.666667	33.83647799	-23.83647799	52.5408805	0.3
6.666666667	3576.666667	33.83647799	-27.16981132	25.37106918	0.2
3.333333333	3583.333333	33.83647799	-30.50314465	-5.132075471	0.1

EL87-257

cell diameter (D) (μm)	distance along growth ring (μm)	mean diameter (md)	D - md	deviation from the mean [Σ(D - md)]	diameter in microscope scale bar units
36.66666667	0	42	-5.3333333	-3.2	1.1
40	36.66666667	42	-2	↓5.2	1.2
60	76.66666667	42	18	12.8	1.8
63.33333333	136.6666667	42	21.3333333	34.13333333	1.9
66.66666667	200	42	24.6666667	58.8	2
66.66666667	266.6666667	42	24.6666667	83.46666667	2
66.66666667	333.3333333	42	24.6666667	108.1333333	2
60	400	42	18	126.1333333	1.8
63.33333333	460	42	21.3333333	147.4666667	1.9
60	523.3333333	42	18	165.4666667	1.8
56.66666667	583.3333333	42	14.6666667	180.1333333	1.7
60	640	42	18	198.1333333	1.8
66.66666667	700	42	24.6666667	222.8	2
63.33333333	766.6666667	42	21.3333333	244.1333333	1.9
40	830	42	-2	242.1333333	1.2
50	870	42	8	250.1333333	1.5
40	920	42	-2	248.1333333	1.2
43.33333333	960	42	1.33333333	249.4666667	1.3
46.66666667	1003.333333	42	4.66666667	254.1333333	1.4
50	1050	42	8	262.1333333	1.5
53.33333333	1100	42	11.3333333	273.4666667	1.6
46.66666667	1153.333333	42	4.66666667	278.1333333	1.4
43.33333333	1200	42	1.33333333	279.4666667	1.3
43.33333333	1243.333333	42	1.33333333	280.8	1.3
53.33333333	1286.666667	42	11.3333333	292.1333333	1.6
56.66666667	1340	42	14.6666667	306.8	1.7
53.33333333	1396.666667	42	11.3333333	318.1333333	1.6
53.33333333	1450	42	11.3333333	329.4666667	1.6
50	1503.333333	42	8	337.4666667	1.5
46.66666667	1553.333333	42	4.66666667	342.1333333	1.4
50	1600	42	8	350.1333333	1.5
46.66666667	1650	42	4.66666667	354.8	1.4
43.33333333	1696.666667	42	1.33333333	356.1333333	1.3
50	1740	42	8	364.1333333	1.5
46.66666667	1790	42	4.66666667	368.8	1.4
43.33333333	1836.666667	42	1.33333333	370.1333333	1.3
53.33333333	1880	42	11.3333333	381.4666667	1.6
36.66666667	1933.333333	42	-5.3333333	376.1333333	1.1
40	1970	42	-2	374.1333333	1.2
40	2010	42	-2	372.1333333	1.2
36.66666667	2050	42	-5.3333333	366.8	1.1

EL87-257					
cell diameter (D) (μm)	distance along growth ring (μm)	mean diameter (md)	D - md	deviation from the mean [Σ(D - md)]	diameter in microscope scale bar units
33.33333333	2086.666667	42	-8.6666667	358.1333333	1
33.33333333	2120	42	-8.6666667	349.4666667	1
36.66666667	2153.333333	42	-5.3333333	344.1333333	1.1
33.33333333	2190	42	-8.6666667	335.4666667	1
33.33333333	2223.333333	42	-8.6666667	326.8	1
33.33333333	2256.666667	42	-8.6666667	318.1333333	1
36.66666667	2290	42	-5.3333333	312.8	1.1
26.66666667	2326.666667	42	-15.333333	297.4666667	0.8
23.33333333	2353.333333	42	-18.666667	278.8	0.7
26.66666667	2376.666667	42	-15.333333	263.4666667	0.8
13.33333333	2403.333333	42	-28.666667	234.8	0.4
20	2416.666667	42	-22	212.8	0.6
16.66666667	2436.666667	42	-25.333333	187.4666667	0.5
20	2453.333333	42	-22	165.4666667	0.6
13.33333333	2473.333333	42	-28.666667	136.8	0.4
10	2486.666667	42	-32	104.8	0.3
10	2496.666667	42	-32	72.8	0.3
6.666666667	2506.666667	42	-35.333333	37.46666667	0.2
6.666666667	2513.333333	42	-35.333333	2.133333333	0.2

EL87-257

cell diameter (D) (µm)	distance along growth ring (µm)	mean diameter (md)	D - md	deviation from the mean [Σ(D - md)]	diameter in microscope scale bar units
70	0	48.88888889	21.1111111	12.6666667	2.1
73.33333333	70	48.88888889	24.4444444	37.11111114	2.2
83.33333333	143.3333333	48.88888889	34.4444444	71.55555559	2.5
80	226.6666667	48.88888889	31.1111111	102.6666667	2.4
73.33333333	306.6666667	48.88888889	24.4444444	127.1111111	2.2
66.66666667	380	48.88888889	17.7777778	144.8888889	2
60	446.6666667	48.88888889	11.1111111	156	1.8
63.33333333	506.6666667	48.88888889	14.4444444	170.4444445	1.9
50	570	48.88888889	1.11111111	171.5555556	1.5
46.66666667	620	48.88888889	-2.2222222	169.3333334	1.4
50	666.6666667	48.88888889	1.11111111	170.4444445	1.5
46.66666667	716.6666667	48.88888889	-2.2222222	168.2222223	1.4
50	763.3333333	48.88888889	1.11111111	169.3333334	1.5
46.66666667	813.3333333	48.88888889	-2.2222222	167.1111111	1.4
50	860	48.88888889	1.11111111	168.2222223	1.5
50	910	48.88888889	1.11111111	169.3333334	1.5
56.66666667	960	48.88888889	7.77777778	177.1111111	1.7
60	1016.666667	48.88888889	11.1111111	188.2222223	1.8
63.33333333	1076.666667	48.88888889	14.4444444	202.6666667	1.9
66.66666667	1140	48.88888889	17.7777778	220.4444445	2
70	1206.666667	48.88888889	21.1111111	241.5555556	2.1
66.66666667	1276.666667	48.88888889	17.7777778	259.3333334	2
60	1343.333333	48.88888889	11.1111111	270.4444445	1.8
70	1403.333333	48.88888889	21.1111111	291.5555556	2.1
66.66666667	1473.333333	48.88888889	17.7777778	309.3333334	2
50	1540	48.88888889	1.11111111	310.4444445	1.5
56.66666667	1590	48.88888889	7.77777778	318.2222223	1.7
60	1646.666667	48.88888889	11.1111111	329.3333334	1.8
53.33333333	1706.666667	48.88888889	4.44444444	333.7777778	1.6
56.66666667	1760	48.88888889	7.77777778	341.5555556	1.7
60	1816.666667	48.88888889	11.1111111	352.6666667	1.8
53.33333333	1876.666667	48.88888889	4.44444444	357.1111111	1.6
50	1930	48.88888889	1.11111111	358.2222223	1.5
56.66666667	1980	48.88888889	7.77777778	366	1.7
53.33333333	2036.666667	48.88888889	4.44444444	370.4444445	1.6
50	2090	48.88888889	1.11111111	371.5555556	1.5
56.66666667	2140	48.88888889	7.77777778	379.3333334	1.7
56.66666667	2196.666667	48.88888889	7.77777778	387.1111111	1.7
53.33333333	2253.333333	48.88888889	4.44444444	391.5555556	1.6
53.33333333	2306.666667	48.88888889	4.44444444	396	1.6
50	2360	48.88888889	1.11111111	397.1111111	1.5
50	2410	48.88888889	1.11111111	398.2222223	1.5
46.66666667	2460	48.88888889	-2.2222222	396	1.4
50	2506.666667	48.88888889	1.11111111	397.1111111	1.5

EL87-257

cell diameter (D) (μm)	distance along growth ring (μm)	mean diameter (md)	D - md	deviation from the mean [Σ(D - md)]	diameter in microscope scale bar units
46.66666667	2556.666667	48.88888889	-2.2222222	394.8888889	1.4
46.66666667	2603.333333	48.88888889	-2.2222222	392.6666667	1.4
50	2650	48.88888889	1.11111111	393.7777778	1.5
43.33333333	2700	48.88888889	-5.5555556	388.2222223	1.3
40	2743.333333	48.88888889	-8.8888889	379.3333334	1.2
40	2783.333333	48.88888889	-8.8888889	370.4444445	1.2
36.66666667	2823.333333	48.88888889	-12.222222	358.2222223	1.1
33.33333333	2860	48.88888889	-15.555556	342.6666667	1
33.33333333	2893.333333	48.88888889	-15.555556	327.1111111	1
40	2926.666667	48.88888889	-8.8888889	318.2222223	1.2
36.66666667	2966.666667	48.88888889	-12.222222	306	1.1
33.33333333	3003.333333	48.88888889	-15.555556	290.4444445	1
30	3036.666667	48.88888889	-18.888889	271.5555556	0.9
33.33333333	3066.666667	48.88888889	-15.555556	256	1
33.33333333	3100	48.88888889	-15.555556	240.4444445	1
23.33333333	3133.333333	48.88888889	-25.555556	214.8888889	0.7
16.66666667	3156.666667	48.88888889	-32.222222	182.6666667	0.5
16.66666667	3173.333333	48.88888889	-32.222222	150.4444445	0.5
13.33333333	3190	48.88888889	-35.555556	114.8888889	0.4
10	3203.333333	48.88888889	-38.888889	76.00000003	0.3
6.666666667	3213.333333	48.88888889	-42.222222	33.77777781	0.2
6.666666667	3220	48.88888889	-42.222222	-8.444444411	0.2

C-27

EL87-268					
cell diameter (D) (μm)	distance along growth ring (μm)	mean diameter (md)	D - md	deviation from the mean [Σ(D - md)]	diameter in microscope scale bar units (40X)
42.56	0	39.80148148	2.758518519	2.758518519	8
37.24	42.56	39.80148148	-2.561481481	0.197037038	7
53.2	79.8	39.80148148	13.39851852	13.59555556	10
58.52	133	39.80148148	18.71851852	32.31407407	11
53.2	191.52	39.80148148	13.39851852	45.71259259	10
50.54	244.72	39.80148148	10.73851852	56.45111111	9.5
47.88	295.26	39.80148148	8.078518519	64.52962963	9
42.56	343.14	39.80148148	2.758518519	67.28814815	8
47.88	385.7	39.80148148	8.078518519	75.36666667	9
47.88	433.58	39.80148148	8.078518519	83.44518519	9
47.88	481.46	39.80148148	8.078518519	91.5237037	9
47.88	529.34	39.80148148	8.078518519	99.60222222	9
45.22	577.22	39.80148148	5.418518519	105.0207407	8.5
47.88	622.44	39.80148148	8.078518519	113.0992593	9
45.22	670.32	39.80148148	5.418518519	118.5177778	8.5
53.2	715.54	39.80148148	13.39851852	131.9162963	10
58.52	768.74	39.80148148	18.71851852	150.6348148	11
53.2	827.26	39.80148148	13.39851852	164.0333333	10
53.2	880.46	39.80148148	13.39851852	177.4318519	10
58.52	933.66	39.80148148	18.71851852	196.1503704	11
47.88	992.18	39.80148148	8.078518519	204.2288889	9
47.88	1040.06	39.80148148	8.078518519	212.3074074	9
45.22	1087.94	39.80148148	5.418518519	217.7259259	8.5
47.88	1133.16	39.80148148	8.078518519	225.8044444	9
47.88	1181.04	39.80148148	8.078518519	233.882963	9
47.88	1228.92	39.80148148	8.078518519	241.9614815	9
42.56	1276.8	39.80148148	2.758518519	244.72	8
37.24	1319.36	39.80148148	-2.561481481	242.1585185	7
37.24	1356.6	39.80148148	-2.561481481	239.597037	7
37.24	1393.84	39.80148148	-2.561481481	237.0355556	7
39.9	1431.08	39.80148148	0.098518519	237.1340741	7.5
42.56	1470.98	39.80148148	2.758518519	239.8925926	8
39.9	1513.54	39.80148148	0.098518519	239.9911111	7.5
37.24	1553.44	39.80148148	-2.561481481	237.4296296	7
37.24	1590.68	39.80148148	-2.561481481	234.8681481	7
31.92	1627.92	39.80148148	-7.881481481	226.9866667	6
37.24	1659.84	39.80148148	-2.561481481	224.4251852	7
34.58	1697.08	39.80148148	-5.221481481	219.2037037	6.5
34.58	1731.66	39.80148148	-5.221481481	213.9822222	6.5
37.24	1766.24	39.80148148	-2.561481481	211.4207407	7
37.24	1803.48	39.80148148	-2.561481481	208.8592593	7

EL87-268					
cell diameter (D) (μm)	distance along growth ring (μm)	mean diameter (md)	D - md	deviation from the mean [Σ(D - md)]	diameter in microscope scale bar units (40X)
26.6	1840.72	39.80148148	-13.20148148	195.6577778	5
23.94	1867.32	39.80148148	-15.86148148	179.7962963	4.5
26.6	1891.26	39.80148148	-13.20148148	166.5948148	5
29.26	1917.86	39.80148148	-10.54148148	156.0533333	5.5
29.26	1947.12	39.80148148	-10.54148148	145.5118519	5.5
26.6	1976.38	39.80148148	-13.20148148	132.3103704	5
26.6	2002.98	39.80148148	-13.20148148	119.1088889	5
26.6	2029.58	39.80148148	-13.20148148	105.9074074	5
23.94	2056.18	39.80148148	-15.86148148	90.04592593	4.5
21.28	2080.12	39.80148148	-18.52148148	71.52444444	4
15.96	2101.4	39.80148148	-23.84148148	47.68296296	3
15.96	2117.36	39.80148148	-23.84148148	23.84148148	3
15.96	2133.32	39.80148148	-23.84148148	4.80796E-10	3

C-34